DESIGN OF AN ACTUATION SYSTEM FOR A HAPTIC GLOVE

A Thesis Submitted to
the Graduate School of Engineering and Sciences of
İzmir Institute of Technology
in Partial Fulfillment of the Requirements for the Degree of

MASTER OF SCIENCE

in Mechanical Engineering

by
Kaan Erol KURT

July 2022
İZMİR

ACKNOWLEDGMENTS

I would like to express my sincerest gratitude to my supervisor Assoc. Prof. Dr. Mehmet İsmet Can Dede for his endless support, guidance and patience during my studies.

I would like to thank my dear friends Asuman Didar Bingöl, Uygar Aydın, Uğur Nalbant and Tarık Büyüköztekin for their continuous supports in my most difficult times.

I would like to express my sincerest gratitude to my parents for their unlimited support, patience and faith in me.

ABSTRACT

DESIGN OF AN ACTUATION SYSTEM FOR A HAPTIC GLOVE

In this thesis, the design of a magneto-rheological fluid-based brake (MR brake) system that is aimed to be used on a conceptually designed force feedback virtual reality glove is presented. The reasons of MR brakes are assigned for this task is that they can provide high torque output in smaller volumes/masses, their ability to operate with low power requirements and their safe natures.

During their designs, in addition to ensuring their usability for a haptic glove application, solutions have been presented and applied for the sticky wall and high off-state torque problems observed in the MR brake systems. In addition to these, a novel study has been carried out to overcome the low torque-to-mass ratio problem observed in drum-type MR brake architectures used for applications requiring small sizes due to their high manufacturability.

The design starts with the determination of the requirements. Later, the mathematical models were developed to estimate the output torques to be obtained from the MR brake and the solid models of the parts were created respectively. In order to estimate the performance of the developed system, magneto-static finite element analyses (FEA) were carried out. The models were updated in line with the analysis results and, the production phase was started after all the design criteria are met. A prototype MR brake system was produced, assembled and tested in order to experimentally verify the analysis results. In the tests carried out, it was observed that all the determined design criteria were met and the developed MR brake system was found to be suitable to be used in a haptic glove application.

Based on the test results, the off-state torque seen in MR brake systems, which can increase up to 25% of the maximum output torque, has been reduced to 3% of the total torque output and found to be 23 mN.m. Additionally, thanks to the improved drum-type design, the typical torque-to-mass ratio seen in drum-type MR brake architectures is increased from 1.4 N.m/kg to 2. 90 N.m/kg within 206 grams of mass and 597 mN.m of dynamic torque range of the developed system.

ÖZET

BİR HAPTİK ELDİVEN İÇİN EYLEYİCİ SİSTEM TASARIMI

Bu tezde, kavramsal olarak tasarlanmış bir kuvvet geri beslemeli sanal gerçeklik eldiveni üzerinde kullanılması amaçlanan manyeto-reolojik sıvı bazlı bir fren (MR fren) sisteminin tasarımı sunulmaktadır. MR frenlerin bu göreve atanmasının nedeni, daha küçük hacimlerde/kütlelerde yüksek tork çıkışı sağlayabilmeleri, düşük güç gereksinimleri ile çalışabilmeleri ve güvenli olmalarıdır.

Tasarımları sırasında, dokunsal eldiven uygulaması için kullanılabilirliklerinin sağlanmasının yanı sıra, MR fren sistemlerinde gözlenen yapışkan duvar ve yüksek kapalı-durum torku sorunlarına çözümler sunulmuş ve uygulanmıştır. Bunlara ek olarak, küçük boyut gerektiren uygulamalar için yüksek üretilebilirlikleri nedeniyle kullanılan davul-tipi MR fren mimarilerinde gözlenen düşük tork-kütle oranı sorununun üstesinden gelmek için yeni bir çalışma yapılmıştır.

Tasarım, gereksinimlerin belirlenmesi ile başlamıştır. Daha sonra MR frenden elde edilecek çıkış torklarını tahmin etmek için matematiksel modeller geliştirilmiş ve elde edilen modeller doğrultusunda parçaların katı modelleri oluşturulmuştur. Geliştirilen sistemin performansını tahmin etmek için manyeto-statik sonlu elemanlar analizleri (FEA) gerçekleştirilmiştir. Analiz sonuçları doğrultusunda modeller güncellenmiş ve tüm tasarım kriterleri sağlandıktan sonra üretim aşamasına geçilmiştir. Analiz sonuçlarını deneysel olarak doğrulamak için prototip bir MR fren sistemi üretimi ve montajı sağlanarak testleri gerçekleştirilmiştir. Yapılan test sonuçları incelendiğinde, belirlenen tüm tasarım kriterlerinin karşılandığı gözlemlenmiş ve geliştirilen MR fren sisteminin bir haptik eldiven uygulamasında kullanılabilirliğinin uygun olduğu görülmüştür.

Test sonuçlarında, MR fren sistemlerinde görülen ve maksimum çıkış torkunun %25'ine kadar ulaşabilen kapalı-durum torkunun, maksimum tork çıkışının %3'üne denk geldiği ve 23 mN.m olduğu bulunmuştur. Ek olarak, iyileştirilmiş davul-tipi tasarım sayesinde, sıradan davul-tip MR fren mimarilerinde görülen tipik 1.4 N.m/kg tork-kütle oranı, sistemin sahip olduğu 206 gram kütle ve 597 mN.m dinamik tork aralığında 2.90 N.m/kg'a yükseltilmiştir.

I dedicate this thesis to my dear mother, Meryem Nil Kaan.

TABLE OF CONTENTS

LIST OF FIGURES

Figure **Page**

Figure **Page**

Figure **Page**

Figure **Page**

LIST OF TABLES

Table **Page**

CHAPTER 1

INTRODUCTION

The word “haptic” comes from Ancient Greek “haptikos” which means the sense of touch or suitable to touch. In order to understand the nature of the objects and their features, humans rely on their sense of touch. Haptic information is used for holding and manipulating objects in real environments. The objectives of haptic feedback systems can be counted as; they provide information to the user and let them feel and interact with objects in virtual or distant environments and the manipulation of the object remotely. One of the main difficulties in understanding haptics is about the sense of touch. The sense of touch perceived by the body covers a collection of various sensations from different joints, muscles and skin. Because of this reason, creation of the sense of touch is not a simple task and cannot be achieved by a single principle. These sensations are classified into two main groups based on the sensory channel they have perceived by different biological receptors found in skin and other soft tissues; which are tactile feedback and force feedback.

Tactile feedback covers the creation of pressure patterns on the surface of the users’ skin. Small receptors spread throughout the skin are responsible from gathering these patterns and the brain interpret this information as a rich set of sensations. The tactile feedback channels are the main source of information about an object’s surface properties and the fine shape and also contributes to the perception of texture, size and weight of that object. Tactile feedback devices rely on actuators spread over the surface of a skin to reconstruct a user’s sense of touch. These actuators can be thought of as a "pixel" grid. Each pixel consists of an actuator that can produce controlled pressure on the skin. Tactile feedback devices create continuous senses on the surface of the skin by adjusting the pressure applied by these actuators spread over the skin. An object placed on a slippery and non-resistant surface can be touched to experience the effect of tactile feedback in real life. However, haptic perception cannot be achieved by only tactile feedback which is cutaneous and perceived by sensitive nerves in the skin. Human body

is also sensitive to the forces acting on the musculoskeletal system which are detected by sensitive nerves in muscles and ligaments. These receptors are responsible for the perception of force feedback.

Force feedback is applied to body segments such as fingers or arms, and is important in the perception of overall shape, weight, and impact forces. Force feedback devices should be able to move with the user, produce forces and have high mobility. Force feedback devices are divided into two categories which are biomimetic devices and non-biomimetic devices. Devices that act similar to human body are called biomimetic devices and as opposite, non-biomimetic devices do not act like human body. In general, biomimetic devices are more capable, but they need to be designed to fit every user which is a challenging task. Another important distinction within force feedback devices is between active and resistive devices. Resistive devices use brakes to restrict the user's movement where active devices use motors to restrict a user's movement and able to actively move their bodies. Passive devices are more advantageous in terms of control, and they can generate higher forces due to their structures compared to the active devices which need powerful motors to generate same amount of forces. The downside of passive devices is the narrow range of interactions. A good force feedback device should keep the unwanted forces (the weight of the device, friction and etc.) at a minimum level, move with the user in the range of their motion and match the forces in a virtual or distant when a user touches an object.

Haptic feedback systems cover the combination of both tactile and force feedbacks and can be classified into three types according to their mechanical grounding configuration: the grounded type, the non-grounded type, and the wearable type. In this work, the development of a haptic glove under the category of wearable haptic feedback systems with force feedback features will be presented.

Haptic gloves are gloves which allows users to get in communication with the computers to interact with distant or virtual objects and feel them with the use of haptic technology. They are wearable devices that allows users to touch and manipulate virtual/distant objects by providing pressures, forces and torques to the fingertips and hence provide users to experience the sense of touch in virtual reality environments. Haptic gloves have two main functions which are: creation of the forces and motions on the users' fingers via using actuators, and the measurement of the kinematic configuration (position, velocity, acceleration) and contact forces of the user's fingers via using sensors.

However, due to the complex anatomy, physiological structure and the dexterity of the human hand, it is not an easy task to design a glove with haptic feedback that enables its user to interact virtual/distant environments. Main challenges in the haptic glove designs can be narrowed down into the following:

- Size: The designed glove should fit on different sizes of human hands.
- Weight: The total weight of the glove should be kept as light as possible in order to be carried on the hand and not tire the users during their manipulations.
- Flexibility: After being worn, the glove should exhibit flexible features to not hinder the fingers' flexion/extension and abduction/adduction motions.
- Dynamic range of the force feedback: The glove should provide sufficient force feedback to the fingers and fingertips of the user. For daily activities such as grasping, pinching and pick-place operations, the glove should be able to generate at least 7 N of force feedback signals with 2 Hz frequency (Rice, Leonard, and Carter 1998).
- Safety: The user wearing the glove must be protected from any source of hazards and damages (electrical shock, fingers push/pulled without control and such).

In this thesis, the presented work starts with the research of force feedback gloves available in the market and developed in a laboratory environment. The problems observed in the investigated gloves were determined and possible improvements were evaluated. Based on the examinations, it has been observed that the problems occur in the surveyed gloves are mostly caused by the actuators used within the systems and therefore, an alternative actuator design to solve related problems has been researched. As a result of the research, magnetorheological fluid-based brake systems were found to be suitable to be used in a haptic feedback glove application due to their advantages. In addition to the problems to be solved in the surveyed gloves, the problems occur within the magneto-rheological fluid-based brake systems were determined and combined to decide the necessary design requirements. After the design criteria were determined, mathematical models were created and solid model designs were started. During the design of the developed brake systems, the manufacturer was always kept in touch so that the required productions would not exceed the capacity of the machining benches. Created solid models were iteratively improved by taking magnetic analyses results into account and

updated until the desired requirements were met. After the results obtained from the magnetic analyzes were approved, the production of the parts was completed and their assembly was carried out. A test setup was created to perform the tests of the assembled brake systems. Thanks to the experimental tests carried out, it was validated that the developed MR brake system met the targeted performance criteria, and the study was completed by extracting its detailed features.

1.1. Thesis Objective and Motivation

It has been revealed after the literature review that in haptic glove designs (both developed in the laboratory environment and commercially available ones), the actuator systems used to provide sufficient force feedback are mostly have at least one heavy and bulky element that must be carried by the user or to be placed in the ground. Additionally, gloves with non-grounded actuators cannot provide sufficient force feedback to the user. In order to overcome this issue, the research interest turned towards magneto-rheological fluid-based brake (MRF Brakes or MR brakes) systems. When the results of the researches were examined, it was seen that MR brake systems can provide higher torque/force outputs within a smaller volume by consuming less electrical power compared to the active actuators. Additionally, since there are no elements connected to the ground, the movements of the users will not be impeded. However, there are 3 main problems that must be resolved to use MR brake systems in haptic glove applications.

The first of these problems is known as the “sticky wall” or “stiction” problem in the literature (An and Kwon 2004; Rosenberg and Adelstein 1993). The root of this problem is, when MR brake systems are activated, they will constrain motion in every direction that they operate. Due to the locking of the system in both directions, users must overcome the braking force provided by the brake system when they want to cut the contact with the object they are interacting with. For haptic glove applications, the direction that the user is aimed to supplied with the braking torque is in the flexion motion of the fingers while grasping an object. During the extension of the fingers, the object being held is released and no torque should be applied to the fingertips of the user. Thanks to the studies conducted by Karabulut (2018), it has been demonstrated that the sticky wall problem can be solved mechanically with the help of one-way bearings without using

any software or control algorithms. In Karabulut's design, one-way bearings are embedded inside the brake system and dynamic sealing elements used to prevent their contact with the magneto-rheological fluid. However, due to the use of dynamic sealing elements the off-state torque increases and besides, a one-way bearing embedded inside the system will cause problems related with the concentricity during the assembly of the parts with small dimensions and narrow tolerances. Additionally, if the braking direction is needed to be switched, the brake system has to be disassembled completely. In this work, one-way bearings aimed to be used to solve stiction problem is placed on the outside of the brake system in an easily accessible position so that, in cases that require maintenance or repair, these operations can be carried out without the need of disassembling the whole system. Another advantage of this design is the flexibility it provided so that in cases the brake system is aimed to be used for different applications, disassembly or reversing the direction of the one-way bearing can be achieved easily.

The second problem is known as the off-state torque and related with an undesired torque occurred in MR brakes (Blake and Gurocak 2009), which is the minimum torque value that an MR brake displays while no current is supplied to the system. High off-state torque reduces the dynamic torque range that the system can provide and negatively affects the mass-torque ratio which is an important metric used to represent the performance of MR brake systems. Additionally, in haptic glove applications, the off-state torque should be reduced as much as possible so that the user wearing the glove can move their fingers freely during their interactions. The root cause of the high off-state torque problem occurred in MR brakes is detected to be the friction occurred between the rotary parts and the dynamic sealing elements used to seal MR fluid inside the brake system. In this work, to reduce the off-state torque, a new sealing design with a few simple parts was proposed so that the MR fluid within the system is used as a sealing element and the dynamic sealing elements can be extracted from the system.

The third and the last problem is their manufacturability in small sizes with narrow tolerance limits. When the results of the literature review are examined, it has been observed that MR brake systems can be designed by using different architectures where each architecture has its own advantages and disadvantages. It has been observed that the manufacturability of the architectures that can provide high torque output became lower and for architectures that can be manufacturable in smaller sizes the torque output is reduced. In this work, in order to provide small scale manufacturability and high torque

output, a new design is proposed. In the proposed design, parts with non-magnetic features were introduced and utilized in both rotary and stationary parts to control the magnetic flux path created within the brake system. By implementing non-magnetic parts in the magnetic flux path, the magnetic flux vectors were forced to pass over MR fluid several times and increasing the torque output of the developed brake system.

Another issue encountered in the literature review on the haptic gloves covers the systems used to transmit the force obtained from the actuators to the fingertips. In most of the force feedback gloves, the torque provided by the actuators is insufficient to stop the motion of the fingers and therefore being raised with the help of gears. The force/torque on these gears is then transferred to the fingertips by using the exoskeleton structures and linkages. The use of gears reduces backdrivability of the system since the unwanted frictional loads exist in the actuator were also multiplied. Likewise, the use of linkages also introduces additional frictional forces at the joints, increase the overall volume and mass that should be carried over hand and fingers which reduces the comfort level of the user wearing the glove.

The main objectives that are aimed to be achieved in this thesis are classified for MR brake can be counted as:

1. Determination of the design criteria based on the manufacturability in small sizes and narrow tolerance limits.

2. Based on the design criteria, design and development of a new MR brake that is able to generate sufficient torque output to stop the motion of fingers without using gears.

3. Development and implementation of the solutions to reduce off-state torque caused by the friction between rotary parts and sealing elements; and overcome sticky wall problem.

4. Improvement of the brake design using magnetostatic finite element analysis.

5. Manufacturing the parts and assembly of the MR brake prototype.

6. Performing validation and characterization tests of the MR brake prototype to reveal the design criteria are met or not.

1.2. Main Contributions

The main contributions of this thesis are as follows:

1. Design of a new MR brake architecture that is manufacturable in small sizes and able to provide high torque output.

As mentioned earlier, among the MR brake types, multi-disc type MR brakes give the highest torque output, but production requirements in small sizes and narrow tolerance ranges are not possible due to the increasing cost of manufacturing. For this reason, a new design has been developed based on the drum-type MR brakes which have fewer and less complex shaped parts when compared with other architecture types. The main problem in the drum type MR brakes is the torque obtained during braking is low due to the magnetic flux vectors pass through the fluid only twice. In proposed solution, T-shaped non-magnetic materials were introduced to the magnetic flux path so that, magnetic flux vectors are forced to pass over the MR fluid multiple times thus increasing the torque output significantly.

2. Implementation of a solution for stiction problem occurred in MR brakes.

In order to deal with the stiction problem, a solution including the use of the one-way bearings is proposed. One-way bearings aimed to be used in this solution are not intended to be placed inside the brake system, but to be located at the point where the brake system will be connected to the force transmission system. In this way, when it is desired to change the braking direction of the MR brake system, this process can be achieved by simply changing the direction of the bearing on the junction point, without the need to disassemble the entire system.

3. Implementation of a solution to reduce off-state torque exist in MR brakes.

To reduce the off-state torque caused by friction between rotary parts and the dynamic sealing elements, an alternative sealing design is proposed, in which the MR fluid itself is used as a sealing element. In this solution, areas where MR fluid can flow out of the brake system have been identified. For these regions, new magnetic flux routes were created by using magnets and materials with high magnetic permeability so that the MR fluid situated in this flux route act as a fluid O-ring by aligning in the direction of

magnetic flux lines between two surfaces and provide sealing ability without using any mechanical parts.

1.3. Thesis Outline

This thesis consists of 6 Chapters; Introduction, Literature Review, Actuation System Architecture, MR Brake Design, Experimental Tests and Validation, and Conclusion.

Chapter 2 begins with information on how haptic glove models used in virtual reality are classified. After giving this information, the actuator systems used on the gloves are categorized based on their purpose of uses. After the introducing these components, results of a detailed research was given as a list in which, the features of the haptic gloves are found and given. For this list, gloves developed in the laboratory environment and the ones that are commercially available are taken into consideration.

In Chapter 3, actuation system architecture of the developing glove is given. The actuation system architecture composed of magnetorheological brakes and force transmission systems. General information about magnetorheological fluid-based brakes were provided and the conceptual design of a force transmission system that is aimed to be used to transmit the resistive torque obtained from the MR brakes to the fingertips of the user were presented.

In Chapter 4, the design of the magnetorheological fluid based brakes that are aimed to be used in the developped haptic glove are presented in details. Topics including the design criteria, mathematical models, material selection, internal design and the new sealing design to reduce off-state torque are discussed in this section. Additionally, the results of magnetic analyses before the manufacturing of the prototype were also provided.

In Chapter 5, the experimental validation tests performed over the manufactured MR brake prototype are given. Starting from the information about the data acquisition and control systems used for the tests, information about the test procedures and the results to reveal the specifications of the design were presented.

Lastly, the conclusion of this thesis was presented in Chapter 6.

CHAPTER 2

LITERATURE REVIEW

In this section, the results of the research on the virtual reality gloves with haptic feedback will be given. In the first section, information about the classification of gloves is given. Following this, the types and functions of the actuator systems used on gloves are examined. Then, the results of a detailed research on gloves with haptic feedback developed in the laboratory environment and used commercially is shared. In this research, detailed specifications of the gloves were revealed, tabulated and the results were provided.

2.1. Classification of Haptic Gloves

In order to simplify the analysis of different haptic gloves, gloves were examined under three main categories in the literature. These categories are traditional gloves, thimbles and exoskeletons (Perret and vander Poorten 2018) respectively. Even though all these three classes have similar objectives to be achieved; technical approaches and constraints they possess to achieve them varies greatly. In the section below, these three categories will be further analyzed and described.

2.1.1. Traditional Gloves

By “traditional gloves” category, a wearable glove made of a flexible fabric is meant. Traditional gloves allow separate movement of fingers and fit the shape of different hands. Sensors that measure the kinematic configuration of fingers and actuators that provide feedback to users’ skin or musculoskeletal system are sewn into the fabric or fixed outside these gloves.

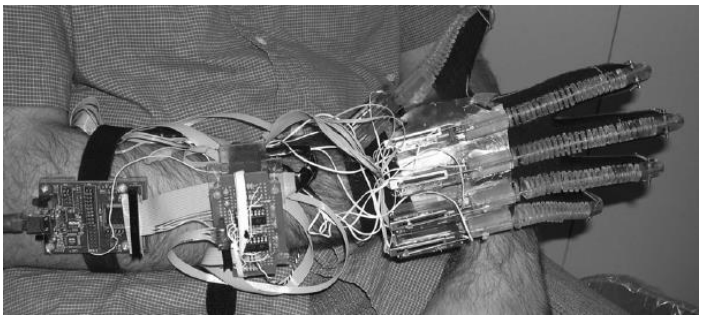

Figure 1: A traditional type haptic glove.

(Source: Winter & Bouzit, 2007)

Two difficulties are encountered during the design and production of a traditional glove. First, sensors and actuators have to be as small as possible in order to be placed and fit inside the fabric so that they can be placed near fingers without restraining the motion of the hand. Secondly, all the equipment including sensors and actuators used in traditional gloves have to be flexible and able to resist continuous and repetitive deformations, flexions, extensions and stretching without getting damaged and losing any functionality. Traditional gloves can be used as data gloves to provide information about the orientation of the hand and fingers together with the actuators for tactile and force feedback.

2.1.2. Thimbles

By "thimbles" category, a fingertip attachment worn by the user such that an actuator is placed at the tip of the finger is meant. In order to obtain haptic feedback at multiple fingers via using thimbles, several modules can be worn concurrently.

By doing it so, multiple tactile sense of touch can be achieved. Unlike exoskeletons and traditional gloves, thimbles are unable to provide force feedback to the user and only provide vibro-tactile feedback. Three difficulties were encountered during the design and manufacturing of thimbles. First, integration of actuators, sensors, power supplies and wireless modules to a single compact device is challenging. Secondly, the thimble device should be light-weighted in order not to restrain the motion of the hand and fatigue of fingers due to carrying a discomforting load at the fingertip. And lastly,

thimbles must be designed to be adjustable for different finger sizes and radii so that, when it is worn by different users, it should not squeeze or slip from fingers of users.

Figure 2: A thimble type device.

(Source: VRTouch, 2017)

2.1.3. Exoskeletons

By “exoskeleton” category, an articulated mechanism structure that is used to transmit forces to users’ hands and fingers is meant.

Exoskeleton gloves are hard to adjust for different hand shapes, sizes and finger lengths. In order to overcome this problem, most exoskeleton gloves were developed with different mechanism structures that help the exoskeletons run in parallel with fingers so that the necessity of precise adjustments were reduced. When compared with traditional gloves and thimbles, exoskeleton gloves are heavier and bulkier but they are able to provide greater force feedback to user’s hands and fingers. Force is transmitted to the fingers and hands of the user through the intermediate linkages used between hand and exoskeleton depending on the type of the actuator. Positions of actuation units and actuators greatly varies within the exoskeleton gloves; however, back of the palm (metacarpal regions), inside the palm and the top of finger joints are common places that actuators placed in exoskeleton type haptic gloves.

Figure 3: An exoskeleton type haptic glove.

(Source: CyberGlove, n.d.)

2.2. Actuators Used in Haptic Gloves

Actuators in haptic systems are the most important components since they are responsible to stimulate the sense of touch in various forms. The type and the design of the actuators greatly affects the quality of kinesthetic and tactile sensations perceived by the user. In haptic glove systems, the motion of the hands and the fingers of the user using the system are measured by the sensors and transmitted to the virtual reality environment to be processed. Based on the processed information, haptic feedback is then provided to the fingers and fingertips of the user by using the actuators available in the system during interactions in the virtual environment. Depending on the characteristics of the actuators used in the system, the haptic feedback felt by the user can be perceived from their skin as tactile feedback or from their musculoskeletal system as kinesthetic feedback. In this section, actuators used in the haptic gloves to stimulate tactile and kinesthetic sense of touch will be given.

2.2.1. Actuators for Tactile Feedback

Tactile feedback is a type of feedback that is perceived by mechanoreceptors in the skin, in which the stimulation of detailed surface features, texture, temperature and

overall shape is created with different patterns applied by the actuators. Since mechanoreceptors spread over the hand intensify in fingertips, actuators used in the haptic feedback gloves are placed mostly under fingertips. The requirement of creation of patterns in small volume under fingertips combined with the high frequency of operation requirements are main challenges to be dealt with for the tactile feedback actuators. In this section, the actuators that are and can be used in glove applications are mentioned for the tactile feedback to be sent to the user's skin.

2.2.1.1. Electromagnetic Actuators

Electromagnetic actuators (EMA) in haptic gloves are mainly used as tactile feedback elements and their use in kinaesthetic devices are limited. Electromagnetic actuators work based on the conversion of electrical energy to mechanical energy. EMAs consist of a coil and a shaft (plunger) that moves together with a permanent magnet or a ferromagnetic material. Coil is wound around the shaft so that depending on the polarity and magnitude of the supplied electrical current, a magnetic field is generated around the shaft since the coil itself becomes an electromagnet that has its own magnetic poles. The directions of the magnetic poles created by the electromagnet and the permanent magnet have, the shaft moves accordingly and creates forces (Kern 2009; Kim and Chang 2007).

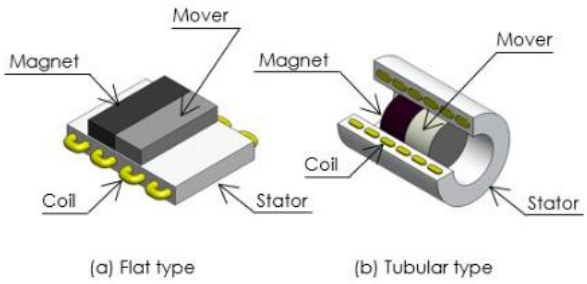

Figure 4: Electromagnetic actuator types

(Source: Ghazaly et al., 2016).

Electromagnetic actuators' control is relatively simple since the only control variable is the electric current fed to the actuator. The gloves Gloveone, SenseGlove, AvatarVR, Cynteract, Maestro Gloves, VRtouch and Tactai Touch use electromagnetic actuators to provide tactile feedback to users.

2.2.1.2. Eccentric Rotary Mass Actuators

Eccentric rotary mass actuators (ERM) use an unevenly sized and unbalanced mass to create vibrations via rotating the mass where the amplitude of the vibrational output can be controlled by changing the frequency of the control signal applied to the motor. When the ERM is supplied with power, the unbalanced mass starts to rotate and creates a centripetal force. By attaching ERMs to fingertips, to force acts on the attachment point and causes a displacement. Based on the angular velocity of the ERM, the frequency of the displacement per second increases and felt as vibrations by the user.

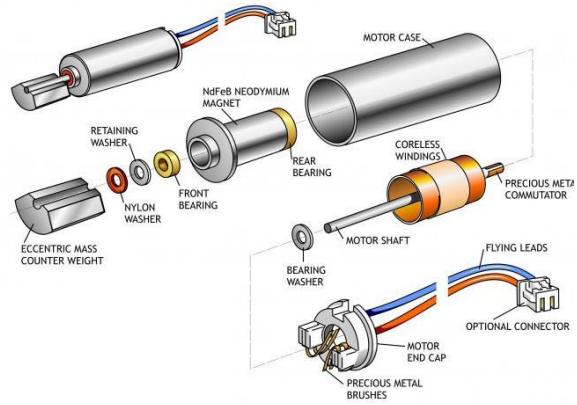

Figure 5: ERM actuator inner structure.

(Source: Precision Microdrives, n.d.)

2.2.1.3. Linear Resonant Actuators

Linear resonant actuators (LRA) create vibrations by moving a mass in vertical direction via using a magnetic coil. They can operate in a narrow range of high frequencies but provide more flexible output amplitude with low power voltage requirements (Kim and Chang 2007; Ghazaly et al. 2016). Since the actuation is done in a linear motion vertically, better tactile sensation can be obtained as compared with ERMs. SensoGlove, Plexus, GloveOne and AvatarVR use multiple LRAs attached to fingertips to provide tactile feedback.

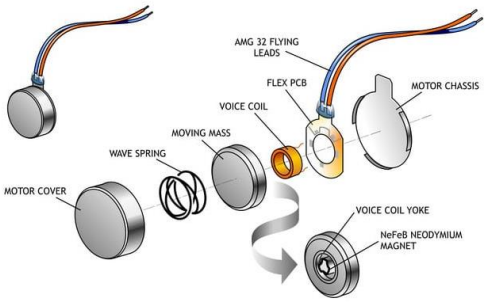

Figure 6: LRA actuator inner structure.

(Source: Precision Microdrives, n.d.)

2.2.1.4. Piezoelectric Actuators

Piezoelectric materials are ceramic–based special materials which can generate force and motion when they to exposed an electrical charge. Actuators using piezoelectric materials are called piezoelectric actuators which consist of cantilever beams with piezoelectric materials attached on them. When a voltage is applied on piezoelectric materials, they generate force and provide motion by bending the cantilever beam. Piezoelectric actuators' deflection is directly proportional to the applied voltage where it could be set to a specific position or set in vibrating mode. Response time of these actuators are about 1 ms which is 50-100 times faster than ERMs. Additionally, it is possible to control the amplitude of the output signal and frequency of deflection independently where complicated signals can be obtained(Schweber 2021). A major disadvantage of piezoelectric actuators is the high voltage requirement (~200 Volts) for the driving signal where additional piezo driver integrated circuits have to be implemented to the system (Kern 2009).

2.2.2. Actuators for Force (Kinesthetic) Feedback

Kinesthetic feedback is a type of feedback that involves limiting or stopping the motion of the joints and limbs by applying a counterforce/torque produced by actuators, while being perceived by the fibers and tendons in the musculature. Kinesthetic feedback stimulates information such as its rough shape, weight, flexibility and stiffness of the

interacted object. Unlike tactile feedback actuators that are small in size and aim to produce force signals with low amplitudes and high frequencies, actuators used for kinesthetic feedback are bulkier and required to produce higher amount of forces/torques with lower operating frequencies. In this section, the actuators used in haptic glove applications with force feedback features will be mentioned.

2.2.2.1. DC Motors

A Direct Current (DC) motor is a type of actuator where electrical energy when a current supplied is converted to mechanical energy to create rotation. DC motors have two main components to perform such an objective, which are a stator and an armature. The stator includes the stationary parts of the motor and provides a magnetic field to rotate the armature. An electromagnetic field is generated by using the stationary magnets and coil inside the stator via applying current to the coil sequentially. Since the coils are activated-deactivated with a current sequentially, a rotating magnetic field is created to generate torque that rotates the armature (Kern 2009). CyberGrasp, EXOS Wrist DK2, HGlove, Exo-Glove, RML Glove LRP Glove and Sensor Glove use DC motors in their haptic gloves to provide kinesthetic feedback.

2.2.2.2. Servo Motors

Servo motors are used in exoskeleton type haptic gloves in order to provide force-feedback to fingers of users. However, in tactile feedback applications, their use are limited. Servo motors are used as rotary/linear actuators in haptic gloves due to their ability of precise control of linear/angular position, velocity and acceleration. They include a sensor coupled with a control device to provide position control inside their compact body precisely. The control of servo motors are done by sending electrical signals in variable widths. This technique is called pulse width modulation (PWM). By controlling the duty cycle of the generated PWM signal, the motor can be turned to the desired position where linear and angular position control of the mechanism can be

performed (Krishnan 1987). Cynteract, Maestro Gloves and Dexmo haptic gloves use servo motors to provide force feedback to the user.

2.2.2.3. Pneumatic Actuators

Pneumatic actuators are used to convert pressure and volume flow into displacement and force. These actuators rely on gas pressure build up from the air pumped to the chamber. When enough pressure is build up inside the chamber to overcome the outside atmospheric pressure, force will be exerted to a piston in the chamber and thus the movement of the piston is obtained (Mourad Bouzit, Popescu, et al. 2002). The use of pneumatic actuators observed in haptic glove applications was seen only in exoskeleton type architectures. HaptX and Rutgers Master II haptic gloves use pneumatic actuators to provide force feedback to users. Additionally, in HaptX gloves, thanks to the small air tubes at fingertips tactile feedback is also provided via the small pneumatic actuators.

2.2.2.4. Electromagnetic Brakes

Electromagnetic brakes are used as passive actuators in haptic gloves which restrict the movement of fingers or complete hand of the user via generating resistive forces in the opposite direction of the exerted force by the user. They are mainly used in exoskeleton type haptic gloves to provide force feedback. Depending on the number of the brakes and their powers, different mechanisms can be used to restrict the motion of fingers and hands. Electromagnetic brakes use electrical energy to create a magnetic field which will be then used to transmit torque mechanically. When a current is applied to the electromagnetic brake, the coil inside will be energized and generate a magnetic field that turns the coil into an electromagnet. The magnetic flux generated by the coil attracts the armature mounted on the rotating shaft and merges the armature to the brake surface which will stop the rotation of the shaft due to the applied friction forces in a short amount of time. Conversely, when the current fed to the electromagnetic brake is cut, the attraction of armature will be over and springs will push the armature back to its original position away from the brake surface (Jenkins 1963; Lindberg 1993). Sense Glove DK1,

Passive Force Display (Koyanagi, Fujii, and Furusho 2005) and Multi-Fingered Force Feedback Glove (Koyama et al. 2002) use electromagnetic brakes in their haptic gloves to provide force feedback to users.

2.2.2.5. Magnetorheological Fluid Based Brakes

Magnetorheological fluids (MRFs or MR-fluids) are mixtures of micrometer sized ferromagnetic particles within a non-conductive carrier fluid. MRF's primary advantage is their adjustable rheological properties which can be continuously changed depending on the existence and intensity of the magnetic field. When MRF is exposed in a magnetic field, rheological properties, especially yield stress, of the fluid will chance and solidify. The viscosity of the MRF fluid is directly proportional to the intensity of the applied magnetic field until the point of saturation so that, with increasing magnetic field intensity, the fluid becomes quasi-solid and further increase of magnetic field intensity after saturation point will not affect the MRF (LORD Corp. 2016).Thanks to these features, MR fluids were used to build high-power and low-inertia resistive actuators for haptic glove applications to provide force feedback which are more efficient compared to conventional actuation methods (Johnston, Kruckemeyer, and Longhouse 1998). MR Glove (Blake and Gurocak 2009), Smart Glove (Nam, Park, and Yamane 2008) and MRAGES (Winter and Bouzit 2007) are haptic gloves that MRF based brakes were used as passive actuators to provide force feedback.

2.4. Commercial and Lab-Based Haptic Gloves

In this section, 25 different haptic gloves including the commercially available ones and the ones were developed in the laboratory environment will be discussed. The discussion also include information about the types of gloves, number of fingers that gloves can be worn, weights of gloves, actuation principles they possess, availability of tactile-force feedback and magnitudes of force/torque feedbacks, ability to track or sense the positions of hands and fingers and degrees of freedoms for motion tracking and force feedbacks, their wireless availabilities, communication protocols between gloves and the

host computer and lastly update rates. In the Table 1, features of haptic gloves found on the internet and scientific papers can be seen, and further details will be given in the following sub-sections.

As can be seen in the Table 1, some of the information is not provided by the developers or not applicable in the literature. In order to find information about these missing features, developers/researchers were contacted. Whenever any information is provided, the table will be updated in the light of their responses.

Table 1: Comparison of different haptic gloves.

Device	Commercial/Lab	Developer Company/Team	Type	Mass(g)	# of fingers	Actuator Type	Tactile feedback	Force-feedback	Force Feedback DoF	Force/Torque Feedback	Hand Tracking / Position Sensing	Motion Tracking DOFs	Wireless	Communication with Host PC	Update Rate (Hz)
CyberGrasp	C	CyberGlove Systems	Exo	450	5	DC Motor	N	Y	5(1 per finger)	12 N	N	18 (with CyberGlove)	N	RS232	150
Rutgers Master II	L	Bouzit et al.	Exo	185	4	Pneumatic	N	Y	4	16 N	Y	12 (3 per finger)	N	RS232	440
Gloveone	C	Neurodigital Technology	TG	NA	5	EMA	Y	N	-	-	Y	10 (with Leap Motion)	Y	USB Bluetooth	NA
AvatarVR	C	Neurodigital Technology	TG	NA	5	EMA	Y	N	-	-	Y	10(with Leap Motion)	Y	USB Bluetooth	NA
Senso Glove	C	Senso	TG	NA	5	LRA	Y	N	-	-	Y	5	Y	NA	400
Cynteract	C	Cynteract	TG	NA	5	Servo Motors	N	Y	5(1 per finger)	NA	Y	3(wrist) + 5(fingers)	Y	USB Bluetooth	NA
Maestro	C	ContactCi	TG	590	5	EMA Servo Motors	Y	Y	5(1 per finger)	NA	Y	5	Y	Wi-Fi Bluetooth	NA
VRTouch	C	GoTouchVR	Thm	20	1	1 LRA	Y	N	-	-	N	-	Y	USB Bluetooth	NA
Dexmo	C	Dexta Robotics	Exo	300	5	Servo Motors	N	Y	5(1 per finger)	5.5 N	Y	11 (3 for thumb, 2 for rest)	Y	USB Wi-Fi	NA
HaptX	C	HaptX	TG	450	5	Pneumatic	Y	Y	5(1 per finger)	18 N	Y	30	N	Bluetooth	240 Hz
Sense Glove DK1	C	SENSEGLOVE	Exo	320	5	EM Brakes	N	Y	5(1 per finger)	16 N	Y	20 (hand)+3 (wrist)	Y	USB Bluetooth	120 (USB) 60 (BT)

(cont. on next page)

Table 1 (cont.)															
HGlove	C	Haption	Exo	750	3	DC Motor	N	Y	6 (2 per finger)	5 N	N	6 (with Virtuose 6D)	N	Ethernet	1000
Plexus	C	Plexus Immersive Corp.	TG	NA	5	LRA motors	Y	N	-	-	Y	21	Y	Bluetooth	180
EXOS Wrist DK 2	C	exiii	Exo	350	Wrist	DC Motors	N	Y	2	200 N.mm	Y	2	Y	USB Wi-Fi	NA
Exo-Glove	L	In et al.	Exo	194	3	DC Motor	N	Y	6 (2 per finger)	12 N	N	NA	NA	NA	NA
RML Glove	L	Ma et al.	Exo	180	2	DC Motor	N	Y	4(2 per finger)	7 N Cont.	Y	6 (3 per finger)	Y	ZigBee	50
LRP Glove	L	Coiffet et al.	Exo	NA	5	DC Motor	N	Y	14 active 5 passive	120 N.mm	N	6 (with Polhemus Isotrack)	N	RS232	NA
Sensor Glove II	L	Kunii et al.	Exo	NA	5	DC Motor	NA	Y	20	NA	NA	NA	N	NA	NA
MFFG	L	Koyama et al.	Exo	NA	3	EM Brakes	N	Y	3(1 per finger)	250 N.mm / 3 N	Y	12(4 per finger)	NA	NA	NA
PFDG	L	Koyanagi et al.	Exo	700	3	EM Brakes	N	Y	3(1 per finger)	29 N	Y	6(2 per finger)	N	NA	NA
MR Glove	L	Blake et al.	Exo	900	3	MR Brakes	N	Y	6(2 per finger)	399 & 821 N.mm	N	22 (with CyberGlove)	N	NA	NA
Smart Glove	L	Nam et al.	TG.	348	5	MR Brakes	N	Y	5(1 per finger)	26 N	Y	5 (1 per finger)	NA	NA	NA
MRAGES	L	Winter et al.	TG.	160	5	MR Brakes	N	Y	5(1 per finger)	6 N	Y	5(1 per finger)	Y	USB ZigBee Bluetooth	NA
LFFG	L	Zheng et al.	Exo	245	5	Pneumatic	N	Y	5 (1 per finger)	4 N	N	WiseGlove	N	USB	70
Exo-Glove PM	L	Yun et al.	Exo	350	3	Pneumatic	N	Y	3 (1 per finger)	~22 N	N	NA	NA	NA	NA
Wolverine	L	Choi et al.	Exo	55	4	DC Motor	N	Y	3	100 N	Y	6	Y	Bluetooth	100

2.4.1. Cybergrasp

CyberGlove Systems Company, developed a commercial haptic glove CyberGrasp. This glove is an exoskeleton type glove that can be worn 5 fingers where the total mass of the glove is 450 grams. Five DC motors in the actuation unit, one for each finger, were used to provide resistive force feedback via pulling exotendons routed around the exoskeleton to the actuation unit.

Each glove joint is connected to the actuation unit by cable-driven mechanisms where forces exerted by actuators are transferred to the fingertips through cables. The actuation unit can be fixed to the ground or worn as a backpack; however, due to the cable length limit, effective working area for the gloves and actuation units is a sphere with a radii of 1m. The glove is able to provide 12 N continuous force on fingertips in the flexion direction that 5 degrees of freedom force feedback (1 for each finger) can be obtained.

Figure 7: CyberGrasp Exoskeleton Glove

(Source: CyberGlove, n.d.)

The CyberGrasp is not designed to track motion; however, it is compatible with CyberGlove, which can track the motion of hand and fingers in 18 degrees of freedom via using 15 flex sensors (3 for per finger), and an IMU to determine the orientation of the fingers. The communication with the host computer is established by using RS 232 protocol, where the force and position data is transferred at a rate of 115 kbps (CyberGlove 2007).

The main disadvantages of the Cybergrasp can be counted as, heavy weight of the force control module (20 kilograms), limited workspace (1 m radius) and high-power consumption of the force control module (120 Watts).

2.4.2. Rutgers Master II

Bouzit et al. (2002) developed an exoskeleton type haptic glove, Rutgers Master II (RM II), for virtual interactions and rehabilitation. RM II can be worn to four fingers except for the little finger and weighs 185 grams in total (pneumatic pump and power supply units' masses are excluded and not available).

Figure 8: The Rutgers Master II

(Source: Bouzit et al.,2002)

RM II is operated by four pneumatic actuators located in the palm of the hand which are connected to finger segments via using structural linkages and able to provide 12 N of continuous force to the fingers with 4 degrees of freedom (1 for each finger). Additionally, the static actuator friction is indicated to be 0.014 N.

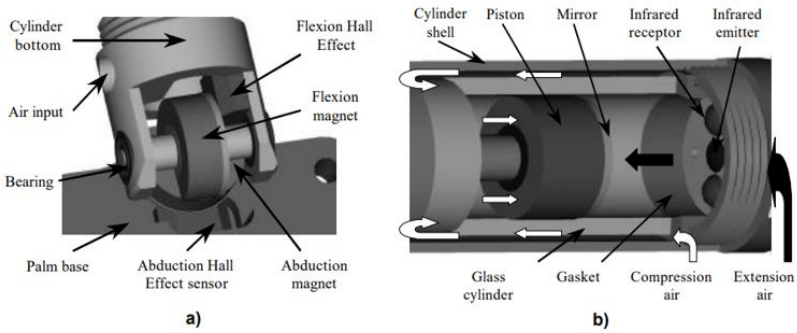

Figure 9: Placement of Hall-effect Sensors (a) and Infrared Sensors (b)

(Source: Bouzit et al.,2002)

Each structure link has 3 sensing joints and 5 degrees of freedom so that the exoskeleton mechanism is able to move in 20 degrees where the motion can be tracked in 12 degrees of freedom. These sensing joints were introduced to the system in order to eliminate the need of a separate sensing glove to determine the kinematic configuration of hand and fingers. Hall-effect sensors and infrared sensors are integrated within actuation cylinders where hall-effect sensors are used to measure the flexion and adduction/abduction angles (Figure 9-a) and infrared sensors are used to measures the translation of the piston inside an air cylinder (Figure 9-b).

RM II communicates with the host computer by using RS 232 protocol at a rate of 115 kbps and 435 position and force data is sent per second. Effective working area for complete system is indicated as a sphere with a radii of 2m.

The main drawback of RM II is, the placement of actuators inside the palm restricts the working area of the hand and prevents complete fist closure (M. Bouzit and Burdea 2006; Mourad Bouzit, Popescu, et al. 2002; Mourad Bouzit, Burdea, et al. 2002). Additionally, even though the weight and power requirements of pressure tanks were not specified in their work, the device is still connected to the ground due to the heavy weight of the pressure tanks and the workspace is limited to 1 m radius.

2.4.3. Gloveone and AvatarVR

Neurodigital Technologies Company developed two different traditional glove type haptic gloves, “Gloveone” and “AvatarVR”. Many information about the gloves are not applicable; however, both of the gloves are worn into 5 fingers and use 10 different vibrotactile actuators (LRAs) in order to provide tactile feedback.

Five of the actuators are placed under each fingertips, two of the actuators are placed behind the hand and the last three actuators are placed under the palm. Hand tracking is done via using auxiliary sensors like Leap Motion or Intel RealSense.

For fingers, Gloveone uses flexible sensors to measure the position of the fingers, where AvatarVR uses 9-axis IMU for each finger. Communication between the computer and the glove can be established via using USB for applications requiring low latency or

using Bluetooth for where movement freedom is desired (AvatarVR, n.d.; Perret & Poorten, 2018).

Figure 10: AvatarVR & Gloveone

(Source: AvatarVR, n.d.)

2.4.4. Senso Glove

Senso Company developed commercially available traditional glove type haptic glove named "Senso Glove" which can be worn to 5 fingers. Senso Glove can only provide tactile feedback thanks to 6 linear resonant actuator motors placed under the distal phalanges of each finger and also one at the wrist. 8 IMU sensors were used to track the motion of the hand and fingers. Senso Glove communicates with host computer wirelessly via using ZigBee and Bluetooth communication protocols to transfer data (“Senso” 2015).

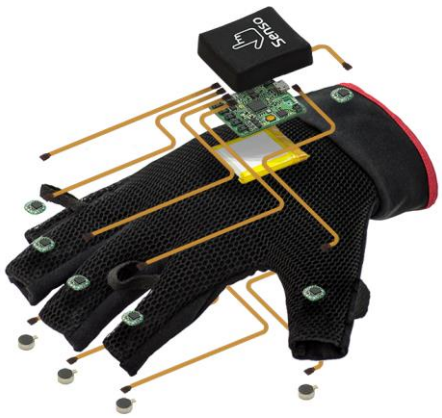

Figure 11: Senso Glove

(Source: Senso, 2015)

2.4.5. Cynteract

The Cynteract Company has developed a commercially available traditional type haptic glove “Cynteract” for rehabilitation purposes. The glove can be worn to five fingers where each finger is actuated by wires connected to servo motors inside the control unit which is worn over the forearm region. The glove can provide 1 degrees of freedom of force feedback for each finger (5 DoF in total); however, the magnitude of the force output is not specified.

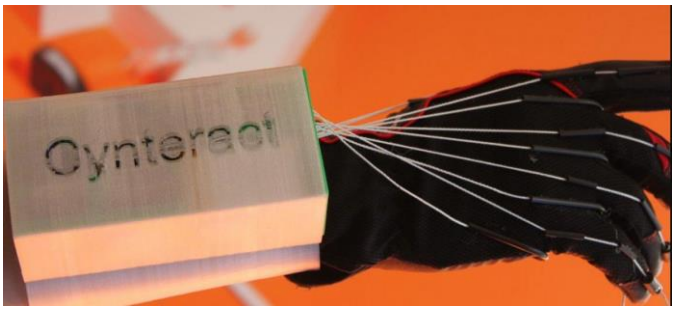

Figure 12: Cynteract Glove

(Source: Cynteract,2013)

The glove is able to track 8 DoF of motion where the orientation of the hand is determined by a 9-axis IMU (3 DoF) and the orientation of the fingers were measured by flex sensors attached on each finger (5DoF) (“Cynteract” 2013).

2.4.6. Maestro

ContactCi has developed a commercial traditional type haptic glove that can be worn into 5 fingers and weighs 590 grams. Maestro use exotendons restriction mechanism where 5 exotendons are connected to 5 servo motors inside a module mounted on the forearm. The amount of force and torque feedbacks are not provided; however, the device is able to provide force feedback in 1 degree of freedom for per finger (5 DoF in total) in

the flexion direction. Additionally, Maestro is equipped with 5 ERM actuators placed at fingertip pads to provide tactile feedback to the user.

Figure 13: Maestro Glove

(Source: Contact CI, n.d.)

Maestro can track the motion of hand via using a Vive Tracker (6 DoF) and the rotation of fingers were measured by flex sensors (5 DoF). The communication between host computer and Maestro can be established via using Wi-Fi and Bluetooth communications (“Contact CI” n.d.; Perret and vander Poorten 2018).

2.4.7. VRtouch

GoTouchVR Company has developed a commercial thimble type haptic device. VRtouch is attached to a single finger via using magnetic clips. Each device contains a single electromagnetic actuator placed at fingertip to provide tactile feedback by pressurizing the fingertip. Maximum suggested number of devices is 3 per hand to increase multi-finger touch feeling.

The main drawback of VRTouch is, due to sizes of the modules, the movement of the fingers are hindered and collisions between modules frequently occurs.

The communication between the device and the host computer is established by using Bluetooth protocol. The USB connection can also be established; however, it greatly restricts the free movement of the fingers (“VRtouch DK Data Sheet” 2017).

Figure 14: VRtouch Thimble Modules

(Source: VR Touch, 2017)

2.4.8. Dexmo

Dexta Robotics has developed the exoskeleton type haptic glove Dexmo which can be worn in 5 fingers and weighs 300 grams. In the first design of the glove, mechanical brakes were used as passive actuators; however, in their final design, brakes were replaced with servo motors. 5 servo motors are used to provide torques to the fingertips where 500 N.mm of continuous torque (5.5 N of continuous force) feedback can be provided each finger with one degree of freedom per finger (5 DoF in total) by consuming 10 Watts of electrical power for each actuator.

Dexmo is able to capture motions of hands and fingers with 11 degrees of freedoms where 3 of the DoFs are captured from the rotation, splitting and bending of the thumb and 8 of the DoFs are captured from the splitting and bending of the fingers (2 DoF per finger). The communication between the glove and computer can be established by both USB and Wi-Fi protocols via using dongles (DextaRoboticsInc 2019).

Figure 15: Dexmo Exoskeleton Glove

(Source: Dexmo, 2019)

2.4.9. HaptX

The company HaptX Inc. has developed an traditional type glove “HaptX” which is worn into 5 fingers and weighs 450 grams. 5 pneumatic actuators connected to the fingers are able to provide 18 N of resistive force feedback to the fingers in extension and flexion directions. As a result, HaptX glove is able to provide force feedback in 5 degrees of freedom (1 for per finger). Additionally, the air used to power the pneumatic actuators is also supplied to the integrated air channels placed at fingertips through smart silicon-based textile (130 air channels per finger) to provide tactile feedback.

Figure 16: HaptX Exoskeleton Glove

(Source:HaptX,2013)

Motions of hands and fingers can be captured by a motion tracking system which can detect magnetic fields generated by the magnetic sensors placed on the glove. In this way, motions can be tracked in 30 degrees of freedom in HaptX glove precisely. The information about the communication protocols used between HaptX gloves and the host computer is not available; however, update frequency for motion tracking is indicated to be 240 Hz (HaptX Inc 2013).

The main disadvantage of the HaptX is the air controller (18 kg), smart compressor (16 kg) and motion tracking system (4 kg) have to be placed on the ground due to their large volumes and heavy weights which significantly limits the effective workspace.

Figure 17: Complete System for HaptX Glove

2.4.10. SenseGlove

Sense Glove Company developed a commercial exoskeleton type force feedback glove which can be worn to 5 finger and weighs 320 grams. Electromagnetic brakes are used as passive actuators which can provide 16 N of continuous resistive force to each finger in the flexion direction. Force feedback degrees of freedom in Sense Glove DK1 is 5 (1 for per finger).

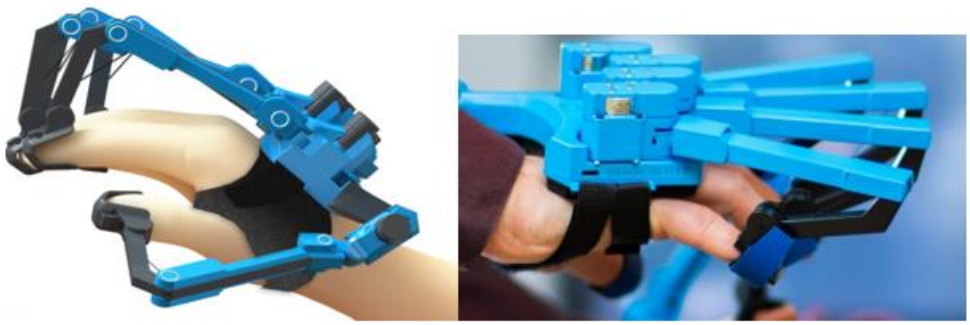

Figure 18: SenseGlove DK1

(Source: SenseGlove, 2017)

The SenseGlove is able to track fingers in 20 degrees of freedom tracking. (4 degrees per finger). Besides that there is also a 9-axis IMU on the wrist provides 3 degrees

of freedom of motion tracking of the wrist. In total, 23 degrees of freedom for motion tracking can be obtained.

Communication between the glove and host computer can be established in both wired and wireless. Wireless communication protocol the haptic glove uses is not specified; however, wired connection can be established via using USB communication (SenseGlove, 2017).

2.4.11. HGlove

Haption has developed HGlove, a commercial exoskeleton type haptic glove that can be worn over 3 fingers and weighs 750 grams. Unlike other exoskeleton type haptic gloves, it allows interactions only with the thumb, index finger and middle finger. The device is worn around the palm and thumb using two straps with hook and loop fasteners. Two DC motors per fingers were used as actuators to exert forces on the fingertips. Forces generated by DC motors are transmitted to fingertips through a two-bar mechanism where the first link of the mechanism is connected to a gear to increase the magnitude of the exerted forces.

Figure 19: HGlove

(Source: Haption, n.d.)

HGlove has 9 degrees of freedom for movement where 6 (no force feedback in 3 abduction movements of per finger) are active DoFs for force feedback. HGlove provides 5 N continuous (or 130 N.mm torque) and 12 N peak force feedback in the direction of

flexion and extension (2 DoFs force feedback per finger; 6 DoF in total). It is suggested to connect HGlove to Virtuoso 6D device to restrain the motion of hand in translational directions in precise tele-robotics operations.

The communication protocol between the host computer and HGlove is established via using Ethernet protocol and the update rate is indicated to be 1000 Hz (Haption n.d.).

2.4.12. Plexus

Plexus developed by Plexus Immersive Corp. is a haptic glove worn in 5 fingers which is able to provide tactile feedback each via using their new designed linear resonant actuators. Flexible silicone materials were used in Plexus in order to protect internal electronics from water.

Plexus is able to measure the motion of fingers with 21 degrees of freedoms with 0.01 degree precision; however, external devices such as Vive Tracker, Oculus Touch, Vive controllers, and Windows VR controllers are required for absolute positional tracking of hand. Plexus communicates with host computer via using Bluetooth communication protocol where 180 Hz refresh rate can be obtained (Plexus 2021).

Figure 20: Plexus with Vive Tracker (a), Oculus Touch (b), Vive Controller (c) and Windows VR Controller (d) (Source: Plexus, 2021)

2.4.13. EXOS Wrist

EXOS Wrist DK 2 developed by excii is a haptic device which is worn into wrist and palm and weights 350 grams. 2 DC motors were used to provide torque feedback up to 200 N.mm in the direction of palmer/dorsal flexion and radial/ulnar abduction.

Figure 21: EXOS Wrist DK 2

(Source: Exiii, 2018)

Optical encoder sensors placed on the axle of DC motors provides 2 degrees of freedom for motion tracking. Communication between the device and host computer is established via using USB for wired and Wi-Fi for wireless connection (exiii 2018).

2.4.14. Exo-Glove

Exo-Glove is a soft wearable exoskeleton type haptic glove developed by In et al. which is worn in 3 fingers (thumb, index, middle) and weighs 194 grams. Exo-Glove use 3 DC motors as actuators which are connected to mechanical pulley systems attached to each fingertip.

The fingertips of the gloves were equipped with 2-axis load cells to measure exerted forces. The glove is able to transmit a 5 N for pinch and 12 N of grasp forces. 2 degrees of freedom of force feedback in extension and flexion directions is provided to each finger (6 DoF in total).

Exo-Glove can measure the angle of the fingers via using resistor bend sensors placed at the back sides of the ginger; however, no information were provided in terms of the tracking the hand or fingers' motions or the degrees of freedom for tracking the motion (Yun, Kang, and Cho 2017; In et al. 2015).

Figure 22: Exo-Glove

(Source: In et al., 2015)

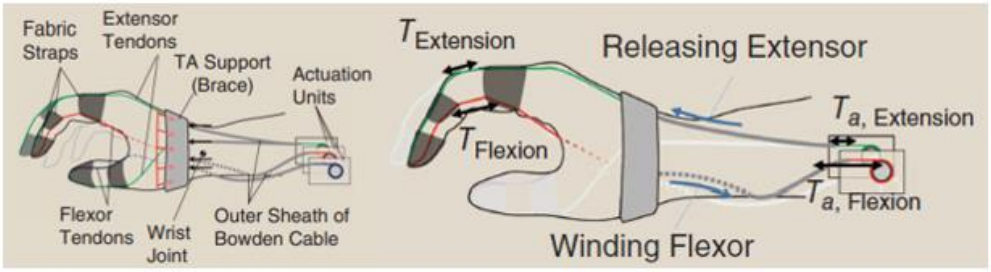

Figure 23: Exo-Glove Layout

(Source: In et al., 2015)

2.4.15. RML Glove

The "RML Glove" developed by Ma et al. is a exoskeleton type haptic glove that is worn in 2 fingers (index and middle) and weighs 180 g. In RML glove, actuation of fingers is done via using 2 DC motors (brushed) geared to pulleys through nonbackdrivable worm gears. In this actuation unit, a two-cable pull–pull transmission is used and therefore, the force is exerted in both directions for extension and flexion,

thereby driving the distal links to follow or resist finger movement (2 DoF force-feedback per finger).

The advantage of this haptic glove design can be appointed to the nonbackdrivable worm gears used actuator unit. The worm gears provide self-locking ability to the glove which can create 35 N of resistive force. Without self-locking of the worm gear, the glove can provide 7 N of continuous output force to the fingertips.

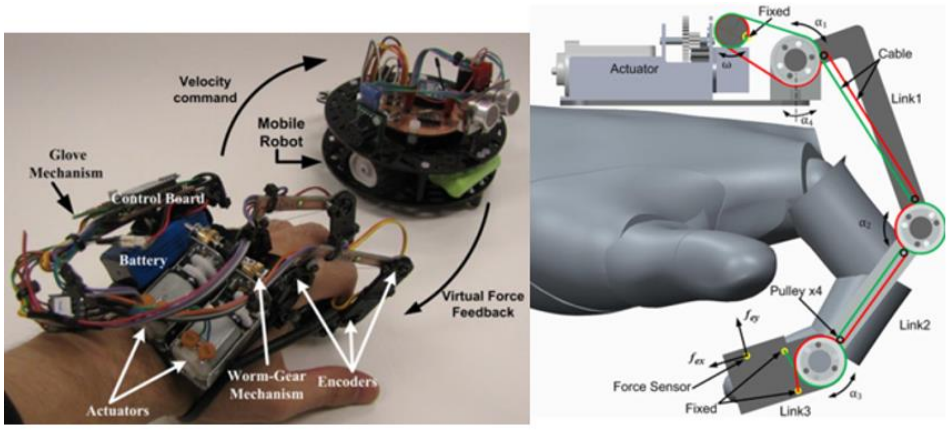

Figure 24: RML Glove

(Source: Ma & Ben-Tzvi, 2015)

3 angular optical encoder sensors were used (for each finger) to determine the joint positions and angles of the finger mechanism on the glove. Additionally, force sensitive resistor (FSR) sensors were placed in fingertip pads to measure normal forces.

Communication between the RML Glove and the mobile robot or the host computer is accomplished through wireless RF XBee modules using ZigBee communication protocol and the communication update rate between the host computer (and mobile robot) and the glove is indicated to be 50 Hz(Ma and Ben-Tzvi 2015a).

2.4.16. LRP Force Feedback Glove

LRP FFG developed by Richard et al. is an exoskeleton type glove that can be worn in 5 fingers. 14 DC motors combined with pulleys and flexible links in order to

actuate glove joints through cable driven mechanisms where 120 N.mm continuous resistive torque per individual finger joint can be generated. The glove have 14 active DoFs in flexion/extension directions and 5 passive DoFs in abduction and adduction directions in terms of force feedback. Feedback forces act normal to the finger segments for most of the motions.

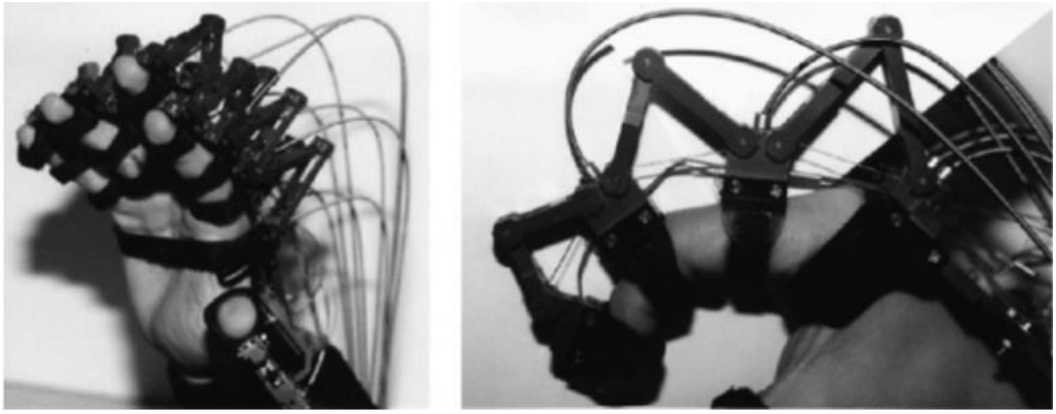

Figure 25: LRP Force Feedback Glove

(Source: Richard & Coiffet, 1999)

In LRP FFG, two types of sensors were used. Optical encoders are used to measure the linear displacement of the cables in order to estimate angles at the finger joints. And strain gauges are used to measure tension forces created on cables in order to estimate generated torques applied at each finger joint.

LRP FFG itself does not provide 3D position / orientation of the user hand. A Polhemus tracking system is therefore used which provides 6 DoF motion tracking of position and orientation of the human hand in space. Communication between the control the LRP FFG and host computer is performed via using RS-232 serial communication protocol, while the host computer communicates with another workstation through using Ethernet protocol (Richard and Coiffet 1999).

2.4.17. Sensor Glove II

Sensor Glove II developed by Kunii et al. is an exoskeleton type haptic glove that can be worn in 5 fingers. Although little information is available about the properties of the Sensor Glove II, it is known that the glove is actuated via using DC motors at each finger joint and is able to provide force feedback in 20 degrees of freedom. Actuation is done via wire transmission. Similar to LRP FFG, joint angles are measured with optical encoders and transmitted torques are measured by using strain gauges attached to the links (Kunii et al. 1997).

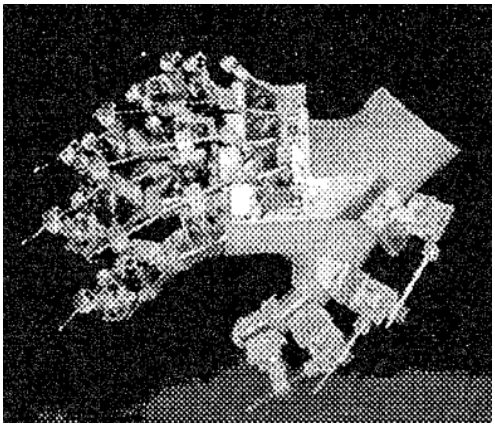

Figure 26: Sensor Glove II

(Source: Kunii et al., 1997)

2.4.18. Multi-Fingered Force Feedback Glove

Koyama et al were developed an exoskeleton type multi-fingered force feedback glove which is worn to 3 fingers (thumb, index and middle). The glove consists of parallelogram linkages, springs and electromagnetic brakes where the motion of the linkage is locked or unlocked by the clutches. The forces applied to the user's fingertips are a result of the deflection in the links and the springs at two of the joints at each finger mechanism. The resistive force generated by electromagnetic brakes are transmitted to the fingertips through parallelogram linkages. The glove can provide 3 N of resistive feedback for each finger in flexion direction (3 DoF of force feedback in total).

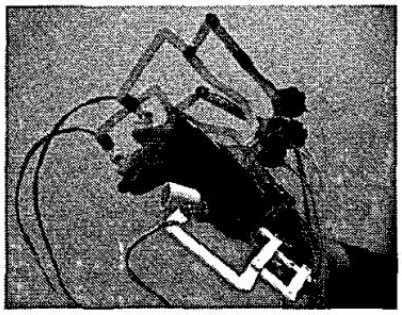

Figure 27: Multi-fingered Force Feedback Glove

(Source: Koyama et al., 2002)

Encoder sensors are implemented to the joints axles of the mechanism to measure angles at fingertips so that 4 degrees of freedoms of motion tracking per finger (12 DoF in total) can be obtained. Then, from forward kinematic analysis for the mechanism, position of the fingertips in space is also determined (Komeda et al., 2005; Koyama et al., 2002).

2.4.19. Passive Force Display Glove

Koyanagi et al. have developed an exoskeleton type passive force display glove (PFDG) that can be worn into 3 fingers (thumb, middle and index) and weighs 700 grams (Joining parts' weights were not provided). Resistive forces are generated by electromagnetic brakes and through wire-pulley systems, transferred to the fingertips. A torsion spring is set to the axis of each brake to maintain tension in the wires. PFDG is able to provide 29 N of force feedback in the direction of flexion per finger (1 degree of freedom force feedback per finger- 3 DoF in total).

PFDG measures bending angles of the joints via using mini potentiometers fixed to the brake axes and curvature of fingers via bending sensors placed at the back of MCP joints. Thumbs curvature is also measured by bending sensors; however, the sensors were place at the palm side of the MP joint. By this way, the degree of freedom for motion tracking is determined as 2 for per finger (6 DoF in total) (Koyanagi, Fujii, and Furusho 2005).

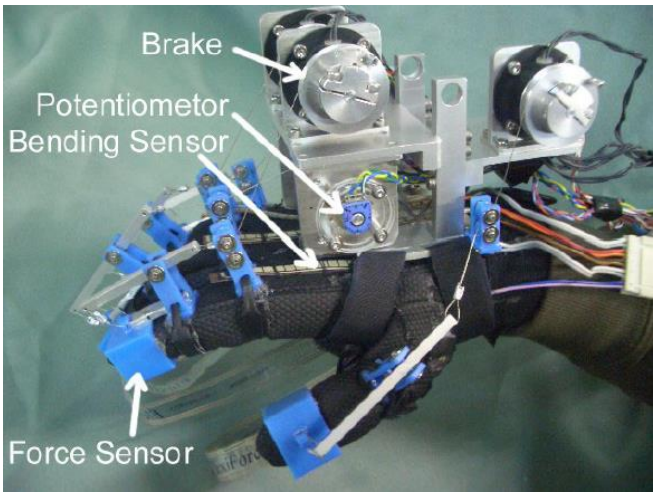

Figure 28: Passive Force Display Glove

(Ichi Koyanagi et al., 2005)

2.4.20. MR Glove

MR glove, developed by Blake et al., is an exoskeleton type of haptic glove in which MR brakes are used as passive actuators to provide resistive force-feedback to the user. The glove weights 900 grams and is worn over 3 fingers (thumb, index and middle fingers) where the braking torque is transmitted to each finger joint through the four-bar linkages. Two different sizes of MR brakes were used for each finger in the glove where the large brakes are placed on proximal joints to meet large resistive torque requirements and the smaller brakes were placed at distal joints to meet smaller torque requirements. The torque outputs for large and small brakes are 821 N.mm (under 0.7 A current supply) and 399 N.mm (under 0.5 A current supply) respectively with an off-state torque of 5 N.mm (raised by 28:181). The glove can provide torque feedbacks by using small and large brakes in 6 degrees of freedom (5 DoF from flexion of the thumb, index and middle fingers, 1 DoF from adduction of the thumb).

Since there are no motion capturing sensors or devices are embedded in MR Glove, it is worn over a commercially available CyberGlove that measures finger joint angles and fingertip position in 22 DoFs (Blake and Gurocak 2009).

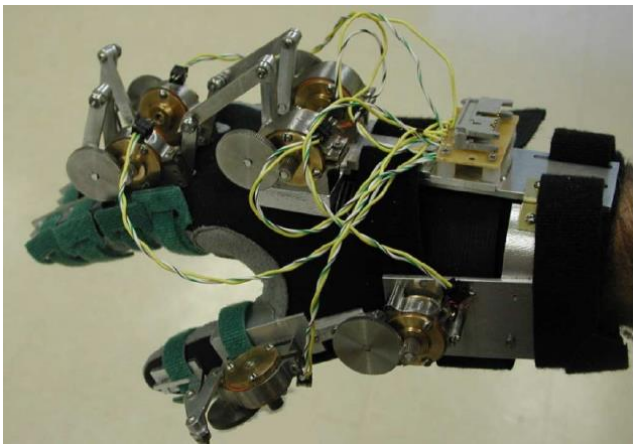

Figure 29: MR Glove

(Source: Blake & Gurocak, 2009)

2.4.21. Smart Glove

Smart Glove, developed by Nam et al., is an exoskeleton type haptic glove which use MR fluid-based brakes as passive actuators to provide haptic feedback to the user. The glove is worn in 5 fingers and weighs 348 grams. The main difference of this glove from other MRF based actuators is the design of the actuation unit.

Figure 30: Smart Glove

(Source: Nam et al., 2008)

The actuation unit consists of several parts such as MR fluid, a cylinder, a piston head and two piston rods. Magnetic field creation is provided by the circuit installed in the piston head. The cylinder filled with the MR fluid and divided two chambers by the piston head. The piston head can move freely in absence of a magnetic field so that the MR fluid is transferred from one chamber to the other through a small gap between piston

head and the cylinder. In this case, only static friction force exists due to the viscosity of the fluid. Actuation and the generation of force is done via the movement of piston head and magnitude of the generated magnetic field. When the electromagnet coil is supplied with current, MR fluid in the gap between the cylinder and piston head will change its dynamic yield stress proportional to the intensity of the applied magnetic field and MR fluid turns quasi-solid state. By this way, movement of the fluid within the chambers is prevented, thus, force is generated. Each actuator on the glove can provide 26 N (with 6 W of electrical power) of resistive force feedback in 1 degree of freedom for per fingertip in the direction of flexion. A downside of the actuators is, 5.54 N of the off-state force exist even there is no current supplied to the system.

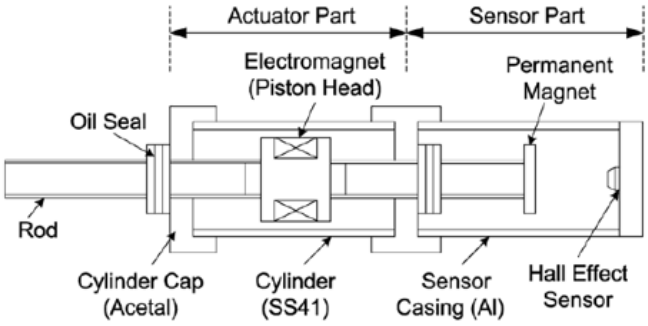

Figure 31: Smart Glove- Design of the Actuator

(Source: Nam et al., 2008)

Motion of the fingers are captured via the movement of piston head with 1 degree of freedom per finger (5 in total). It is done via using a permanent magnet is placed at the end of the piston head. When the permanent magnet moves and gets closer to hall-effect sensor, intensity of the magnetic flux on hall-effect sensor changes therefore the output voltage of the sensor changes. The change in the voltage is interpolated to a 5^{th} order curve in order to measure the change in distance. In their experiments, it was seen that the voltage change is nearly linear with the displacement of the piston head.

The reasons Nam et al. used MRF based actuators in their glove are: MRF brakes can generate high force/torque outputs, have low inertia, safe in case of any system failure, able to provide stable haptic feedback and make the design of the link mechanism easier (Nam, Park, and Yamane 2008).

2.4.22. MRAGES

Winter et al. developed MRAGES (MagnetoRheological Actuated Glove Electronic System) glove which uses a similar actuation principle as Smart Glove. MRAGES is worn in 5 fingers and the entire system weighs just 160 g.

MRAGES measures the motion of fingers via using linear potentiometers placed at the top of each actuator that the movement of piston head can be measured. By manufacturing a rapid prototyped part for the sensor's moving head, connection between the sensor and piston head is established via using a coupling between control cable (connected to moving sensor head) and the moving piston. By this way, 1 degree of freedom of motion for each finger can be tracked (5 in total).

The communication between the host computer and MRAGES is established via using USB protocol so that, calibration of sensors, force feedback settings and sensor readings can be measured/adjusted. Also wireless communication protocols such as 802.15.4 ZigBee and 802.15.1 Bluetooth are being used since the commands and responses are not complicated (Winter and Bouzit 2007).

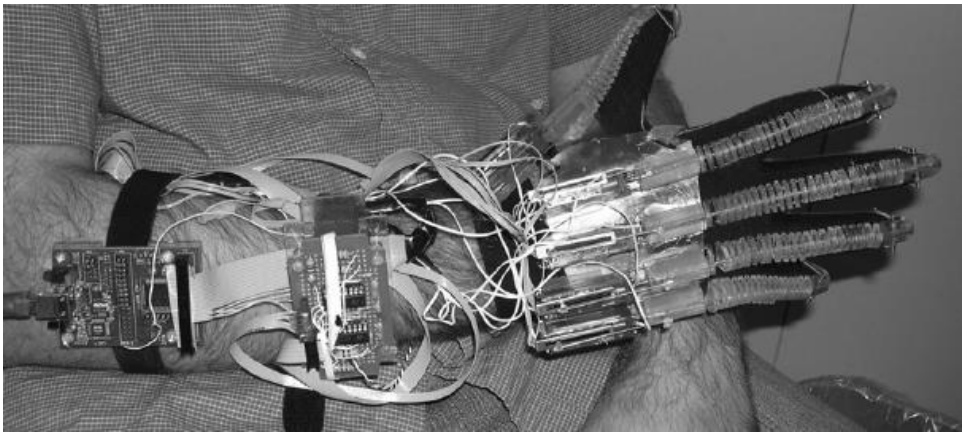

Figure 32: MRAGES

(Source: Winter & Bouzit, 2007)

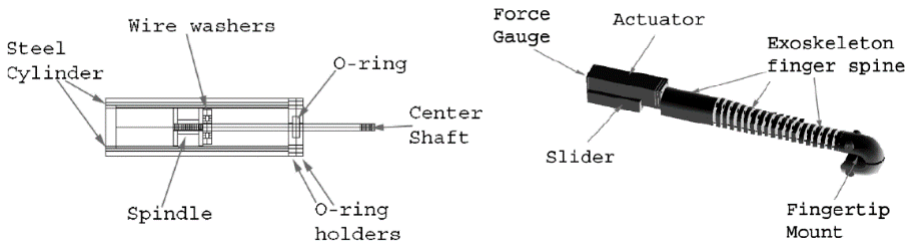

Figure 33: MRAGES- Design of the Actuator

(Source: Winter & Bouzit, 2007)

2.4.23. Lightweight Force Feedback Glove

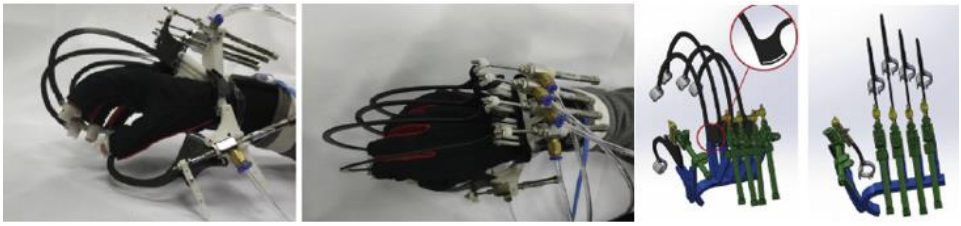

Figure 34: Lightweight Force-Feedback Glove

(Source: Zheng et al., 2018)

Zheng et al. developed an exoskeleton type haptic glove that is worn in 5 finger and weighs 245 grams. 5 pneumatic actuators were used in their design to provide active force feedback to the fingertips. In their work, abduction/adduction motion of the proximal joints were excluded; thus, the system can be analyzed in a plane.

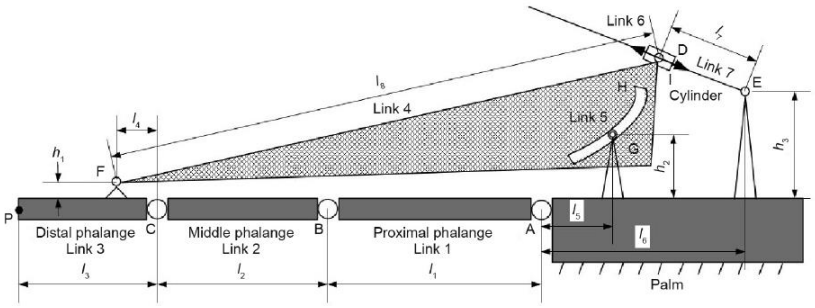

Figure 35: Hybrid Cam-Linkage Mechanism

(Source: Zheng et al., 2018)

Each actuator is connected to a hybrid cam-linkage mechanism to transmit the force into fingertips. The actuation process starts with the injection of air into the pneumatic cylinder (link 7). In this way, resistance force is exerted on the piston rod (link 6). The transmission of the actuated force from piston rod to the fingertip is done through the transmission link (link 4) which consists of three kinematic pairs (tuning pair F, tuning pair D, and higher cam pair H). The mechanism is able to support 2 degrees of freedom of motion for each finger in flexion-extension plane. Beside this, the glove is able to produce 4 N (with low static load, 0.1 N) of continuous force at the fingertips with 1 degree of freedom for each finger (5 DoF force feedback in total) by consuming 110 W of electrical power for each actuator. The response time of the pneumatic actuators is indicated to be 130 ms.

In the glove, only 6-axis force/torque sensors were used to measure forces transmitted to the fingertips. Since there are no other sensors used to track the motion, a separate commercial data glove (WiseGlove) is worn to track the motion. The communication between the glove and host computer is established via using USB protocols, where 70 Hz of update rate can be achieved (Zheng et al. 2018).

2.4.24. Exo-Glove PM

Yun et al. developed an exoskeleton type force feedback glove, “Exo-Glove PM”. The glove can be worn in 3 fingers (thumb, index and middle fingers) and weighs 350 grams (950 grams in total with the pressure tanks). The thimble, finger strap and wrist strap parts of the glove are made of silicone in order to ensure the easiness in wearability, provide adjustability for different hand and finger sizes and keep the glove hygienic and washable. Actuator modules were also made of silicon but additionally covered with rubber sheets which restricts the extension of actuators housing when air is supplied to the system. Three pneumatic actuators are linked to the fingertip thimbles via using intermediate modules (such as MCP, DIP and PIP modules) to transmit forces. Exo-Glove PM is able to provide 22-22.5 N of continuous force feedback to the fingertips in the direction of flexion (3 DoF total, 1 per finger). The total power requirement for three actuators is given to be 30 Watts.

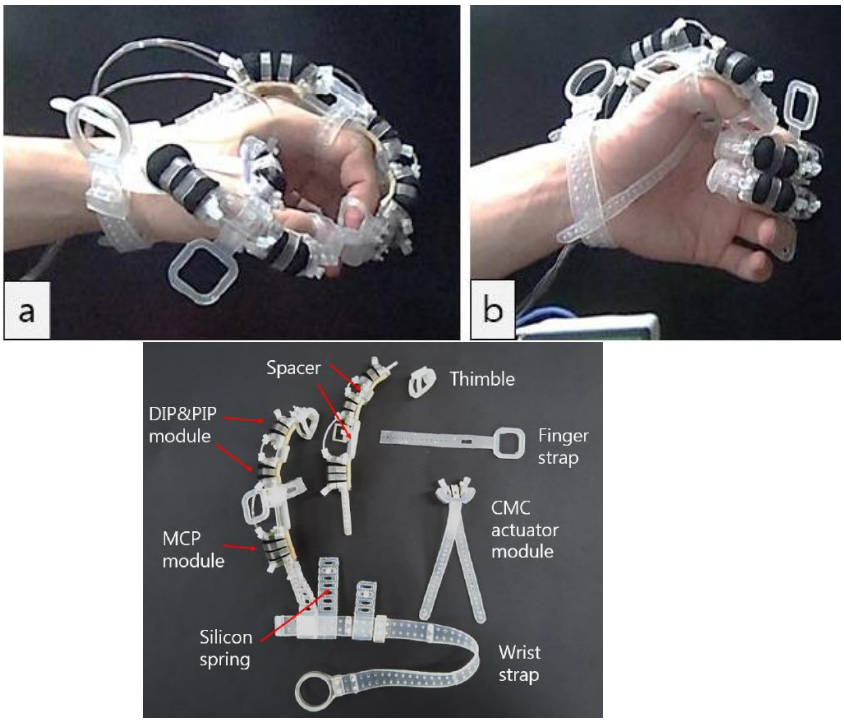

Figure 36: Exo-Glove PM

(Source: Yun et al., 2017)

Exo-Glove PM do not include any sensors or external devices to track hand and finger motions; however, video recordings somehow were used to track the motion and mat-type pressure sensor is used to measure the forces at the fingertips (Yun, Kang, and Cho 2017).

2.4.25. Wolverine

Choi et al. developed an exoskeleton type haptic glove Wolverine. The device can be worn in 4 fingers (thumb, index, middle and ring fingers) and weighs 55 grams in total. Unlike many other haptic glove designs where dorsal side of the hand or forearm regions were mostly used to place actuation units, thumb is used as the base in the proposed design where index, middle and ring fingers are connected to the base with sliding mounts placed on rods made of carbon fiber tubes. All other mechanical components except rods are produced by using a stereolithography 3D printing technology. The sliding mount placed on each rod has a brake mechanism to stop the movement of the mount and lock it onto

the rod. The whole device provides movability 18 degrees of freedom (6 DoF for each finger, thumb is excluded).

Figure 37: Wolverine

(Source: Choi et al., 2016)

The proposed brake mechanism of Wolverine consist of 2 tendons, a lever, a DC motor and a wire to connect the lever to the DC motor and works as follows. When no power is supplied to the system, the hole in the lever and the rod are coaxial so that the sliding mount can move freely on the rod (A).

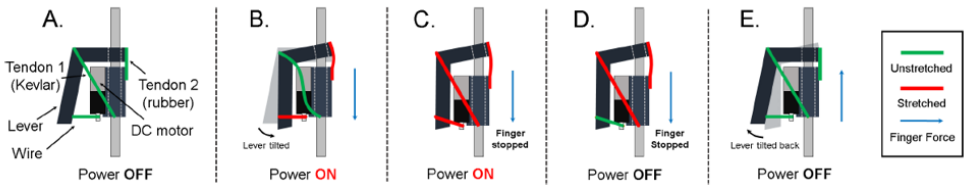

Figure 38: Wolverine- Braking Sequence

(Source: Choi et al., 2016)

In order to lock the sliding mount power, is supplied to the DC motor which actuates the wire between the lever and motor to break the coaxiality. When the lever is tilted, the rod and the hole of lever are not coaxial which causes the sliding mount to jam (B). After jamming, if the user continues to move the mount further, Tendon 1 will also actuated so that it will pull the lever even more and introduces additional braking force

(C). At this point, even the power supplement is cut to the DC motors, the mechanism will prevent the movement of sliding mount and keep it locked (D). Once the user opens his/her hand, Tendon 2 rotates the lever in clockwise direction and stops braking engagement (E) and allow free movement of hands. An important point of this design is, DC motors do not supplied with power in whole braking engagement; instead, they are only used at the initiation. Users' applied force provides self-locking ability to the system. Wolverine is able to provide 100 N of force feedback in the direction of grasp motion (1 degree of freedom for index, middle and ring fingers, 3 DoFs in total) with 3 Watts of power is supplied to each actuator.

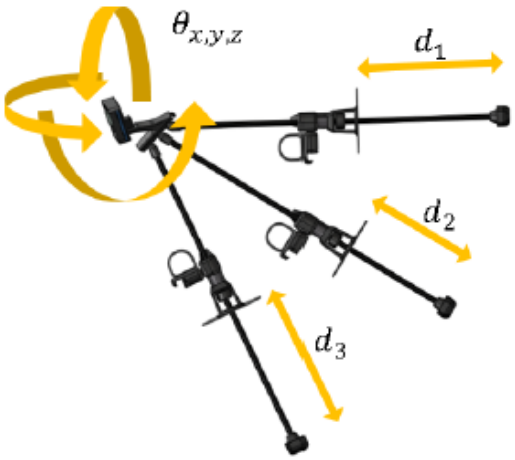

Figure 39: Wolverine Motion Tracking DoFs

(Source: Choi et al., 2016)

The motion is tracked via using different sensors at different places. For the rotations, a 9-axis IMU is used that is placed at the thumb and it was assumed that thumb represents the orientation of the hand in space. For linear motion of the sliding mount, time-of-flight sensors were placed at the end of each rod, which emits infrared lights to measure the distance between sliding mount and the tip of the rod. (6 DoF for tracking motion). The communication between Wolverine and host computer is established via using Bluetooth protocol and 100 Hz of update rate is achieved (Choi et al. 2016).

2.5. Conclusion

In this chapter, information about haptic gloves were presented. Based on the conducted research, 25 different gloves that can provide haptic feedback have been revealed. It has been observed that 18 of these gloves can provide force feedback, 5 of them can provide tactile feedback and 2 of them are able to provide both tactile and force feedbacks.

For tactile feedback applications, 1 thimble type and 6 traditional glove type were detected. Three of these gloves use electromagnetic actuators, two use linear resonant actuators and one uses pneumatic actuators to stimulate tactile sense of touch.

For force feedback applications, 4 traditional glove type and 17 exoskeleton type gloves were detected. Active actuation principle is used in fifteen gloves, and the distribution of the actuators is 11 DC motors and 4 pneumatic actuators. In terms of passive actuation, six of the gloves were detected where 3 of them use electromagnetic brakes and the remaining use magnetorheological fluid-based brake systems. When the scope is narrowed to the force feedback capabilities, it was seen that nine of the gloves that can give a force between 0-10 N, five of the gloves that can give a force between 10-20 N and four gloves are able to provide force feedback greater than 20 N have been identified.

When gloves that are able to provide 0-10 N of force feedback to the fingertips are examined, nine gloves using active and passive actuation principles were found. The main disadvantage of these gloves is that the finger motions cannot be restricted due to the insufficient force feedback their actuators can provide. Since their force feedback is insufficient to model stiff virtual objects, they are unable to provide detailed haptic information to the users and can only provide cues about the object being interacted with.

When gloves that can provide force feedback between 10-20 N are examined, all found to be using active actuation principles and except for the SenseGlove DK1, in CyberGrasp, Rutgers Master II, HaptX and Exo-Glove PM gloves found to have heavy force control units operating at high electrical powers to create the required force to be provided to the fingertips. Since these force control units are way too heavy to be carried by the user, they must be placed on the ground. In this case, the mobility of the user is significantly restricted and limited by the force transmission structures, tubes and cables.

In addition, due to the active action principle they use, in case of a malfunction that may occur in the device, a sudden and strong pulling of the fingers may cause injury.

When gloves that can provide force feedback greater than 20 N are examined, except for the Exo-Glove PM which uses pneumatic actuators, Passive Force Display Glove (PFDG), Smart Glove and Wolverine were found to use brake systems as passive actuation units. As the different brake systems used in these gloves are examined, it can be inferred that since the users have no connection with the ground, their mobility is much less restricted, and a much higher force feedback can be provided at a lower power consumption. In addition, since the brake systems can operate at low power consumptions and can only resist to the movement due to their passive working principles, it has been concluded that these systems can be positioned closer to the hand and fingers due to their safer natures.

Apart from the actuators and their capabilities, following observations were done in terms of motion tracking of the fingers based on the glove types. While exoskeleton type gloves were found to be taking the advantage of placing rotary sensors such as encoders and potentiometers at the joint locations to determine rotation angles between links, flex sensors were mostly used in traditional type gloves which were sewn over finger phalanxes to measure the flexion angles of the fingers directly. For thimble modules, only inertial measuring units (IMU) were used; however, the use of IMUs are not limited with thimbles and extended over all types of the gloves. Except these sensors, in cases as seen in Rutgers Master II and Smart Glove, different types of sensors can directly embed into the designed actuator. It was also seen that, besides the sensors, fingers motions were also seen to be measured with separate image processing and motion capture hardware such as Leap Motion which can track 10 DoF of finger motions.

In the next Chapter, information about the conceptual design and actuation system architecture of a wearable system over a separate external data glove able to measure and track finger motions will be given.

CHAPTER 3

ACTUATION SYSTEM ARCHITECTURE

In this Chapter, information about the architecture of the actuation system to be used the developing haptic feedback glove will be presented. There are two main components that make up the actuation system of the haptic glove which are the magnetorheological fluid-based brake systems and the force transmission system.

When the actuators of the gloves presented in the literature review examined, three main problems were observed. These problems are insufficient force feedback, heavy ground units and safety issues. To deal with these issues, magnetorheological fluid-based brake systems are found to be great candidates and chosen as the main actuation units to be used in the developing haptic glove in the scope of this thesis. In the first part of the Chapter, information about magnetorheological fluid-based brakes is presented.

Besides the actuators, when the force transmission systems in the gloves in the literature review are examined, it has been observed that the mechanisms and linkages are detected to be heavy structures that restrict the motions of the users' fingers during their manipulations. In addition, it was seen that unwanted frictional forces occur between mechanism joints and are transferred to the user. To prevent these problems in force transmission systems, it is aimed to transfer the force obtained from the brakes to the fingertips with the help of cables, since they are flexible, small and light in weight which provides additional freedom to the finger motions of the user. Since MR brake systems are actuators that resist movement and cannot provide any movement to the system, the most important problem to be dealt with while using cables together with MR brakes is, prevention of cable slack during finger motions. In the second part of the Chapter, the conceptual design of a force transmission system consists of cables and spring-based cable winding structures that can be used to the transfer the output torques/forces obtained from the MR brake systems to the fingertip of the user is included.

3.1. Magnetorheological Fluid Based Actuators

The challenge in haptic glove applications is to design an actuator which is small enough to be placed on the user's hand and fingers and at the same time be designed to limit or stop their movements when the user grasps a virtual or distant object while keeping the friction minimum to increase the transparency of the haptic feedback. In addition, reducing the overall mass of the glove and determination of the position of the actuators on the glove in such way that the free and natural movement of the user's hand and fingers are minimally affected are also important design requirements. An important aspect to consider when meeting these requirements is the degree of freedom that the glove can move and provide force feedback to the users' fingers. Since the human hand has 27 degrees of freedom and it is not possible to use an actuator for each finger joint. Therefore, it is necessary to design a mechanism (linkages, cable-driven types, etc.) structure so that the force/torque generated by actuators/brakes can be transmitted to the fingertips of the user in the most effective way. In order to meet these requirements, an efficient actuator should be selected or designed by considering their advantages and disadvantages; where magnetorheological fluid-based brakes, by considering these issues, are suitable candidates for haptic glove applications due to their passive force feedback features. In this section, information about the MR brake systems will be presented.

3.1.1. Working Principle of MR Brakes

Magnetorheological fluids (MRFs or MR-fluids) are mixtures of micrometer sized ferromagnetic particles within a non-conductive carrier fluid that has low viscosity. They respond to the changes in magnetic field instantly and reversibly so that, when the MRF is exposed to a magnetic field, rheological properties of the fluid will change instantaneously. The main rheological property that is aimed to be controlled is their variable yield strength. With increasing magnetic field strength, the fluid starts take a semi-solid form due to the alignment of the ferromagnetic particles in the direction of the magnetic flux density vectors. When the application of the magnetic field is over, it returns to the fluidic state back.

In order to develop brake systems by using MRFs, 3 parts are required beside the MRF; which are a coil, a rotary shaft and a casing respectively. The coil is used to create an external and controllable magnetic field by controlling the current supplied to the wound wires around a core that has high magnetic permeability. The shaft is required to provide motion and transfer the braking torques/forces obtained within the brake system. Lastly, the casing is required to keep the system together by carrying the shaft and the coil. Additionally, casing can also be used as the magnetic core required for the coil.

As shown in Figure 40, the MRF is filled in the gap between the shaft and the casing. When there are no current supplied to the coil, magnetic particles can move freely within the carrier fluid. By supplying current to the coil, an external magnetic field is created. Based on the direction of magnetic flux density vectors created by this magnetic field, magnetic particles are aligned by following magnetic flux vectors. After alignment of magnetic particles, chain structures were formed between the rotating shaft and the static casing. Also, the magnitude of the magnetic flux passing over the fluid determines the variable yield strength value of the particles in these chain structures. In order to break these chains attached on the shaft and casing from their ends, a shear force on the surface of the shaft have to be reached.

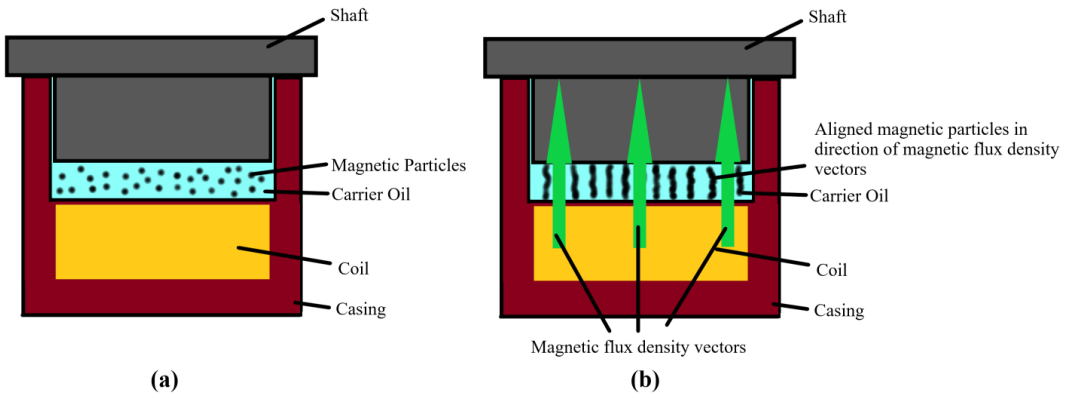

Figure 40: An MR brake's inner structure without (a) and with (b) current.

Therefore, by controlling the current supplied to the coil, a resistive braking force/torque to break the bonds of the particles can be obtained. Braking torque is the main design parameter for a MR brake to be determined. To estimate the braking torque would be obtained from the system, three design parameters have to decided:

- The dimensions of the surface of the shaft that is in contact with the MRF.
- Operational current interval and number of turns of the coil wires that are wound to a magnetic core.
- The magnitude and the directions of the magnetic flux density vectors passing over the MRF situated in the gap between the shaft and the casing.

3.1.2. Advantages and Disadvantages

As a result of the literature review, the main problems observed in the surveyed force feedback gloves can be narrowed down into the following: insufficient force feedback (DC motors), heavy ground units (DC motors and pneumatic actuators), safety issues (any active actuators), and heavy weight (electromagnetic brakes and MR brakes).

An actuator to be used in force feedback applications must be able to generate large forces/torques to simulate interaction with stiff objects. Based on the work of Redmond et al. (2010) and Rice et al. (1998), it was revealed that human hand generates 7 N of continuous force with frequencies under 2 Hz while performing daily life activities such as pick/place and grasp/hold. However, the required force for power grip motion can be increased up to 100~300 N. When the capabilities of the actuators were investigated, the nearest values of forces required for power grip motion could be obtained by using MR brakes since they can produce high shear stress, depending on the physical and chemical properties of the MR fluid. MRFs can typically generate high yield stresses between the 50 to 100 kPa range interval (Shafer and Kermani 2011). By using magnetorheological fluids (MRFs), a passive actuation system can be constructed such that the amount of transmitted torque/force can be controlled by the intensity of an applied magnetic field that affects the rheological properties of the MR fluid. Thus, the yield stress of the MR fluid can be controlled by adjusting the intensity of the applied magnetic field.

Based on the researches of Rankin et al. (1998) and Zinn et al. (2016), heavy, bulky and grounded haptic interfaces reduce the immersivity of VR/AR interactions of the user wearing the glove. Therefore, an actuator to be used in a haptic glove device is expected to have a low mass-to-torque ratio. The lightweight and compact sizes of MRF-

based passive actuators without any grounded power units allow the user interacting with the device to experience more persuasive interactions with virtual/distant environments.

It is highly desirable for a haptic device to produce high torques as well as have low inertia. The use of gear reduction to increase the torque capacity results in a decrease in the backdrivability and a significant increase in inertia felt by the user; thus, contributing to the greater part of the inertial load. Since MRF-based brake systems are able to generate resistive torques/forces high enough to stop the motion of the fingers, the gears can be completely extracted from the system so that only the reflected inertia of the output shaft will be felt by the user (Ma & Ben-Tzvi (2015).

Based on the research of Winter & Bouzit (2007), the high bandwidth of the actuation system is a vital necessity for a haptic system that collaborates with the transparency of the device. As stated in the work of Rice et al. (2018), the required frequency to stimulate haptic feedback for finger motions of daily activities is about 2 Hz where the MR fluid inside the brake systems responds within a few milliseconds to an applied magnetic field. Although the actuation response is delayed due to field propagation, MRF-based brake systems have sufficient bandwidth to respond hand and finger motions for glove applications.

Another advantage of MRF-based actuators is their safety. Since MRF-based actuators have low power requirements and providing passive force feedback that only resist the users' inputs, they can be placed close to the user's hand and fingers, unlike other actuators. In case of an accident, the user will not severely shocked by the electric shock or the fingers pulled back causing injuries. Several injuries of users have been reported in an event of failure with the use of active actuators that fingers are pulled back by the cables, which raised the safety concerns (Ma and Ben-Tzvi 2015b).

MRF-based actuators have two main disadvantages which are their nonlinear behavior and high off-state torque (Gang, Choi, and Sohn 2016; Najmaei et al. 2014). MRF-based actuators show hysteresis due to the ferromagnetic materials used in the fluid. This translates into a hysteresis relationship between input current and output torque, resulting in tracking errors, unwanted harmonics, and unwanted stick slip movements. To develop a reliable relationship between output torque and input current, it is important to both understand and model actuator hysteresis precisely. Another important issue is the off-state torque observed in the MR brakes. Even no current is supplied to the brake

systems, there exist a resistive force/torque that needed to be overcame first to start the motion of the fingers. As mentioned in the Section 2.4.21 and Section 2.4.22 the off-state force/torque observed in these MR brakes are about 25% of the total force output. Therefore, the reasons behind this situation have to be analyzed and a proper solution have to be developed.

In the Table 2, the advantages and disadvantages of the MRF actuators were collected together in order to provide clarity to the reader.

Table 2: Advantages and Disadvantages of MRF-based Actuators

MRF-based Actuators (Clutches & Brakes)		
#	**Advantages**	**Disadvantages**
1	Passive force feedback	Hysteresis due to ferromagnetic materials
2	Lightweight and compactness	High off-state torque
3	Low mass-torque ratio	
4	Low inertia	
5	High bandwidth and low response time	
6	Low power requirement	
7	Safety	

3.1.3. MR Brake Types and Architectures

MR brake system architectures are classified based on the motion of the shaft (translational or rotational) and the axis on which braking force/torque will be produced. Therefore, MR brake systems are examined under two main categories which are the linear-type MR brakes and rotary-type MR brakes respectively.

In linear type MR brakes, a piston-cylinder type structure is used to ensure that the shaft moves linearly within the brake system. When the designs were examined, it was observed that the coil part used to create the magnetic field required for braking was placed on the shaft, and the MR fluid was filled between a shell with high magnetic permeability and the shaft that acts as a piston.

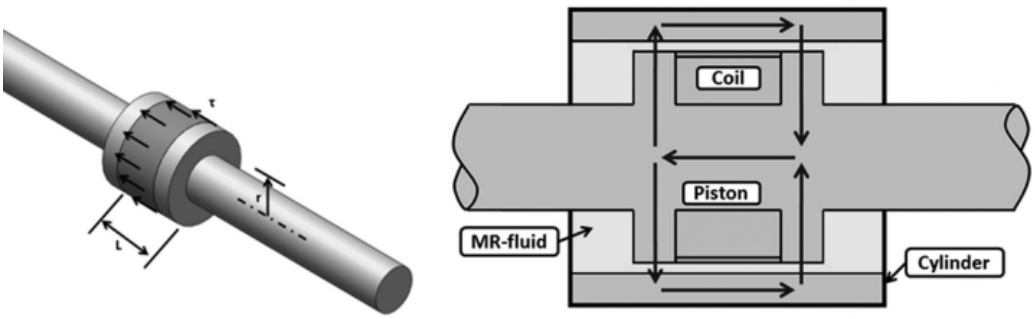

Figure 41: Linear type MR brake architecture.

(Source: Alkan et al., 2013)

The advantage of linear type MR brake systems is their compact structures within a small volume. One of the main disadvantages of linear type MR brakes is the high off-state torque they exhibit. The pressure difference between the chambers divided by piston shaft (the right and left parts of the piston) during the motion causes large forces to occur, even when the MR fluid is not activated. In addition, due to the large area that the coil is placed, the magnetic flux density obtained on the magnetic flux path decreases and causes the system to produce low force output. Due to these disadvantages, linear type MR brakes are rarely used and no further information found about the different design sub-categories.

In rotary type MR brake systems, the shaft's linear motion is restricted and only rotational motions are permitted. Due to the absence of pressure chambers seen in linear type brake systems and the use of a piston-cylinder-like structures, the off-state torque of rotary type MR brake systems is considerably less compared to the linear-type MR brakes. Based on the work of Avraam et al. (2010), 5 main sub-design categories for rotary type MR brakes were found. These sub-categories can be counted as: drum type, inverted-drum type, T-shape type, disc type and multi-disk type rotary MR brakes.

In drum type MR brakes, the coil is placed in the cylindrical shell and magnetic field is generated radially. This type of MR brake is the simplest configuration in terms of manufacturability. However, due to magnetic flux lines passing through MR fluid only two times, produced braking torque is the least compared to other MR brake architectures. Additionally, their rotor inertia is higher than other configurations due to the increased radius of the rotating shaft to achieve greater torque values.

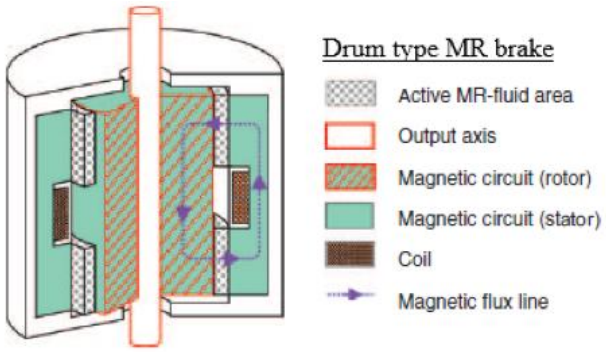

Figure 42: Drum type MR brake architecture.

(Source: Avraam et al., 2010)

An improved version of drum type MR brakes is known as inverted drum type MR brakes. Compared to drum type MR brakes, they produce the same braking torque since magnetic flux lines pass over the MR fluid two times; however, inertial properties were improved in this architecture thanks to the new coil position taken from the outer shell to the shaft, resulting reduced rotor inertia due to the reduced rotating mass.

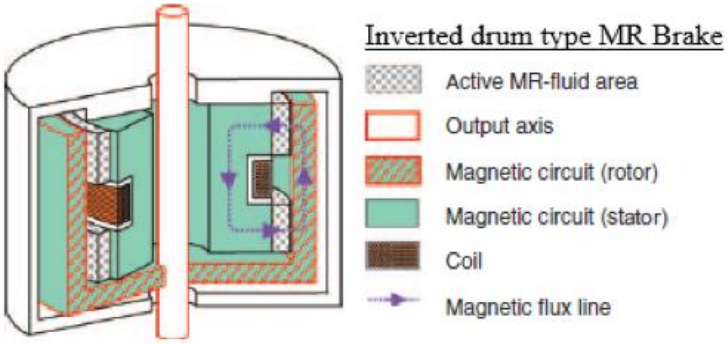

Figure 43: Inverted drum type MR brake architecture.

(Source: Avraam et al., 2010)

T-shape type MR brakes are improved versions of the previously mentioned architectures. Due to the structure and the reduced mass of the rotating part, the inertial properties are improved. At the same time, by using two coils, the magnetic flux is provided to pass over the MR fluid four times. This architecture has two disadvantages. The first is the high-power consumption due to the use of two coils to increase the braking torque. The second is that the production costs increase since the parts to be produced become more complex in shape and the number of parts increases while keeping the tolerance intervals narrow.

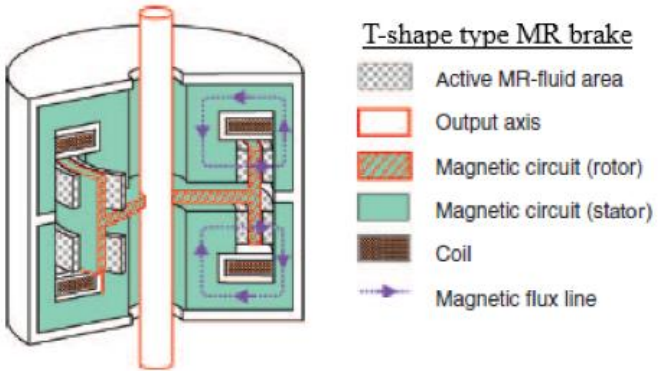

Figure 44: T-shape type MR brake architecture.

(Source: Avraam et al., 2010)

Another widely used MR brake architecture is the disc type MR brakes. The main difference observed in this architecture, unlike the previous types, is the region where the braking is taking place and the MR fluid works. When the magnetic flux path in this

region is examined, it is observed that the magnetic flux vectors affect almost the entire radius of the radial part of the disk, forming many different force arms for the force generated by the MR fluid. Thanks to these infinitesimally small force arms, the braking torque increases considerably compared to other architectures. Disk type MR brakes are easy to manufacture due to their compact structure and fewer sub-part requirements.

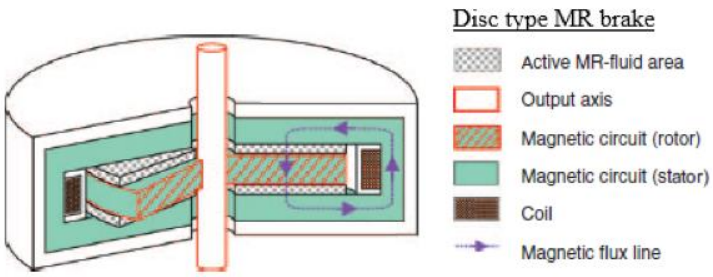

Figure 45: Disc type MR brake architecture.

(Source: Avraam et al., 2010)

By increasing the number of the disks of a disk type MR brake, the braking torque can be increased significantly. Multi-disk type MR brake architectures are simply disk type brakes with additional number of discs. Their dynamic range (maximum torque/off-state torque) and torque/ volume ratio are superior to other architectures, however, due to the parts with complex shapes and narrow tolerances, they are hard to manufacture for smaller volumes.

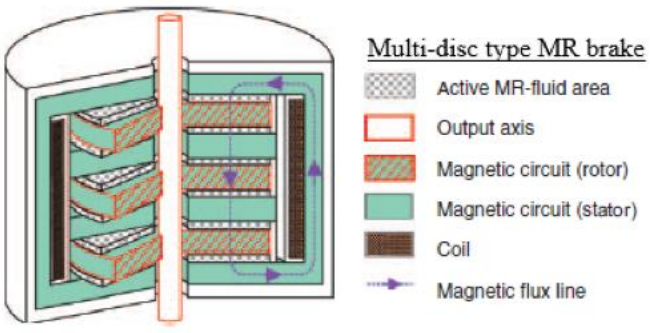

Figure 46: Multi-Disc type MR brake architecture.

(Source: Avraam et al., 2010)

Based on the collected information, data given in Table 4 was prepared. It can be concluded that, rotary type MR brakes are superior to linear type MR brakes in terms of their high dynamic torque range and low off-state torques. Within the rotary-type MR brakes, drum and disc type of MR brakes are superior over others in terms of manufacturability in small sizes due to the parts with simple geometries and the low power consumption they possess. The major issue observed on these types of brakes were their low torque outputs. The reason for this situation is, the magnetic flux vectors pass through the MR fluid only twice. If the magnetic flux vectors are forced to pass through the MR fluid multiple times, the torque outputs to be obtained from these systems can be increased, making these systems more suitable for use in haptic glove applications.

Table 3: Comparison of different MR brake architectures.

Features	Type of the MR brakes					
	Linear	Drum	Disc	Inverted Drum	T-shaped	Multi-Disc
Rotor radius	NA	+	-	++	+	--
Off-state torque	--	++	+	++	+	-
Torque/mass ratio	--	--	-	--	-	++
Dynamic range	--	-	--	-	+	++
Power requirement	++	++	+	++	-	--
Mechanical simplicity & manufacturability	++	+	+	-	--	--
++ : Best + : Good - : Bad -- : Worst						

3.2. Force Transmission System

In haptic systems, the force/torque obtained from the actuators must be transferred to the user so that the tactile or force feedback must be felt accurately in the intended location. The elements to be used in the force transmission system should be selected by considering the features of the actuator in use and their deficiencies should be eliminated during in the designs. In this section, the conceptual design of a force transmission system that can efficiently transmit the braking torque produced by MR brake systems to the fingertip of the user wearing the glove are presented.

3.2.1. Design Requirements

The braking torque obtained from the developed MR brake systems must be properly transferred to the fingertips so that the user can feel force feedback while in contact with an object during his/her movements in the virtual reality environment. A force transmission system is needed to establish the connection between the MR brakes and the fingertips so that, the generated torque will be transferred through the transmission elements and transmit the haptic feedback to the user. The requirements for the system to be developed are as follows:

- The system should connect 3 MR brakes to the fingertips of the thumb, index and middle fingers for pinching a virtual object. Since a total of 3 brake systems aimed to be used in the system, 1 degree of freedom of force feedback must be provided in each finger.
- The system planned to be built has to fit over the limited space on the dorsal side of the hand and fingers.
- The structure has to be small in volume in order to prevent attaching and hitting objects in the surrounding during the user's interaction with VR environment.
- It should be light weighted to allow long-term use and increase comfort level since the users will carry the whole system over their hand during manipulations.
- In addition to the off-state torque observed in the brakes, unwanted forces/torques that will be felt by the user due to the use of this system should be kept as small as possible.
- Gears should not be used while transmitting torque; since gears reduce the backdrivability of the system and also multiply the off-state torque that will be felt at the fingertip.
- Different motions of the hand and fingers, such as flexion/extension and abduction/adduction, should not be hindered. Therefore, the structure should exhibit flexible properties to allow all connected fingers to move freely.
- The effect of this structure on the control of the system should be minimal.
- Force transmission systems have to be suitable to be worn and taken off together with the developed brake systems.

3.2.2. Conceptual Design

When the force feedback gloves in the literature are examined, it has been observed that two types of transmission systems are mainly used to transfer the force obtained from the actuators to the fingertips; which are the mechanisms and the cables respectively. Among the 20 force feedback gloves examined, it was observed that 9 of the gloves use mechanisms and 9 of the gloves use cables to transfer the forces between their actuators in use to the fingertips of the users. Additionally, RML Glove and LRP gloves were found to be use both mechanisms and cables together within their systems. After performing a detailed review of the works, the results given in Table 4 are revealed. By considering the data given in Table 4 and taking the design requirements into consideration, the most efficient way to transmit the resistive torque generated by the MR brakes to the fingertips of the user is revealed to be by using cable transmission.

Table 4: Comparison of force transmission systems.

	Advantages	Disadvantages
Cables	- Low inertia due to absence of mechanical parts and links. - Allows collecting the masses of actuators on the back of the hand, reducing the load on the fingers providing more freedom. - Effective in single DoF force/torque transmission applications.	- Ineffective in multiple DoF transmission. - Cables must be kept taut during manipulations.
Mechanisms	- Effective in multi-DoF force/torque transmission applications.	- High inertia and friction. - Weights of the links and actuators are loaded on fingers.

Using cables as force transmission elements is a frequently applied solution in robotics and wearable system designs where the main reasons for using such transmission instead of mechanisms and linkages can be counted as:

- It allows the actuators to be positioned further from the joints so that the transmission of the force/torque generated by the actuators to the required position can be achieved remotely.
- They provide greater degrees of freedom of movement to the user wearing or using the device.
- They significantly reduce the total weight of the device.
- Since the cables are flexible and small in volume, cable transmission systems provide smaller, more compact, more portable wearable systems.

Besides these advantages, two main problems are observed in cable transmission systems:

- If the cable tension in the system cannot be maintained during the movements require sudden winding and unwinding, the cable may come off the grooved pulley rail (cable derailing).
- If the cable winding system is not designed correctly, the friction occurred between the cables and/or other parts may damage the system and cause the force to be transferred to the desired position lower than the required value.

Therefore, it is important to design the transmission system going to be implemented to the system by taking these problems into consideration. Cable transmission systems are mostly used with active actuators (such as DC motors) in the literature due the ability of the motors to rotate clockwise and counterclockwise directions allows both winding and unwinding of the cables while keep them taut. However, MR brakes do not capable of providing any motion; when an external motion is provided, MR brakes will generate resistive torque in the opposite direction of motion provided by the user. In order to explain why cable transmission together with MR brakes solely would be problematic, an example scenario given in below:

In the glove system to be used, the cables passing over the fingers of the glove are obliged to transfer the resistive torque generated from the MR brakes placed in the dorsal side of the hand to the fingertips of the user. The user must bend their finger towards their palm (finger flexion) while grasping an object in a virtual environment. During the

bending motion of the fingers, a curve occurs between the base and the tip of the finger and the outer length increases, causing the cable to be pulled. While the cable is being pulled, the movement of the user is limited according to the determined braking procedure. However, when the user opens (extends) his/her fingers again, the curvature formed previously will disappear and the slacks in the cables will be observed when the fingers become completely straight. This situation is illustrated at Figure 47.

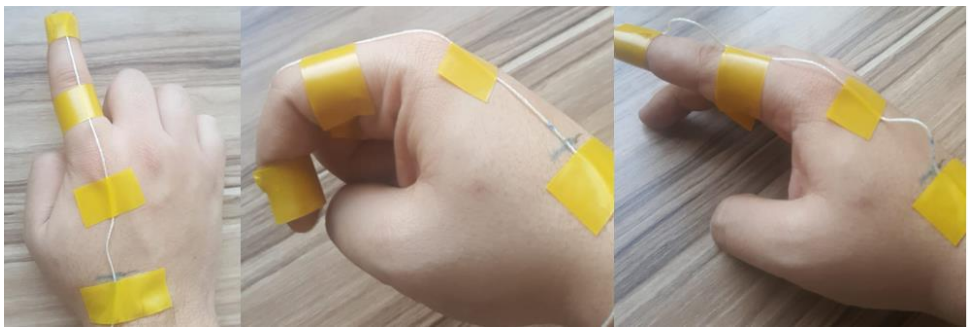

Figure 47: Cable slack after finger flexion and extension.

MR brakes planned to be used in the glove cannot be used to wind the slack cable since they can only generate resistive torque against an external rotation. Therefore, if no external structure is used for the glove to wind the cable after users' finger motions, the cable cannot be wound and kept taut. If this slack in the cable is not prevented, the users will not be able to receive any force feedback from the system in any of their further subsequent movements (except for those where the fingers must bend more).

To prevent cable loosening after finger flexion and extension, a common option widely used in the literature is to use active actuators such as DC motors. However, this option is not valid and not applicable to this design due to the following limitations and disadvantages:

- The area at the dorsal side of the hand is limited and MR brake systems will almost cover all this area.
- The weight carried by users over their hands will increase in collaboration with the number of connections between brakes and fingertips since a DC motor has to be placed for each of these connections to wind the cables during manipulations.
- Additional complexities such as electrical power, signal filtering and control will be added to the overall system.

In order to overcome factors stated above and keep the cables taut during user's manipulations and interactions, a spring-based solution is designed. The requirements for the spring-based cable winding structure are listed below with respect to their importance as following:

- Keep cables attached to the pulley (which is connected to the shafts of the MR brakes with one-way bearings) taut during extension, flexion and hyperextension motions of the fingers.
- It shall create a force just to exceed the off-state torque observed at the brakes while the fingers are not flexed or extended.
- Light in weight.
- Small in volume.

As mentioned in the last element of the design requirements, the force transmission system and the MR brakes have to be suitable to be worn and taken off together. Therefore, they both must be carried by the same platform. This requirement is added by the sponsor company since the glove system is aimed to be sold as haptic feedback system that can be bought separately and connected to an external data glove on demand. Therefore, the first step is to design a platform that is able to carry 3 MR brakes, which are oriented in a way that pulleys connected to the brakes can be linked to the tips of the thumb, index and middle fingers.

A hand model was created before further progress in designs including the cable winding structure and attachments worn over the finger to guide the cables towards the fingertips. Based on the works of the researchers (Jasuja O.P. and Singh G. 2004; Habib and Kamal 2010), an average male's finger lengths the dimensions for each phalanges were obtained as given in Table 5. This data is taken as a reference and used to generate hand CAD model.

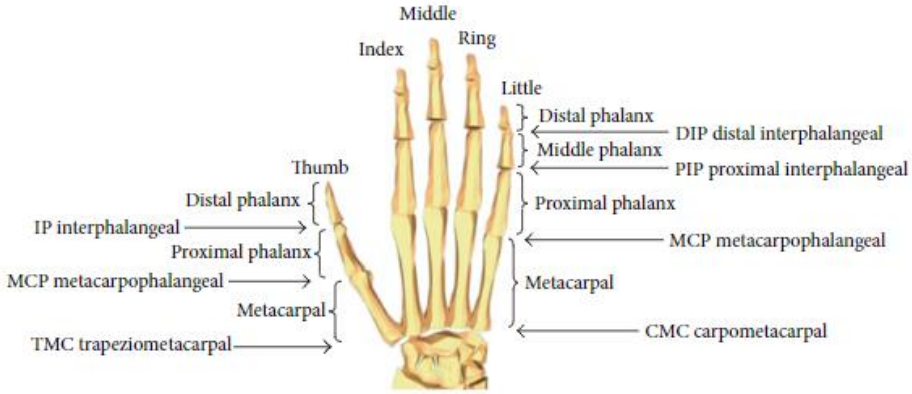

Figure 48: Hand skeleton's anatomical details

(Source: Chen Chen et al., 2013)

Table 5: Mean Phalanx Lengths

(Source: Chen Chen et al., 2013; Habib & Kamal, 2010; Jasuja O.P. & Singh G., 2004)

Mean Average Phalanx Length of the Male Hand			
	Distal Phalanx (cm)	Middle Phalanx (cm)	Proximal Phalanx (cm)
Index	2.32	2.37	2.65
Middle	2.6	2.78	2.8
Ring	2.29	2.56	2.76
Little	1.96	1.92	2.51
Thumb	2.55	-	3.49

After determining the average finger phalanx lengths and creating the hand model respectively, it is necessary to determine the angle of rotation on the joints between the phalanges, which occurs during the motions of the user's fingers. Since the system is aimed to be used for pinching motion with three fingers (3P), rotation angles observed on each joint (during the flexion/extension of the index and middle finger and abduction/adduction for the thumb) has to be determined. Lee & Jung (2015) shown that, while pinching, the size of the object and the posture of the hand (3P for the case of this work) contributes the rotation angles occurred in the finger joints significantly more compared to the shape and the weight of the object. As the size of object to be pinched

became smaller, the flexion/extension angles in DIP, PIP and MCP joints of index and middle fingers and the abduction/adduction angles in CMC joint of the thumb increase.

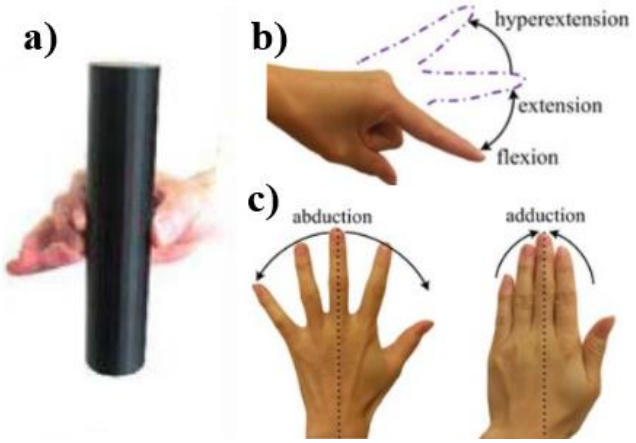

Figure 49: Pinch with 3 fingers (a), finger motions (b and c)

(Source: Lee & Jung, 2015, Wang et al., 2017)

Based on their work, data given in Table 5 is generated and used as a reference to reveal maximum joint angles occurred during pinching motion of hands for different sized cylinders.

Table 6: Maximum joint angles observed in 3P

(Source: Lee & Jung, 2015)

3 Finger Pinch (Thumb, index and middle)			
Finger	Joint & Joint Motion	Object Diameter	
		2 cm	8 cm
Thumb	CMC Ab/Ad	~73°	~55°
	IP F/E	~23°	~27°
Index	MCP F/E	~57°	~28°
	PIP F/E	~22°	~35°
	DIP F/E	~25°	~28°
Middle	MCP F/E	~55°	~32°
	PIP F/E	~41°	~48°
	DIP F/E	~10°	~14°

By using the hand model created by using the values at Table 4, a platform was designed to be placed on the hand and to carry 3 MR brakes directed towards the thumb, index and middle fingers' fingertips. Also, additional fingertip and intermediate attachments were designed in order to properly transfer the torque obtained from the brakes to the fingertips with the help of cables.

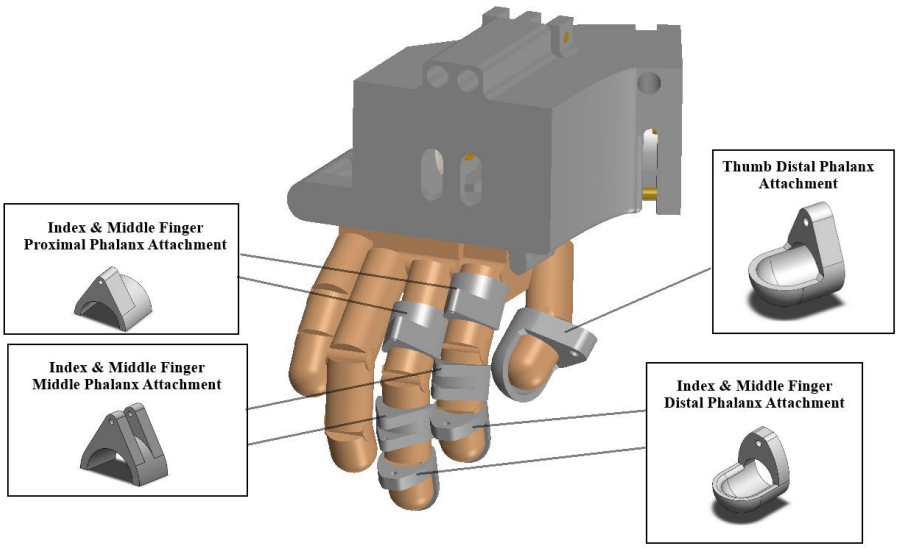

Figure 50: Finger attachments and the platform.

For index and middle fingers, 3 different attachments were designed for each finger phalanx. Cables leaving the platform are guided to the proximal phalanx attachments first. From proximal phalanx, cables were linked to the middle phalanx and distal attachments respectively. For the thumb, only one attachment is used to transfer the torque to the fingertip since it was seen that, if an additional attachment is placed over the proximal phalanx of the thumb, unwanted forces in abduction/adduction direction occur due to the platform's necessary extension to carry the third brake system to limit the motion of the thumb.

After the design and placement of finger phalanx attachments were completed, the joint rotation angles for 3P hand posture given Table 5 were applied each joint to determine the minimum and maximum lengths of the cables required during motion.

The difference between the minimum and maximum lengths of the cables during pinching motion were used to determine the lengths of the cables to be used in the system

and to design the spring-based cable winding structure since the obtained values for each finger indicate the required spring displacement within the structures when the fingers are flexed/extended. The information used in the designs of the cable winding structures for each finger were given in Table 7 and the corresponding parameters were indicated at Figure 51.

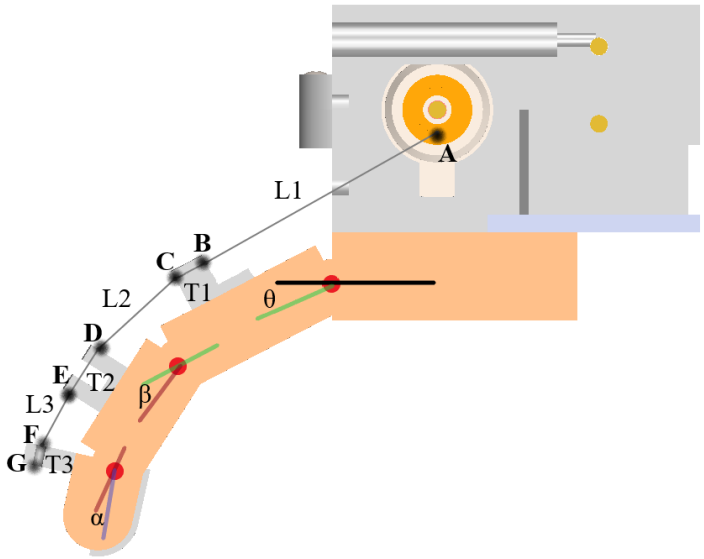

Figure 51: Parameters for the cable displacement during pinching.

Results given in Table 8 reveals that, the required cable lengths for 3P motion is 131.2 and 160 mm for index and middle fingers respectively. The displacement of the springs needed for the cable winding structures for index and middle finger were calculated as 38.3 and 35.39 mm respectively. Same study is repeated for the thumb where the minimum/maximum cable lengths and the required spring displacement is calculated as 92/126 mm and 34 mm respectively. In the design of spring-based cable winding structure, an additional space is left for the linear motion of springs to provide more freedom to the fingers and for the compressed lengths of the springs. Therefore, the additional linear distance left for the springs to be travelled is determined as 65 mm for index and middle fingers (~45% more than required) and 55 mm for thumb (~40% more than required).

Table 7: Parameters required for cable winding structure design.

General Information			
Cable Length	Between Points	Angle	About
L1	A-B	θ	MCP joint
T1	B-C	β	PIP joint
L2	C-D	α	DIP joint
T2	D-E		
L3	E-F		
T3	F-G		

Minimum Cable Lengths (mm)			
θ, β, α = 0°	Length	Index	Middle
	L1	47.8	63.61
	L2	10	20
	L3	4.1	10
	T1	10	10
	T2	15	15
	T3	6	6
	Sum	92.9	124.61

Maximum Cable Lengths (mm)					
Index θ= 57°, β= 22°, α = 25°	L1	70.2	Middle θ= 55°, β= 41°, α = 10°	L1	82.8
	L2	17.4		L2	32.7
	L3	12.6		L3	13.5
	T1	10		T1	10
	T2	15		T2	15
	T3	6		T3	6
	Sum	131.2		Sum	160

Cable Winding Structure Parameters	
Displacement required for index finger (mm)	38.3
Displacement required for middle finger (mm)	35.39

After the clarification of details, the design of the platform that includes the cable winding structures was completed. Within the platform, tubular structures for springs were designed based on the results obtained in Table 6. In order to transport the cables departing from the springs' ends to the pulleys attached over the shafts of the MR brakes, brass cylinders were used as cable guides as illustrated in Figure 52 (for index and middle fingers) and Figure 53 (for the thumb).

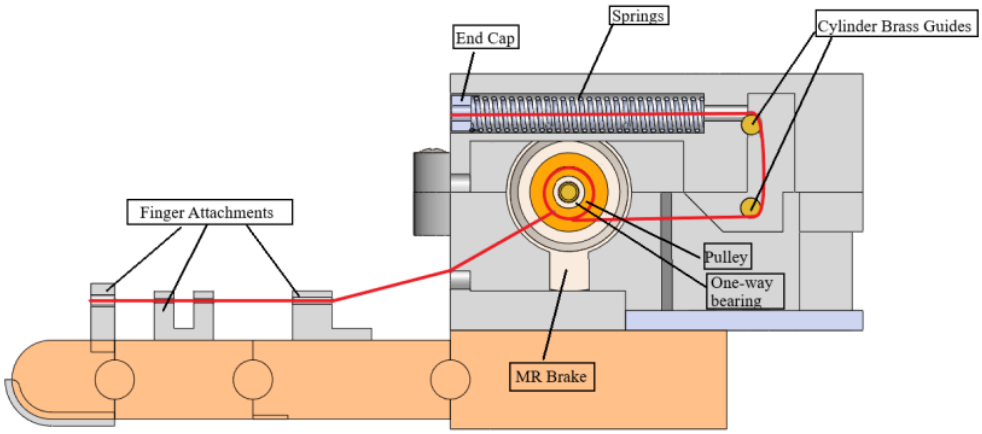

Figure 52: Cable winding structures for index and middle fingers.

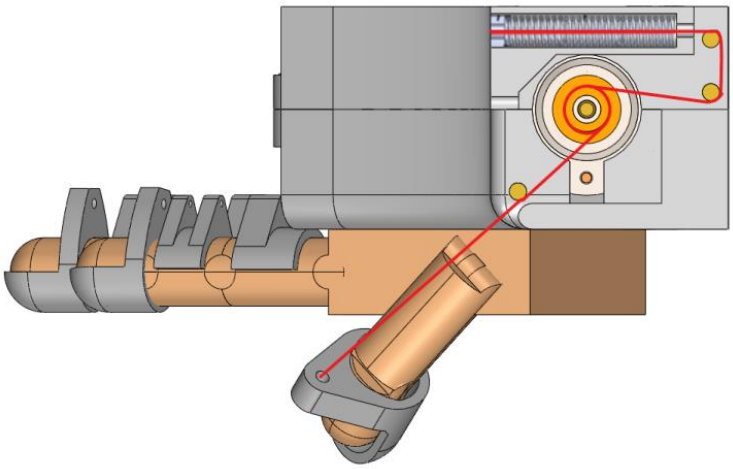

Figure 53: Cable winding structure for the thumb.

An example scenario is given below to present and summarize the actuation of the design:

- When the users wearing the glove want to pinch an object in the virtual reality environment, their fingers start flexion and adduction motions.
- Since the cable lengths between the fingertip attachments and the end caps are constant for each finger, end caps start to compress the springs inside the cable winding structures.
- Based on the force feedback demand, MR brakes will be activated and start to restrict further motions of the users' fingers in the direction of flexion. After the motions are completely restricted, the cables and springs will no longer displace. If any finger motion performed in the direction of extension, the springs will extend thanks to the one-way bearings attached at the junction point between the

pulleys and MR brakes' shafts. By this way, even MR brake systems were completely locked, cables wound around the pulley will not become loose and always kept taut.

- When the users release the virtual object and cut their contact, the MR brakes will be deactivated. While brakes are not active, the off-state torques in the brakes and the spring forces will be felt by the user during their finger motions in the direction of flexion. In the direction of extension, only spring forces are expected to be displayed on the users' fingertips.

3.4. Conclusion

In this Chapter, the actuation system architecture to be used for a haptic glove application is explained.

In the first section of the Chapter, the results of the studies on MR brake systems are presented. Working principles of the MR brakes are explained and they were compared with other actuators based on their advantages and disadvantages. Also, different architectures that are used in the design of these systems have been examined. As a result of the examinations, it has been revealed that rotary-type architectures display lower off-state torques and produce higher torque outputs making them better candidates compared to the linear-type MR brakes to be used in a haptic glove application. Within the rotary-type architectures, drum and multi-disc type MR brake systems stand out from other architectures. While the requirement of lesser number of parts to be produced and their manufacturability in smaller sizes with narrow tolerance ranges stand out for the drum-type architectures, high torque output in multi-disc type architectures put these architectures ahead of others.

In the second part of the Chapter, conceptual design of an effective force transmission system design was presented to inform the reader about how MR brakes are aimed to be used in a glove application and to avoid confusion before proceeding on to the MR brake design will be presented in the next chapter. Different force transmission systems on haptic gloves found in the literature were examined and compared. In line with the results obtained, the conceptual design of a transmission system in which the output force obtained from the MR brake systems will be transferred to the fingertips with

the help of cables has been started. The average finger phalanx lengths and the rotation angles occur between the phalanges during in the 3P motion were researched and a hand model was created. The design of the platform, which is planned to be placed on the hand model, has been realized and the design of a spring-based cable winding system to prevent cable slack during fingers' motion has been given.

In the next Chapter, detailed design of a magnetorheological fluid-based brake system to be used in a haptic glove's main actuation element will be given.

CHAPTER 4

MR BRAKE DESIGN

In the literature, 5 main designs architectures for rotary-type magnetorheological fluid-based brakes were adopted; which can be classified as drum-type, disk-type, inverted drum-type, T-shaped and multi-disk type. Within these, multi-disk and T-shaped designs exceeds in torque/volume ratio; however, dimensional requirements and mechanically complex shaped parts in small volumes makes them nearly impossible to manufacture for haptic glove applications that have limited space over hand and the system volume required to be kept as small as possible. By considering manufacturing capabilities and necessity of the parts with small volumes, the drum type is selected to continue with.

The main disadvantage of drum-type MR brakes is their low torque-to-mass ratio compared to other architectures. The main reason for this situation is the magnetic flux passing over MR fluid that is required to create the braking torque, passes over the fluid only 2 times (when entering and leaving), and the MR fluid reaches higher yield strengths only at these regions. As a common option, surface area of the rotary part (in terms of length and radius) might be increased to obtain higher torque output from a drum-type MR brake. However, due to the limited area in the dorsal side of the hand, this solution is not suitable.

In this section, details of an improved drum-type MR brake design capable of producing high torque output are presented. In the design criteria, the problems observed in the gloves and the problems related with the drum-type MR brake architecture were combined. After the situations that need to be solved given in the design requirements have emerged, the mathematical models required for the design of the brake system have been created and the designs have been carried out. At the end of the section, the results of the magnetic analyzes performed on the developed designs are given and the predicted system properties are presented.

4.1. Design Requirements

The design criteria for the MR brake to be developed and used in haptic glove applications are related with the dynamic torque range, weight and size, respectively. Beside these, reducing the off-state torque and implementation of a solution against the sticky wall problem are also important issues to be dealt in the design.

Dynamic torque range is a feature that indicates the range between the lowest and highest torque output that the system will exhibit based on the current supply state. The minimum torque that the brake system will display is determined only by the viscous and dynamic friction when no current is supplied to the system and known as off-state torque, while the maximum output torque is the highest achievable value when the current is supplied to the system. Based on the radius of the pulley attached to the shaft of the MR brake system, it is aimed for the brake system to produce at least 7 N of resistive force to be supplied to the users' fingertips while pinching an object with their thumb, index and middle fingers.

In order to provide comfort to the user wearing the glove, the weight of the brake systems to be carried on the dorsal side of the hand should be kept minimal so that the users should not feel impeded during virtual reality interactions. Besides the fact that the brake system should be lightweight, there exists a relationship between the dynamic torque capacity and the weight of the system which is an important metric to indicate the performance of an MR brake and is known as the torque-to-mass (TMR) ratio. Based on the work of Qin et al. (2018), typical TMR value for drum-type MR brake is revealed to be 1.4 N.m/kg. It was aimed that the weight of the MR brake should not exceed 250 grams and besides, at least 2.8 N.m/kg of TMR aimed to be achieved within the improved design based on the drum-type architecture.

Dimensional requirements cover the outer diameter and the total length of the brake system. The effect of the yield strength of the MRF over the braking torque is directly proportional to the length and the square of the radius. Therefore, a low-length and high-diameter brake system aimed to be obtained. To be placed over a platform who will be carried over the dorsal side of the hand, it was aimed that maximum allowable length and diameter of the brake systems must not exceed 40 mm and 60 mm respectively.

It was mentioned that the MR brake systems suffers from a resistance torque resulting from viscous and dynamic frictions even no current is supplied to the system. This minimum torque value of the system is known as the off-state torque and determines the minimum impedance of the system. When previously developed brake systems were examined to determine the cause for the high off-state torque, it was seen that the friction between rotary and static parts related with the dynamic sealing elements contributes off-state torque the most. In order to reduce the off-state torque, a new sealing design is aimed to be developed where conventional sealing elements could be extracted from the system.

The last design requirement is, to implement a solution to the solve the stiction problem in the designed MR brake so that the resistive force feedback is going to be felt by the users in only flexion direction of their fingers. A similar approach to the the work of Karabulut (2017) is aimed to be utilized in which one-way bearings were used to solve this problem. In Karabulut's designs, one-way bearings were assembled inside the brake system so that, in order to reverse the braking direction, complete disassembly of the parts is required. In the developing MR brake systems, it was aimed to place one-way bearings in the junction point of the brake system and the force transmission system so that, in any case that the braking direction is required to be switched, it could be switched easily without the need of the disassembling any parts of the system.

The design requirements for the developing MR brake is given in Table 8 to provide clarity to the reader.

Table 8: Design requirements for the MR brake to be developed.

Numerical Requirements	
Maximum allowable diameter (mm)	60
Maximum allowable length (mm)	40
Minimum force output (N)	7
Maximum allowable weight (gr)	250
Non-numerical Requirements	
Stiction problem have to be solved.	
Off-state torque should be kept in minimum.	

4.2. Mathematical Model

The braking torque obtained in magnetorheological fluid-based brake systems depends on two main factors. These factors are the dynamic yield stress and the viscosity of the MR fluid, respectively. Bingham plastic model is used to model the behavior of the total yield stress of magnetorheological fluids under varying magnetic flux and this value is calculated using the following formulation:

$$\tau = \tau_y(H) + \eta \frac{\omega r}{z} \quad (1)$$

- τ: $Total\ yield\ stress.$
- $\tau_y(H)$: $Dynamic\ yield\ stress\ of\ MR\ fluid.$
- η: $Viscosity\ of\ MR\ fluid.$
- ω: $Angular\ velocity.$
- r: $Radial\ position.$
- z: $Fluid\ gap\ within\ rotating\ and\ stationary\ parts.$

While the first term in the right-hand side Equation 1 indicates the dynamic yield stress of the MR fluid under the effects of magnetic field, the second term indicates the shear stress ratio.

In haptic glove applications, the effects of angular velocity and viscosity is assumed to be negligible, considering that the parts in the brake system will rotate very slowly due to the small distance covered during the flexion-extension movements of the fingers and the slow movement of the fingers to feel the interaction forces during the interaction of the user with the objects in the virtual or distant environment. Therefore, Eq.1 can be simplified as:

$$\tau = \tau_y(H) \quad (2)$$

In order to determine the braking torque, following calculations have to be performed. First, the force must be derived from yield yield stress by using Eq. 3.

$$F = \tau_y(H)A \quad (3)$$

$$A = wh \quad (4)$$

$$w = 2\pi r \quad (5)$$

- $A: Surface\ area\ of\ the\ rotating\ parts.$
- $w: Circumference\ of\ the\ rotating\ parts.$
- $h: Height\ of\ the\ rotating\ part.$

By substituting Eq. 5 into Eq. 4 and then into Eq. 3, Eq. 6 is obtained.

$$F = \tau_y(H)(2\pi rh) \quad (6)$$

After obtaining the force, force-torque conversion is done by substituting Eq. 6 to Eq. 7.

$$T = Fr \quad (7)$$

$$T = \tau_y(H)(2\pi rh)r \quad (8)$$

$$T = \tau_y(H)(2\pi r^2 h) \quad (8)$$

In theory, Eq. 8 is valid; however, in practical applications there is an additional torque component that represents the frictional torque which affects the impedance of the system.

$$T = 2\pi r^2 h\, \tau_y(H) + T_{friction} \quad (9)$$

In Eq. 9, r and h are design parameters and can be manipulated. However, the determination of $\tau_y(H)$ is not a straightforward task to perform since there are no exact analytical formulations. In order to determine $\tau_y(H)$, procedures listed below should be followed:

- A coil has to be designed to generate magnetic field and control the braking torque under various currents.
- Numerical simulation (Magnetostatic analysis) has to be performed in order to determine magnetic flux passing over the MR fluid.
- After obtaining magnetic flux (B), magnetic field strength (H) should be determined via using specified B-H curve of the magnetorheological fluid.

Then, yield stress values corresponding to the H previously obtained has to be determined via investigating yield stress-magnetic field strength curve of the MR fluid.

4.3. Design of the Brake System

After the development of the mathematical models, the design of the brake system was started with the material selection for the sub parts. The material choices of the parts in the brake system directly affect the behavior and performance of the system under the magnetic field. In order for the braking torque to be created, the current is supplied through the cables wound on the coil and as a result, a magnetic field is created. The generated magnetic field will flow over the magnetic flux path based on the magnetic permeabilities of the materials on the route. Magnetic permeability is a material property that indicates how much a material can be magnetized under the influence of a magnetic field. The flux vectors created by the magnetic field want to flow over materials with higher magnetic permeabilities, while avoiding being directed on materials with low permeabilities. Thanks to parts with different magnetic permeability values that their materials possess, magnetic flux density vectors can be concentrated over the MR fluid while transitioning from static parts to rotating parts. During this transition, magnetic flux vectors must be aligned vertically between the rotating and fixed parts. If the direction of the magnetic flux vectors between the surfaces cannot be arranged correctly, the desired braking torque response cannot be obtained, no matter how strong the magnetic field is.

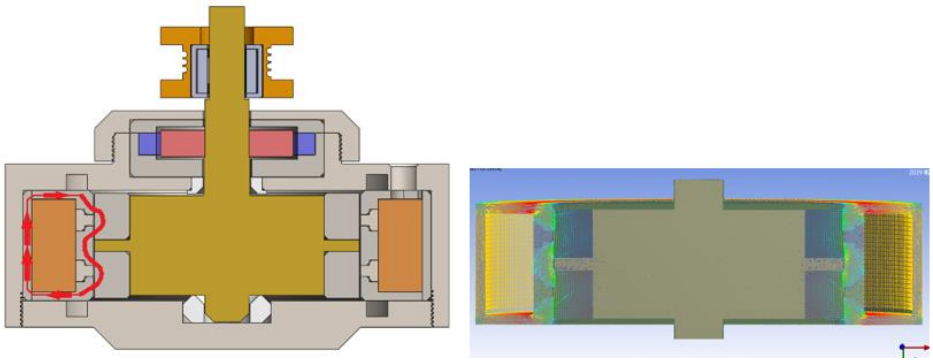

Figure 54: Magnetic flux path created by current.

In the developed brake system, 7 different materials have been used for different purposes in relation to the places where they will be used. Non-magnetic parts' materials are selected as aluminum (6013 grade), PTFE (polytetrafluoroethylene, Teflon), brass, copper, ABS (Acrylonitrile Butadiene Styrene); and those for which magnetic

permeability is desired are manufactured using SAE 1020 steel (C20). Magnets to be purchased except for the manufactured parts were chosen as NdFeB (neodymium) material. The places where the relevant materials are used based on their properties are as follows:

• Brass and Teflon are used as shaft and journal bearing for system due to their low coefficient of friction and high strength,

• Copper, in electrical cables where the coil part will be wound,

• Aluminum, in the magnetic flux path and outer cases/covers since they are easy to manufacture/process and have low density and low magnetic permeability,

• SAE 1020 steel, in magnetic flux route and sealing parts due to its high magnetic permeability,

• Neodymium magnets, in the sealing part, due to their strong permanent magnetization (1~1.5 T) without the need for current,

• ABS is used in the part of the pulley attached at the end of the shaft where the cables will be wound, due to its high strength and easy production/changeability when necessary from 3D printers.

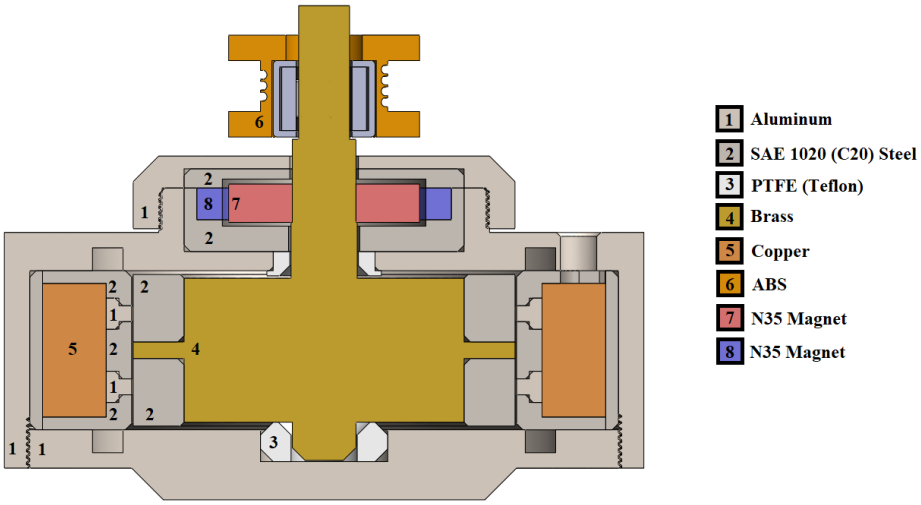

Figure 55: Part-material information.

After the materials for each part were assigned, the design of the parts was started. After the first few iterations of the design were carried out, the manufacturer was

contacted and their opinions were taken based on their manufacturing capabilities. As a result of the negotiations, it was decided to keep the number of aluminum rings aimed to be used in the design as two at most (although introducing more non-magnetic parts to the magnetic flux path increases the maximum torque output). The reasons behind this decision are these parts are difficult to process within narrow tolerance limits due to their high diameter/thickness ratio and they possess the risk of getting damaged during assembly due their low thicknesses. After the number of the aluminum rings were decided, a study was performed to determine the parameters yielding best results. During this study, it was aimed to maximize the magnetic flux density passing over the MR fluid within a limited area, thus the braking torque. The parameters needed to be determined are:

- The thickness, height and shape of the aluminum rings,
- The thickness height and shape of the steel discs attached on the shaft,
- The distance between the non-magnetic parts (aluminum rings and the brass shaft's thin section) on the magnetic flux path.

When the results of the study are examined, following conclusions were done:

- Increasing the thicknesses of the stationary parts on the magnetic flux path (Figure 56- Parts 1,2,3,5) will reduce the magnetic flux density passing over MR fluid since it reduces the area where the coil cables wound and increase the area where the magnetic field strength to be distributed over a wider section, reducing the overall magnetic flux density.

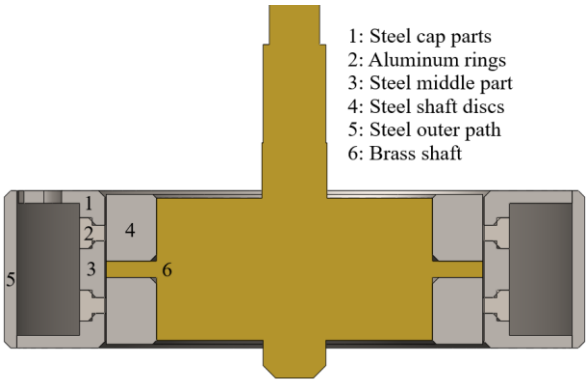

Figure 56: Internal parts of the MR brake system.

- Increasing the thickness of the steel shaft discs will increase the magnetic flux density passing over the MR fluid to a point where further increase in the thickness will have no effect since the steel is magnetically saturated.
- The height of the non-magnetic parts in the magnetic flux path and the distances between them are strongly dependent on each other. If the relationship between the heights of the relevant parts and the distance between each other cannot be established correctly, the magnetic flux density passing through the liquid decreases significantly.
- The shape of the steel shaft discs detected to have no significant effect on the magnetic flux density passing over the MR fluid. However, the shape of the aluminum rings (and the parts connected to the aluminum rings) affects the magnetic flux obtained over MR fluid. Instead of using discs with rectangular cross-sections, by using discs with T-shaped cross-sections the magnetic flux density (and thus, the braking torque) was increased by ~22%.

Dimensions for maximizing the magnetic flux density obtained over the MR fluid in a limited area are obtained as given in Table 9.

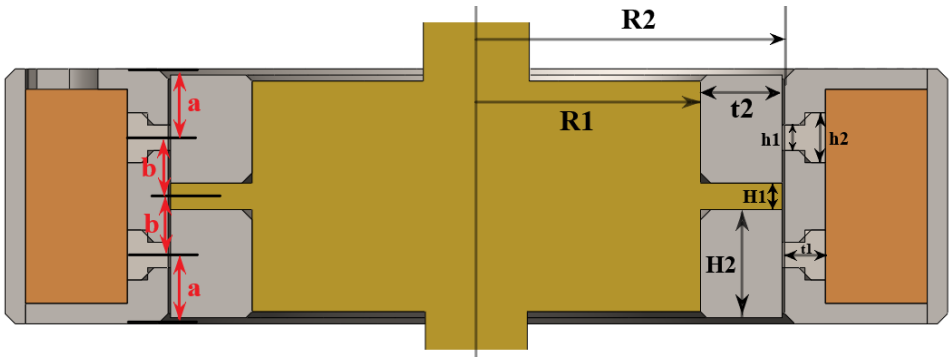

Figure 57: Dimensional parameters used in the maximization of braking torque.

In the light of the magnetic analyzes performed after the creation of solid models whose dimensions were obtained as a result of the study, it was revealed that the developed MR brake system can provide an output torque of 587 N.mm at 1 A operating current.

Table 9: Dimensions of internal parts yielding best results.

Parameter	Best Result (in mm)
a	3.375
b	2.875
R1	11
R2	15.125
H1	1.30
h1	1.25
h2	2.45
t1	2
H2	5.30
t2	4

As mentioned earlier, with the use of MR fluid-based brake systems in haptic devices, the sticky wall or stiction problem occurs. In this problem, when the brake is activated after an input, the rotational motion of the brake system is restricted in both clockwise and counterclockwise directions. Due to the locking of the system in both directions, users must overcome the braking force provided by the brake system when they want to cut the contact with the object they are interacting with. For haptic glove applications, the direction that the user is aimed to supplied with the braking torque is in the flexion motion of the fingers while grasping an object. During the extension of the fingers, the object being held is released and no torque should be applied to the fingertips of the user. As it was mentioned in the Chapter 3, the resistive torque obtained from the brake systems to the fingertips of the users by using cables. In order for cables to be wound around, a pulley is needed. Within the designed pulley, a one-way bearing is

placed and the connection is established in a way that rotational freedom in the extension direction of the fingers is achieved even the brake system is still supplied with the current.

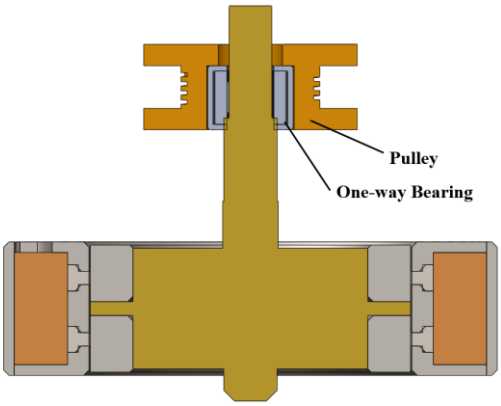

Figure 58: The use of the one-way bearing to overcome the stiction problem.

By placing the one-way bearing to the outside of the system, following advantages were obtained:

- Reduction of assembly difficulties related to concentricity has been achieved.
- Thanks to the fact that the bearing is in an easily accessible position, in cases that require maintenance or repair, the necessary operations can be carried out without disassembling the whole system. Additionally, when the brake system is aimed to be used for a different application, removing or reversing the direction of the one-way bearing can be achieved easily.

4.4. Sealing Design

During the examination of the previously developed MR brake designs in IZTECH Robotics Lab., it was noted that there exist an off-state torque caused by friction between the rotating and static elements due to the dynamic sealing elements used to prevent MR fluid from leaking out from the casing. In order to reduce the off-state torque, an alternative solution for sealing design is researched. In the proposed solution, sealing is achieved by using only the properties of the magnetic fluid, without using any mechanical elements. In the majority of the researches in the literature, ferrofluids were

used as magnetic fluids and thus caused the method to be called as “ferrofluidic sealings”. However, magneto-rheological fluids can also be used and found to be more effective due to their variable yield strength and resistance they possess against higher pressure differentials. In the following sections, detailed information about magnetic fluid sealings were given and analyzed further.

4.4.1. Magnetic Fluid Sealings

Magnetic fluid sealings (Ferrofluidic sealings-FFS and magnetorheological fluid sealings-MRS) are mechanisms applied on rotary equipment to enable rotary motion while preventing the leak of fluids or gases inside the equipment to the outside media. Their principle of operation is based on the creation of a liquid ring, which is formed between the intersection of the outlet of the equipment and outside media, that is kept in place with the help of magnetic fields provided by permanent magnets (PM) and pole pieces.

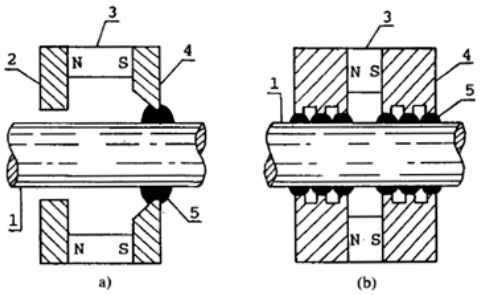

1- Shaft, 2- Flux-return Ring, 3- Permanent Magnet, 4- Pole Piece, 5- Ferrofluid

Figure 59: Single (a) and Multi-stage (b) FFSs

(Source: Jibin et al., 1992)

These combinations of PMs and pole pieces are called sealing stages. The magnetic forces provided by PMs are transferred to the gap between the shaft and pole pieces and cause the magnetic fluid situated in this gap to take shape as a fluid O-ring. The main factor in these sealings that prevent the leakage is known as critical pressure. The critical pressure value determines the capacity of the seal that liquid O-ring structure

can withstand a specific range of pressure difference between inner and outer media without any discontinuity occurred in the ring shape and cause leakage. As the critical pressure increases, the seal can withstand greater pressure differentials between inside and outside media (Jibin and Yongping 1992; Liu, Cheng, and Yang 2005; Szczęch 2019).

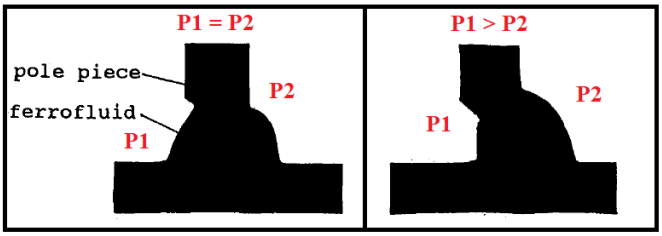

Figure 60: Ferrofluid behavior under different pressures.

(Source: Jibin et al., 1992)

There are two distinct types of failures occur in FFSs and MRSs which are "breakthrough" and "wastage".

In the breakthrough process, the reason of failure is the continuous increase of pressure at one side which disturbs the magnetic fluid O-ring continuity. When the pressure difference between the two media exceeds the critical pressure, the magnetic fluid continuity between the surfaces is disrupted and the part separating the media from each other disappears. If the critical pressure is exceeded slowly, the magnetic fluid can realign and maintain continuity after the pressure differential falls below the critical value again.

In the process of wastage, instead of increasing pressure in one side, the failure is occurred due to continuous removal of magnetic fluid by the other fluids in the sealing environment in long-term uses under a pressure lower than critical pressure.

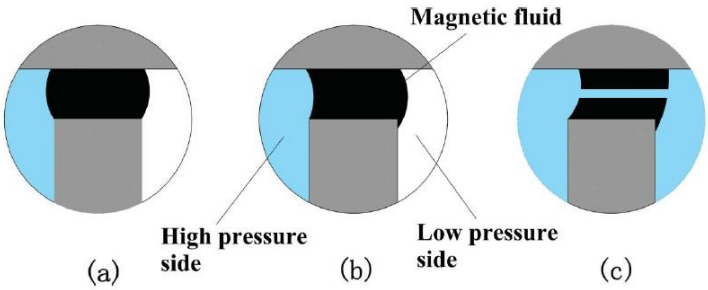

Figure 61: Process of Breakthrough in FFS and MRS

(Source: Li et al., 2018)

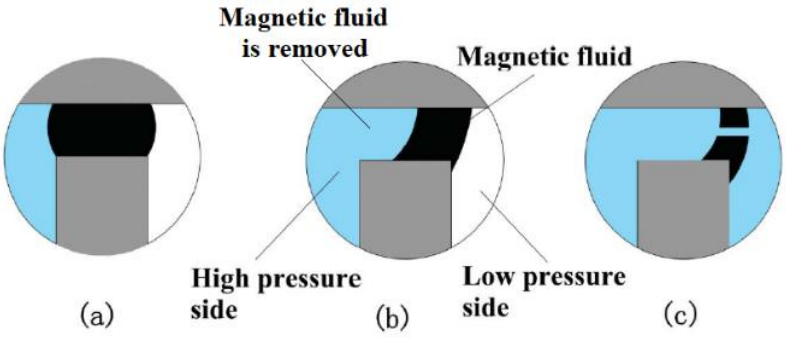

Figure 62: Process of Wastage in FFS and MRS

(Source: Li et al., 2018)

Since magnetic fluid seals are mostly used for vacuum applications to seal the oil around the shaft rotating with high speeds, both breakthrough and wastage process occurs. However, by using magnetic fluid seals together with an MR brake developed for haptic glove applications, following advantages were taken:

- Since the pressure difference between outer media and the inside of the brake system will be quite low compared to the vacuum applications where high-pressure differentials might occur, the chances of breakthrough failures are reduced.
- Even the magnetic fluid is removed as seen in process of wastage, since the fluid in the brake system that is sealed is also magnetic fluid, the chances of the wastage failure are also reduced.

4.4.2. Mathematical Formulation of the Critical Pressure

Ferrohydrodynamic equations were used to express the behavior of magnetic ferrofluids and MR fluids since the flow is greatly influenced by magnetic forces affecting the magnetic particles carried by the fluid (Szczęch 2019; Szczech and Horak 2017; Jibin and Yongping 1992).

In order to determine the critical pressure, FHD Bernoulli equation will be used. This equation is a generalized Navier-Stokes equation by also taking the magnetic properties of the fluid into account and can be expressed as:

$$\rho\left(\frac{\partial v}{\partial t}+\mathbf{v}.\nabla\mathbf{v}\right)=-\nabla\mathbf{p}^{*}+\mu_0 M\nabla H+\eta\nabla^2\mathbf{v}+\rho\mathbf{g} \quad (11)$$

As can be seen in the equation that, in order to move a magnetic fluid against a pressure gradient, the magnetization of the fluid or the gradient of magnetic field has to be controlled. Researchers also made additional assumptions in order to simplify the solution further:

- Incompressible, Newtonian fluid $(\eta = 0)$
- Steady-state flow ($\frac{any\ parameters}{dt} = 0$)
- Magnetic field is magnetostatic ($\nabla \times \boldsymbol{H} = 0$)
- Magnetization is collinear with the field($\boldsymbol{M} \parallel \boldsymbol{H}$)
- Irrotational flow field($\nabla \times \boldsymbol{v} = 0$)
- Gravity is constant
- Fluid without hysteresis
- Magnetization is not affected by temperature

These assumptions reduce the equation to the following form:

$$\mathrm{p}^{*}+\frac{1}{2}\rho\mathrm{v}^2+\rho\mathrm{gh}-\mu_0\int_0^{\mathrm{H}}\mathrm{MdH}=constant \quad (12)$$

Where:

- M magnetization intensity of FFs or MR fluids, $\mathrm{A/m}$;

- μ_0 vacuum permeability, $\mu_0 = 4\pi \text{ x } 10^{-7}$ H/m;
- H external magnetic field strength, A/m.

With further assumptions that neglect the effects of gravity, velocity and surface tension forces; the critical pressure for one stage (with "N" number of sealing stages in total) can be found as:

$$\Delta p_{cri} = \sum_{i=1}^{N}(p_1 - p_2) = \mu_0 \sum_{i=1}^{N} \int_{H_{imin}}^{H_{imax}} M dH \quad (13)$$

In most cases, ferrofluid used for the sealing is kept at magnetic saturation by using strong permanent magnets and proper magnetic circuit design. Because of this reason, the equation for the critical pressure can be expressed as:

$$\Delta p_{cri} = \sum_{i=1}^{N}(p_1 - p_2) = \mu_0 \sum_{i=1}^{N} \int_{H_{imin}}^{H_{imax}} M dH$$
$$= \sum_{i=1}^{N} \int_{B_{min}}^{B_{max}} M dB \approx \sum_{i=1}^{N} M_s(B_{imax} - B_{imin}) \quad (14)$$

- p_1 & p_2: The higher and lower pressure of each side of the ith pole teeth;
- μ_0: Vacuum permeability;
- M: Magnetization of the magnetic fluid;
- M_s: Magnetization saturation of the magnetic fluid;
- N: The number of pole teeth;
- H_{imax} & H_{imin}: The maximum and minimum magnetic field intensities under the i pole teeth;
- B_{imax} & B_{imin}: The maximum and minimum magnetic flux densities under the i pole teeth.

It can be concluded from Eq. 14 that, in order to increase the critical pressure and the sealing capacity of the FFS, magnetic inductance difference obtained in both sides of the magnetic fluid sealing ring should be maximized. This can be achieved by either using

a magnetic fluid with high magnetization value or applying strong magnetic fields that higher magnetic flux densities are applied to the ferrofluid.

Since ferrofluids are considered as Newtonian fluids, their yield stresses are completely ignored when sealing capacity is calculated. However, when magnetorheological fluids are going to be used, elasto-plastic properties of MR fluids must be taken into consideration since the critical pressure is highly associated with both their magnetization and yield stress. Zhang et al. (2018) was examined both magnetorheological fluids and ferrofluids in their research to find their static seal performances.

In terms of critical pressure, magnetorheological fluid-based seals (MRS) possess similar magnetic features but they also provide elasto-plastic performance when they exposed to an external magnetic field. The sealing capacity (critical pressure) for MRSs are composed of two parts which are related with magnetic (p*) properties and variable yield stress (p') of the MR fluids.

$$\Delta \mathrm{p}_{cri} = p^* + p' \quad (15)$$

$$\mathrm{p}^* = \sum_{i=1}^{N} (p_1 - p_2) = \mu_0 \sum_{i=1}^{N} \int_{\mathrm{H_{imin}}}^{\mathrm{H_{imax}}} \mathrm{MdH} \quad (13)$$

$$p' = 2\tau_0 \frac{h}{b} \quad (16)$$

Where:

- τ_0 field dependent variable yield stress of MR fluids;
- *h* length of the sealing clearance;
- *b* fluid gap.

To calculate the critical pressure for the sealing stages, maximum and minimum magnetic flux densities under each tooth should be determined first. Finite element method (FEM) analysis through numerical simulation programs used to determine the magnetic flux density distribution for the designed sealing geometry.

4.4.3. Design

As stated in the beginning of the section, the friction force occurred on the dynamic sealing elements used between the rotating and stationary parts does the highest contribution to the off-state torque observed in MR brake systems. In order to take out dynamic sealing elements and reduce the off-state torque, a sealing design was developed in which the MR fluid within the system is used as a sealing element instead of dynamic seals. FFS and MRS structures mentioned in Section 4.4.1 cannot be directly applied in the developed system due to one minor and one major issue:

• Minor issue: Precise tolerances are required to manufacture and fit tooth structures into the brake design which will increase the cost significantly.

• Major issue: In order to create a magnetic flux path between the teeth and the shaft, the shaft must also be manufactured from a magnetically permeable material. If the shaft is produced using magnetic permeable material, the magnetic flux route formed inside the brake system (more specifically, in the area where the braking torque is generated) is disturbed, causing the brake to act as a standard drum-type MR brake and reducing the output torque significantly.

Based on manufacturing issues and considering these problems, an effective sealing system consisting of only 4 parts was designed. In the developed design, two axially polarized neodymium magnets and 2 SAE 1020 steel parts were used as shown in Figure 63.

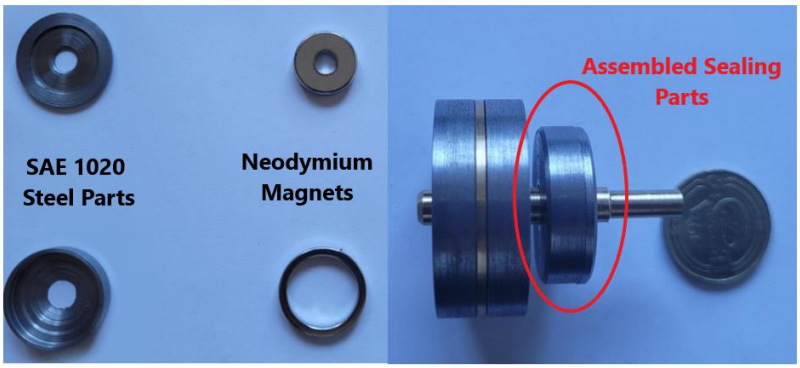

Figure 63: Parts used for sealing (left) and their assembly (right).

The magnets are placed on the shaft and the main body of the brake system, with the north and south poles directed towards each other, as shown in the Figure 64.

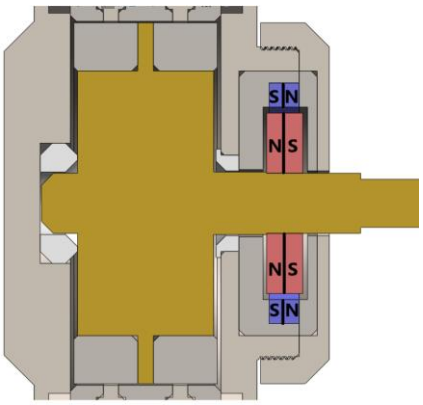

Figure 64: Inner and outer magnet polarizations within the MR brake.

The MR fluid, which fills the area between these magnets, functions as a liquid O-ring by aligning in the direction of magnetic flux path created by neodymium magnets' magnetic fields, as shown in Figure 65. Based on the magnetic analysis results (See Chapter 4.5.2), MR fluid is aligned between the surfaces, indicated with orange region in Figure 65, and magnetically saturated. In order for the fluid to leak outside the brake system, the MR fluid chains between the surfaces have to be broken down first. It has been revealed that, 965 kPa of pressure differential is required to observe leakage of the fluid.

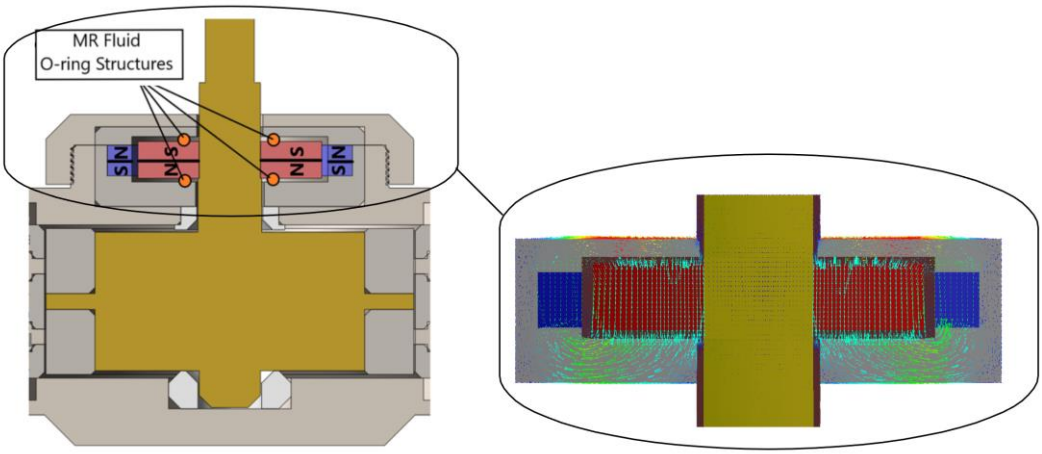

Figure 65: MR fluid alignment for O-ring structure (left) and magnetic flux path created by neodymium magnets (right).

4.5. Finite Element Analysis

In this section, magnetic analysis results for the designed MR brake system will be given. Analysis results for the brake and sealing parts were presented separately since the braking torque obtained from the system dynamically controlled by the magnetic field generated by external current supplied to the coil, whereas the sealing of the MR fluid is handled by static magnetic fields that neodymium magnets have.

4.5.1. Analysis Results for Brake Part

The aim of the magnetic analysis is to get information about the output of the system based on the given inputs under certain conditions. Before manufacturing the parts of the system, firstly, the magnetic analysis of the system was carried out using the magneto-static analysis package of the ANSYS software in order to get a preliminary idea of the desired torque output to be obtained when the current is supplied to the coils. The inputs for the magnetic analysis program are, system's CAD model, the magnetic properties of each material that are situated within the system, the number of electrical cable turns wrapped around the coil and the current passing through the cable. With these inputs, the desired output from simulation program is the magnetic flux density passing over the MR fluid. With the knowledge of magnetic flux density, magnetic field strength acting upon the fluid and thus the resultant yield strength value of the fluid is obtained. As the last step, the force and torque output that the system can provide is calculated by using the yield strength values and solid model information (such as surface area and radius) by using Eq. 9 given in Section 11.1.2.

After importing the system's CAD model to the simulation program, material selection for each part with their respective magnetic features performed. As mentioned in Section 3.3, the MR brake system consists of aluminum, Teflon, brass, copper, ABS, SAE1020 materials and MRF-140CG as MR fluid. Since aluminum, Teflon, brass and copper are non-magnetic materials, their relative permeability is equal to 1. However, SAE1020 and MRF-140CG are non-linear ferromagnetic materials so that they do not possess constant magnetic permeability values. The non-linear B-H curves

given in Figure 66 for SAE 1020 and Figure 67 for MRF 140-CG determines their behavior under magnetic field and were used as inputs in the simulation program respectively.

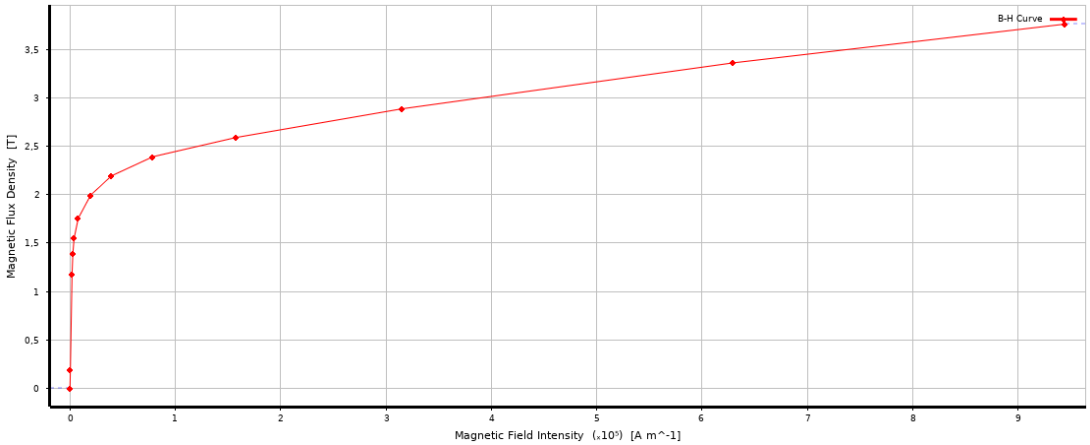

Figure 66: Non-linear B-H curve of SAE 1020 (C20) Steel

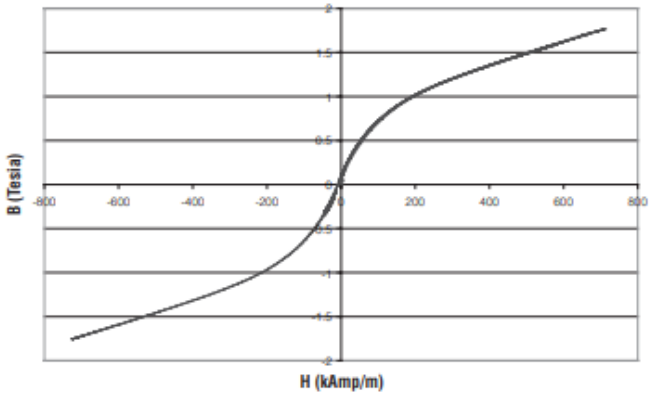

Figure 67: Non-linear B-H curve of MRF 140-CG

After the material information is entered into the system, the number of turns to be made on the coil and the current that will pass over the cables must be entered. Coil design is an issue that directly affects the magnetic flux passing through the MR fluid. If more wires are wound on the coil or the current through the coiled wires is increased, the magnetic flux acting on the MR fluid and thus the braking torque increases. The requirements to consider for these two conditions are:

- As the cables get thinner, their internal resistance increases and the current they can carry decreases. When thinner cables are used, due to their high resistance,

problems such as heating the system and damaging the cables may be encountered.

- More cable winding can be done by enlarging the coil part by keeping the cable to be wound the same; however, the diameters of the outer parts holding the coil part must also be enlarged proportionally. Therefore, in order to make such an update, restrictions such as the limited space on which the brakes can be placed on the hand and the desire to keep the weights of the brakes to a minimum must be taken into account.

Considering these factors, during the design of the coil, a study was carried out in order to maximize the current passing over the cables together with the number of turns in a limited area. The aim of this study is to see which cables can maximize the magnetic flux passing through the fluid when wound on the coil. American Wire Gauge (AWG) 22, 24, 26, 28, 30, 32, 34 standard cables were analyzed and the area for these wires to be wound is kept as Ø34.25 mm in minor diameter (R=17.125 mm), 5 mm in width (H) and 10.5 mm in height (L). The parameters and results for this study are given in Figure 68 and Table 6.

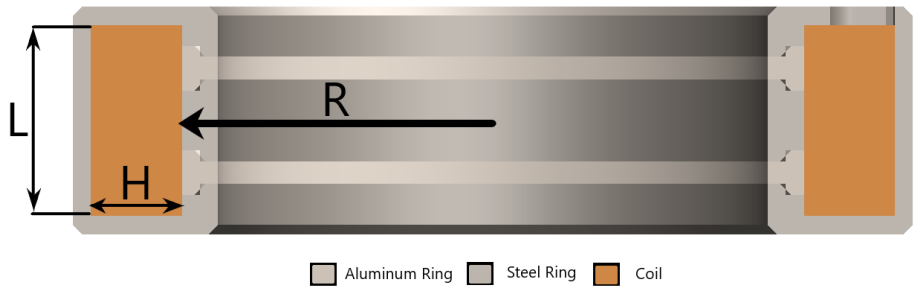

Figure 68: Dimensional Parameters For Wire Selection for Coil

When the results in Table 10 are examined the highest magnetic flux values were obtained when AWG 26, 28 and 30 cables were used, corresponding to 378.66 mT, 378.97 mT and 378.31 mT, respectively. AWG 28 and AWG 30 cable selections were eliminated due to the risks of over-heating and damage during transportation, assembly and movement of the system due to their thin diameters and high electrical resistances. As a result, AWG 26 cables were selected as coil wires; where the input parameters for

simulation software are 250 number of turns to be wound and 1.30 A maximum allowable current.

Table 10: Determined Coil and Wire Parameters

Coil Features				
R (mm)	H (mm)	L (mm)		
17,125	5,000	10,500		
AWG Wire Features				
AWG	Diameter (mm)	Cross-sectional Area (mm^2)	Resistance Per Unit Length (mΩ/m)	Maximum Allowable Current @60° (A)
22	0,644	0,326	53,0	3,00
24	0,511	0,205	84,2	2,10
26	0,405	0,129	133,9	1,30
28	0,321	0,081	212,9	0,83
30	0,255	0,051	338,6	0,52
32	0,202	0,032	538,3	0,32
34	0,160	0,020	856,0	0,18
Magnetic Analysis Results				
AWG	Number of Turns	Total Resistance (Ω)	Voltage Requirement (V)	Average Magnetic Flux @ MR Fluid (T)
22	136	0,77	2	0,36963
24	180	1,63	3	0,37564
26	300	4,32	6	0,37866
28	480	11,00	9	0,37897
30	779	28,38	15	0,37831
32	1224	70,90	23	0,37733
34	2015	185,59	33	0,36672

As a result of the magnetic simulation performed after the necessary information about the coil is entered, the regional results of the magnetic flux density passing over the MR fluid are as seen in Figure 69.

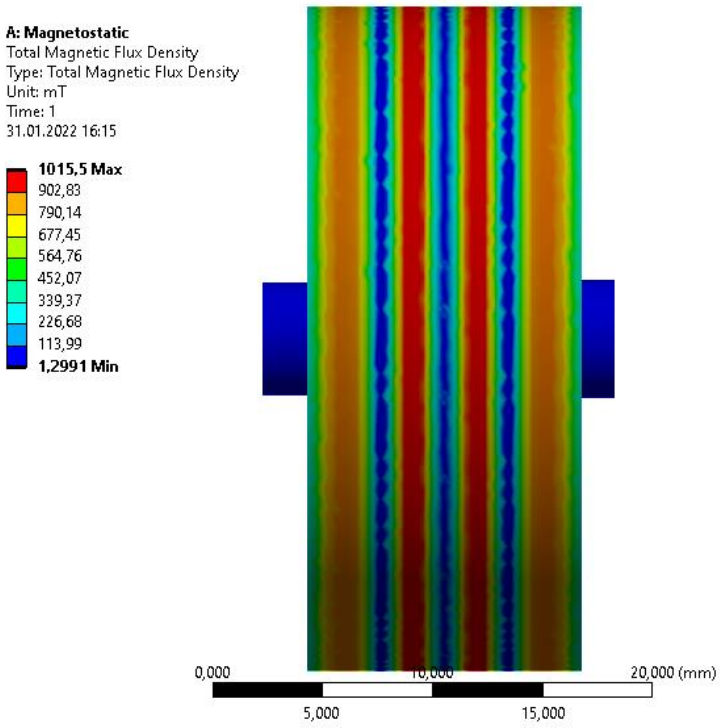

Figure 69: Magnetic flux density passing over MR Fluid

Magnetic flux density vectors illustrated in Figure 70 provide information about the magnitude and direction of magnetic flux density acting upon the MR fluid situated between rotary and stationary parts. The highest magnetic flux density values on the MR fluid were obtained while the magnetic flux vectors on the flux path is transitioning from/to parts with low magnetic permeability (aluminum and brass) to/from parts with high permeability (SAE 1020) and are approximately 1 T. The lowest magnetic flux values were obtained in the regions where the magnetic flux vectors move on the flux path on the highly permeable material before transition happens, and on the surfaces parallel to the magnetic field created by the coil, and it is approximately 1 mT.

The average magnetic flux density acting over the MR fluid and affecting the braking torque (magnetic flux density vectors' radial components only) was found to be 620.97 mT (0.62 T). As a result of the calculations obtained after the simulations, by using the properties of MRF-140-CG fluid given in Figure 71 and Eq. 9, the braking torque that the designed braking system can produce is calculated as 587.24 N.mm. The features of the designed MR brake is given in Table 11.

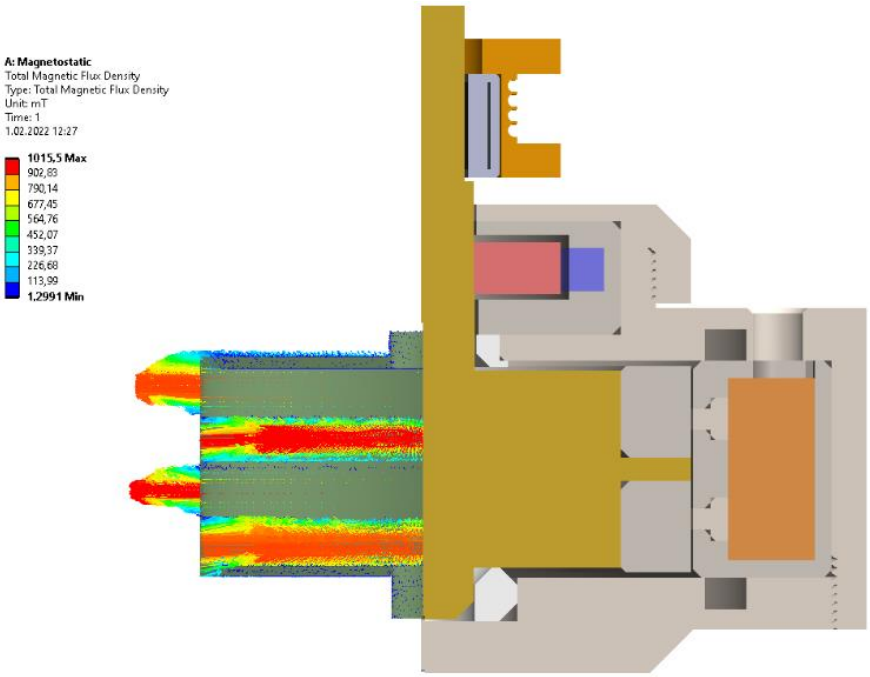

Figure 70: Magnetic flux lines passing over MR fluid situated between rotary and static parts.

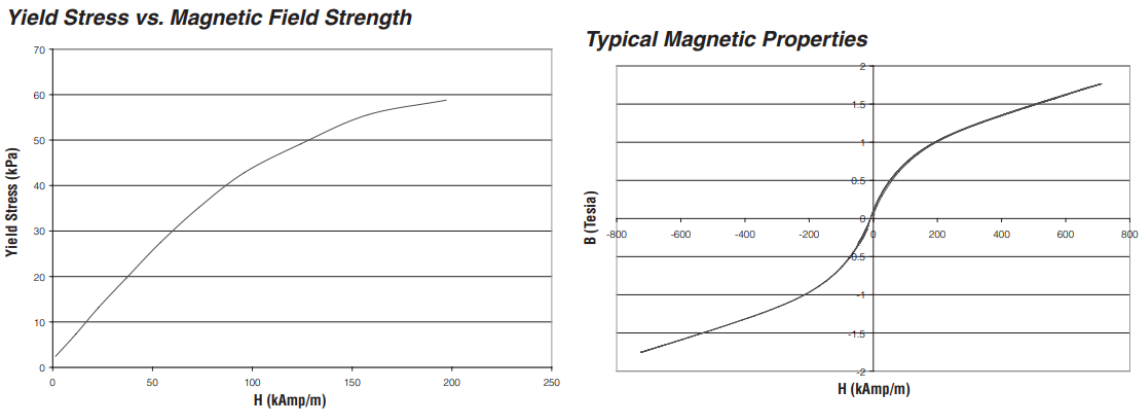

Figure 71: MRF 140-CG Specifications.

Table 11: Final MR Brake Parameters.

Brake Radius (r)	15 mm
Brake Height (h)	12,5 mm
AWG Wire Type	26
Maximum Available Current	1,3 A
Number Of Turns	250
Calculated Internal Resistance	4,32 Ω
Required Voltage	5,62 V
Average Magnetic Flux (B)	0,621 mT
Corresponding Magnetic Field Strength (H)	209,3 Amp/mm
Yield Stress, $\tau_y(H)$	36,76 kPa
Expected Output Torque (T)	587,25 N.mm

4.5.2. Analysis Results for Sealing Part

When the equations derived in the previous sections (3.4.3) are examined, it is necessary to calculate the critical pressure that the O-ring structure formed by the MR fluid between the magnets can withstand without breaking down. The equation sets to be used for critical pressure calculation include Equation 13, 15, and 16.

$$\Delta p_{cri} = p^* + p' \quad (15)$$

$$p^* = \sum_{i=1}^{N} (p_1 - p_2) = \mu_0 \sum_{i=1}^{N} \int_{H_{imin}}^{H_{imax}} M dH \quad (13)$$

$$p' = 2\tau_0 \frac{h}{b} \quad (16)$$

When Equation 15 is examined, it is seen that there are two separate parts affecting the critical pressure. **p*** is the pressure value due to the difference between the minimum and maximum magnetic flux densities passing over MR fluid on the each side of the teeth for each sealing stages in the system. Differently, **p'** can only be obtained with the use of MR fluids instead of the ferrofluids, contains the information such as the circumference

and the gap on which the fluid settles and combines this information with the variable yield strength of the MR fluid.

In the sealing part of the designed MR brake system, the calculation of p* was performed by assuming that the tooth structures are the equally spaced sections on both inner magnet surface and corresponding face that links the outer magnet to the magnetic flux path via steel parts with high magnetic permeability. Twenty points with 0.25 mm steps were taken for the MR fluid attached to the inner magnet surface. Points corresponding to these points on the opposing surface were also determined and selected. Magnetic flux density values on these points were obtained were given in Figure 72.

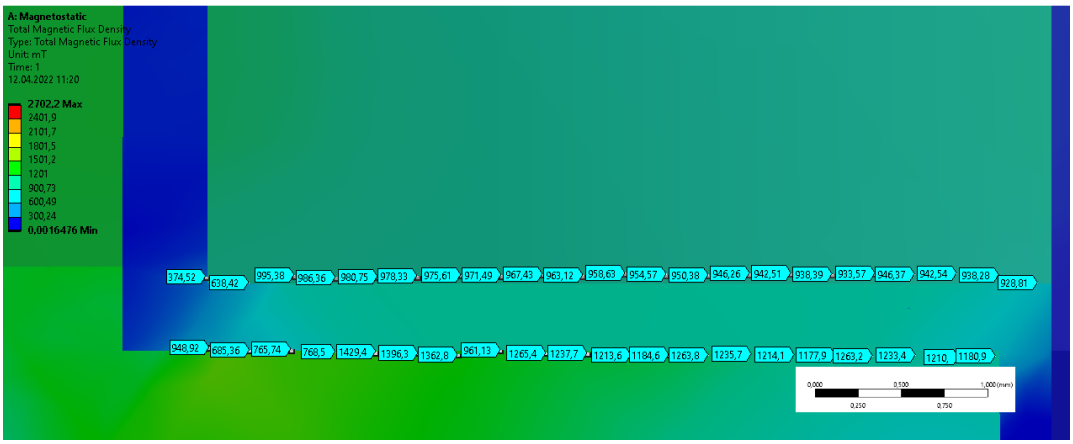

Figure 72: Magnetic flux densities of selected points with 0.25 mm steps.

In order to apply these values into the Equation 13, conversion from magnetic flux density to magnetic field strength has to be performed. Additionally, magnetization saturation of the MR fluid (MR 140 CG), was determined. For both operations, specifications given by LORD Company were followed (given in Figure 71) and following tabular data is generated for each datum.

As the results given in Table 12 are examined, the average **p*** value is calculated as 43.98 kPa assuming that there are 20 sections between the surfaces. However, the average p* value can be calculated more accurately in the same simulation using smaller step sizes since selected points were determined discretely by hand.

In order to calculate the second component of the critical pressure value, **p'**, the magnetic flux density passing over MR fluid has to be determined. With the information

of magnetic flux density, variable yield strength of the MR fluid can be calculated and then combined with the known design parameters such as fluid gap (b) and the length of the sealing clearance (h). The sections where these known design parameters correspond on the sealing section are given in Figure 73.

Table 12: Calculated parameters for P*.

MR Fluid Attached To						**ΔH (kA/m)**	**P* (kPa)**
Inner Magnet Surface			**Corresponding Face**				
B(mT)	**B (T)**	**H1 (A/m)**	**B(mT)**	**B (T)**	**H2 (A/m)**		
374.52	0.37452	91399.8572	948.92	0.94892	399518.4022	308.118545	77.43863659
638.42	0.63842	218535.257	685.36	0.68536	243688.3666	25.15310971	6.321665974
995.38	0.99538	430233.589	765.74	0.76574	288297.8441	141.9357454	35.67234361
986.36	0.98636	424194.302	768.5	0.7685	289867.8495	134.3264523	33.75991966
980.75	0.98075	420455.97	1429.4	1.4294	638380.7274	217.9247573	54.77046533
978.33	0.97833	418847.673	1396.3	1.3963	644331.167	225.4834943	56.67018313
975.61	0.97561	417043.146	1362.8	1.3628	642757.539	225.7143929	56.72821429
971.49	0.97149	414316.226	961.13	0.96113	407493.9017	6.822324528	1.714637169
967.43	0.96743	411636.654	1265.4	1.2654	608048.3792	196.411725	49.36365059
963.12	0.96312	408800.473	1237.7	1.2377	592778.1792	183.9777057	46.2386407
958.63	0.95863	405855.131	1213.6	1.2136	578295.2337	172.4401031	43.33892489
954.57	0.95457	403200.092	1184.6	1.1846	559777.5131	156.5774207	39.35219796
950.38	0.95038	400468.306	1263.8	1.2638	607213.7033	206.7453969	51.9607856
946.26	0.94626	397790.4	1235.7	1.2357	591614.2739	193.8238736	48.71325259
942.51	0.94251	395360.13	1214.1	1.2141	578605.0634	183.2449335	46.05447495
938.39	0.93839	392697.958	1177.9	1.1779	555368.8289	162.6708706	40.88364895
933.57	0.93357	389593.998	1263.2	1.2632	606899.0772	217.3050796	54.61472333
946.37	0.94637	397861.791	1233.4	1.2334	590266.6552	192.404864	48.35661657
942.54	0.94254	395379.545	1210	1.21	576053.9808	180.6744359	45.40843843
938.28	0.93828	392626.994	1180.9	1.1809	557348.0207	164.7210263	41.39890928
MR 140 CG Magnetization Saturation (A/m)			200000	Vacuum permeability (H/m, N/A^2)			1,2566370614 x 10^-6

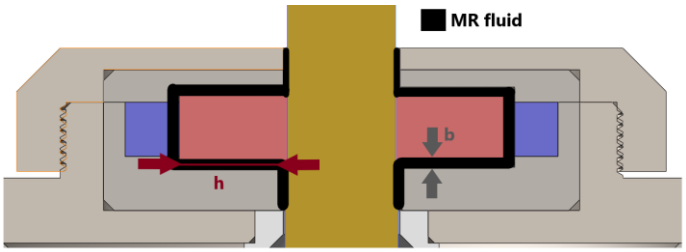

Figure 73: Known parameters to be substituted in Equation 16.

FEA results for the MR fluid situated within the sealing area is shown in Figure 74. Due to the axial polarization of the magnets, the magnetic flux density passing over the MR fluid is maximized at the top and bottom side of the sealing section and reduced greatly in the short sides of the magnets. The maximum and minimum magnetic flux density value in these regions is obtained as 967.48 mT and 194.62 mT respectively.

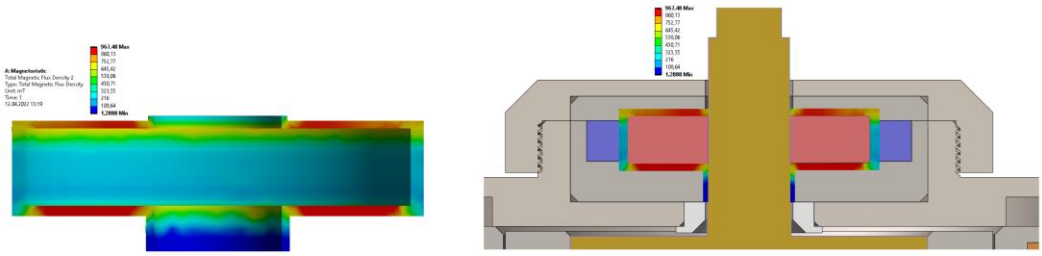

Figure 74: Magnetic flux density on MR fluid (left) and the region on the MR brake (right).

The regions that the magnetic field is concentrated are evaluated and the average magnetic flux density over a 3 mm long region is calculated as 946.92 mT. Magnetic field strength acting over the MR fluid is calculated as 398.26 kAmp/m and the corresponding variable yield strength is calculated as 53.75 kPa. By applying known parameters and calculated values (given in Table 9) in Equation 16, **p'** is calculated as 921.42 kPa.

After obtaining **p'** and **p***, total critical pressure is calculated as 965.36 kPa. This value indicates the maximum pressure difference that the designed MR brake system can operate without losing its sealing property and leaking the MR fluid out of the system. In order to validate the sealing of MR fluid, following calculations were made:

Table 13: Parameters for the calculation of p'.

h (mm)	3
b (mm)	0.35
B (mT)	946.92
H (kAmp/m)	398.26
Tau (kPa)	53.75
p' (kPa)	921.4286

$$P_{cri} > abs(P_{MRF} - 1\ Atm)$$

$$P_{cri} > abs(P_{MRF} - 101.325\ kPa)$$

$$965.35\ kPa > abs(P_{MRF} - 101.325\ kPa\ )$$

$$\rho_{MRF140CG} = 3.64\frac{g}{cm^3} = 3640\frac{kg}{m^3}, \qquad V_{MRF\ in\ the\ brake}: 581.98\ x\ 10^{-9}\ m^3$$

$$m_{MRF\ in\ the\ brake} = 2.12\ x\ 10^{-3} kg, \qquad A_{MRF\ acts}: 1.67\ x\ 10^{-6}\ m^2$$

$$P_{MRF} = \frac{m_{MRF\ in\ the\ brake}\ x\ g}{A_{MRF\ acts}} = 12453.41\ Pa$$

$$965.35\ kPa > abs(12.534\ kPa - 101.325\ kPa)$$

$$965.35\ kPa > 88.79\ kPa\ \ (Validated)$$

Additionally, the maximum linear acceleration value that the sealing can withstand is calculated as 830.44 m/s^2.

4.5.3. Combined Analysis Results

In the result of the magnetic analyzes performed for the sealing and brake parts, the magnetic fields to be obtained in these regions were calculated separately.

In order to understand whether these magnetic fields formed in both regions have any effect on each other, a separate magnetic analysis that covers both results was performed. In this magnetic analysis, the effects of the permanent magnetic field formed by the two neodymium magnets used in the sealing part and the controllable magnetic field generated in the braking section due to the current supplement were examined and the results obtained in the Figure 75 and Figure 76 were obtained.

In the Figure 75, magnitudes of magnetic flux density vectors obtained on the MR fluid settled between the static and rotary parts in the brake system is given. Differently, in the Figure 76, the magnitudes of the magnetic flux density vectors obtained over the the parts (not the MR fluid) is provided.

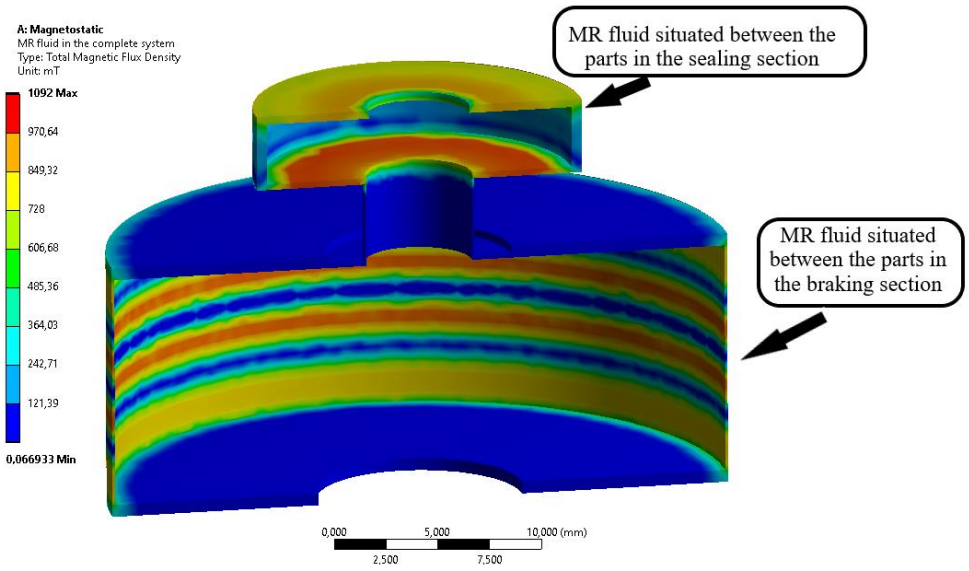

Figure 75: Magnetic flux density passing over the MR fluid (Combined Results).

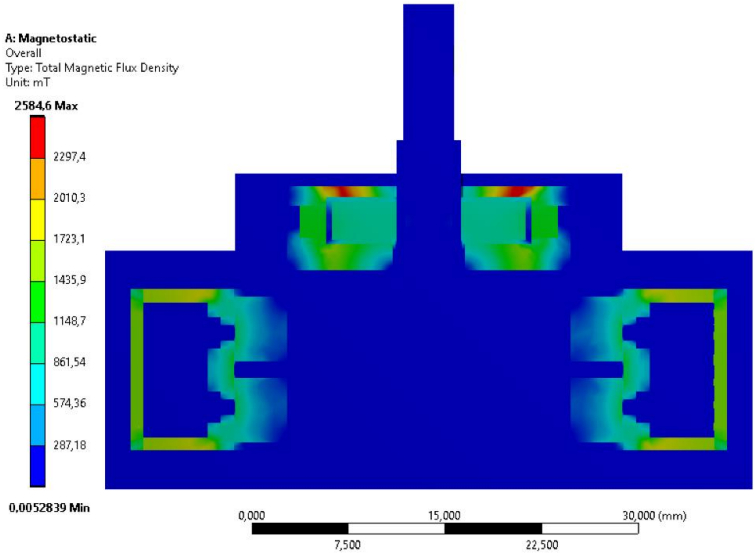

Figure 76: Magnetic flux density passing over the parts (Combined Results).

When the result of the magnetic analysis was examined, it was observed that permanent magnetic field that exist in the sealing part did not affect the magnetic flux

density vectors formed in the braking part. Similarly, the controllable magnetic field that is created in the braking section was also found to have no effect over the magnetic flux density vectors situated in the sealing section. The reason for this is that the outer case and bearing elements separating both the braking and sealing sections from each other are selected as non-magnetic aluminum and Teflon (PTFE) materials respectively and have at least 1.5 mm thickness.

Although the magnetic fields formed in the two regions were found to have no effect on each other as obtained in the simulations, magnetic fields in these regions may affect each other in a real practice. The causes of possible differences that can be observed between the simulation and the real-life application can be linked to the magnetic features of the magnets and the parts produced from soft-magnetic steel.

During the magnetostatic analyses, the magnetic properties assigned for neodymium magnets used in the sealing part are coercive force and residual induction and these values were assumed to be constant. However, these values may differ significantly based on the thickness, outer and inner radiuses of the magnets even though they have the same chemical composition and grades in reality.

Apart from magnets used in the sealing section, B-H curves found for the steel do not cover the information about the applied manufacturing processes during the production. It is known that the manufacturing processes used during the production of the steel (which are used in the sub-parts of the system in the magnetic flux paths) significantly affect the B-H curves of the steel. It has been revealed in the studies of Ito et al. (1983), hot or cold rolling processes applied to the steel and the temperatures applied during the annealing and cooling processes have direct effects on the magnetic properties of the steel due to the change of domain structures of the material.

For these reasons, it is inevitable to observe differences between the simulation outcomes and the real-life use. In order to minimize the differences that can be observed, samples from magnets and steels should be taken and analyzed in laboratories that are capable of determining the exact relationship between magnetic flux densities and magnetic field strengths of these materials, and the information obtained should be input into the simulation program. Thanks to the new simulations that can be performed afterwards, the difference between the results can be reduced and the chances of

observing unexpected situations can be minimized due to the increased accuracy of the simulation.

4.6. Conclusion

In this section, the design of an MR fluid-based braking system planned to be used on a haptic glove to be developed is explained in detail. A drum-type architecture has been chosen as a basis so that the developed MR braking system can be produced in small sizes with narrow tolerances, and with few parts required. The mathematical equations required for the designs of the selected architecture were derived and the material selection of the parts to be used in the system was carried out.

It is known that a major drawback of drum-type MR brakes is their low torque outputs compared to other architectures. To overcome this issue, additional parts produced from non-magnetic materials were introduced and utilized in both rotary and stationary parts to control the magnetic flux path in the proposed MR brake design so that, magnetic flux vectors created by the current flow are forced to pass over MR fluid several times to increase the output torque of the brake system. Since the magnetic flux passing over the MR fluid determines the yield strength of the fluid; with the help of the designed non-magnetic parts in the magnetic flux path, the torque output is significantly increased in the developed improved drum-type MR brake design.

In order to reduce the high off-state torque, which is one of the common problems occur in MR brakes, a new sealing design consisting of only 4 parts has been developed. In this sealing design, with the help of two neodymium magnets and two steel parts, the MR fluid itself is used as a sealing element. With this solution, the effect of friction on off-state torque occurred between the rotary and static parts caused by traditional dynamic elements were reduced significantly.

In order to develop a solution to the "sticky wall" problem, which is another problem seen in MR brake systems, one-way bearings were used. By placing one-way bearings at the part of the shaft outside of the brake system, an advantageous design has been obtained in which the stiction problem was solved and braking direction of braking can be switched easily without the need for the disassembly of the system.

In the light of the magnetic analyzes carried out, information about the output torque of the system and the critical pressure value of the sealing was obtained. The expected output torque of the system in the operating current range (0-1 A) is calculated as 587.25 N.mm. In addition, the maximum pressure difference value that the fluidic O-ring structure created by aligned magnetic particles within the MR fluid can withstand is calculated as 965.35 kPa.

The estimated specifications of the designed MR brake system are given in the Table 14. When the data in the table are examined, an effective improved drum-type MR brake that met all the design criteria is obtained. In the next Chapter, information about the procedures and results of the verification tests performed after the production and assembly of the designed brake system are given. Based on the test results, the suitability of the developed brake system for haptic glove application will be evaluated and the final system specifications will be presented.

Table 14: Specifications of the Designed MR Brake

MR Fluid Features		
Stock Code	MRF 140-CG	
Density (g/cm^3)	3.64	
Maximum yield stress (kPa)	58	
Magnetization Saturation (A/m)	200000	
MR Brake Features		
Architecture	Improved drum-type	
Materials used	Magnetic	SAE 1020 Steel
	Non-Magnetic	Aluminum
		ABS
		Brass
		PTFE
	Magnets	NdFeB
Number of Parts	16	
Expected weight (g)	206	
Coil Features	Coil Wire	AWG 26
	Maximum allowable current (A)	1.3
	Number of Turns	250
Expected Braking Torque (mN.m)	587.24	
Sealing Critical Pressure (kPa)	965.35	
Rotor diameter (mm)	30.25	
Fluid Gap (mm)	0.125	
Outer Shell Diameter (mm)	50	
Total Length (mm)	38	
Moment of Inertia (kg.mm^2)	7.55	
Torque/Mass Ratio (N.m/kg)	2.81	

CHAPTER 5

EXPERIMENTAL TESTS AND VALIDATION

Solid models of MR fluid-based brake system were created and their magnetic analyzes were performed. In order to validate the results obtained from magnetic simulations, the brake system's parts were manufactured and assembled as shown in Figure 77.

Figure 77: Manufactured and assembled MR brake parts.

The resulting MR brake prototype were used in experimental tests to validate the torque capacity of the system obtained numerically in simulation softwares and to validate the method used for the sealing of MR fluid in the brake system. For this validation task, a test rig was built and the prototype MR brake is connected to the test rig. The MR brake system was tightened to the the jig produced by using a three-dimensional printer with the help of M3 screw and nut pairs from the top and bottom sides. The jig is then fixed on the lower platform using M5 screws. The output shaft coming out of the brake system is connected with a coupling, in which a one-way bearing is fixed. The other end of the coupling is paired with the output shaft of the DC motor and connected to the shaft passing through the torque sensor.

The sensor used to determine the current-torque relationship in the experiments is Futek's FSH03985 model response torque sensor, and it measures the torque differences up to 1.1 N.m between the active and fixed terminals, as seen in Figure 78, in line with its working principle.

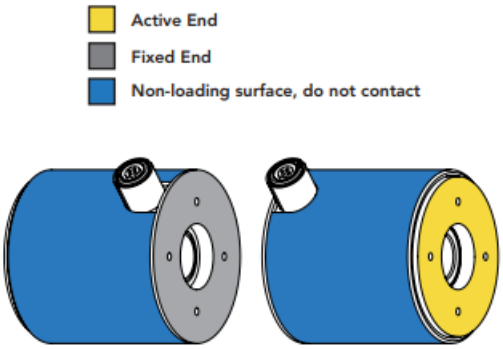

Figure 78: Futek reaction torque sensor's active and fixed end.

The fixed end of the sensor is attached to the test setup on the jig connected to the lower platform. The active end, on the other hand, is combined with the DC motor with the help of an intermediate apparatus, making it possible to measure the response torque between the two ends of the sensor.

In order to measure the torque value to be obtained from the brake system using the sensor, an external motion input must be provided to the system. For this task, a 12 V DC motor of Maxon was selected and connected to the fixed end of the torque sensor with the help of a circular spacer. The continuous torque value that the DC motor can provide alone is 27.5 mN.m. This torque value is increased with the help of a planetary gearbox with a gear ratio of 181:1 connected to the end of the DC motor, making it capable of producing 4.5 N.m (reducer limit) torque continuously and preventing damage to the DC motor during braking. The motor was operated at a constant speed during the experiments, and speed control was achieved by taking the derivative of the measured position information (500 counts per revolution) thanks to the Maxon encoder connected to the back of the motor.

5.1. Systems Used for Data Acquisition

In order to find the current-torque relationship of the developed MR brake prototype, it is necessary to control the DC motor and brake system and to model it using data such as current, torque and position obtained from different sensors. The data acquisition equipment and the elements of the control system used during the tests are shown in the Figure 79 and Figure 80.

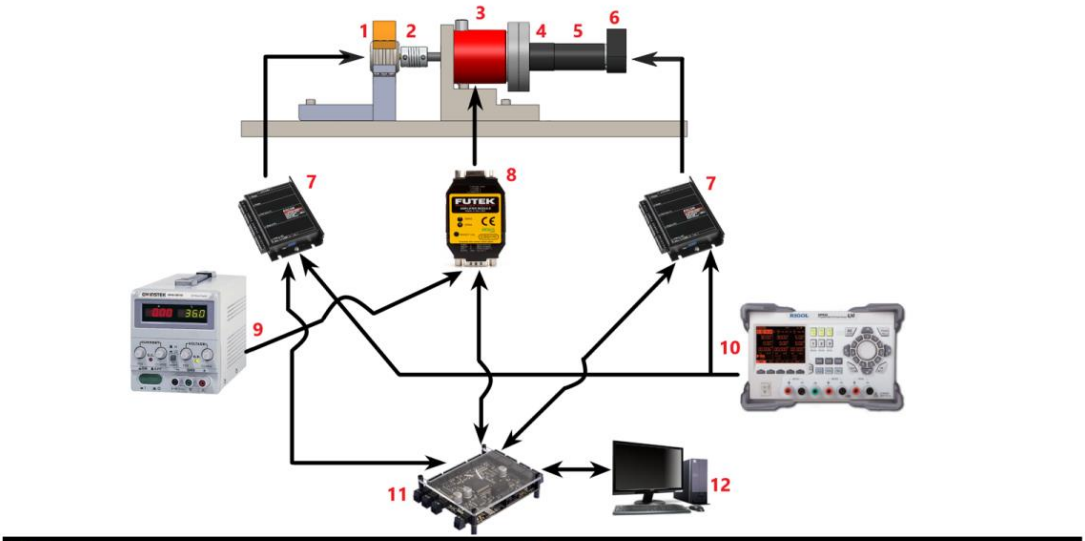

1- MR Brake prototype
2- 8x8 Flexible coupling
3- Futek FSH03985 Reaction torque sensor
4- Maxon Planetary Gearhead (1:181) GP 26 A Ø26 mm, 0.75-4.5 Nm
5- Maxon DC Motor RE Ø25 mm, Graphite Brushes, 20 Watt
6- Encoder HEDL 5540, 500 CPT, 3 Channels, with Line Driver RS 422
7- ESCON 50/5, 4-Q Servocontroller for DC/EC motors, 5/15 A, 10-50 VDC
8-Futek CSG110 Strain Gauge Amplifier
9- GW Instek SPS-3610 DC Power Supply
10- Rigol DP832 Power Supply
11- V-DAQ RT-4 UBS based Real-Time Control & Data Acquisition System
12- Host PC

Figure 79: The data acquisition system and components used for the tests.

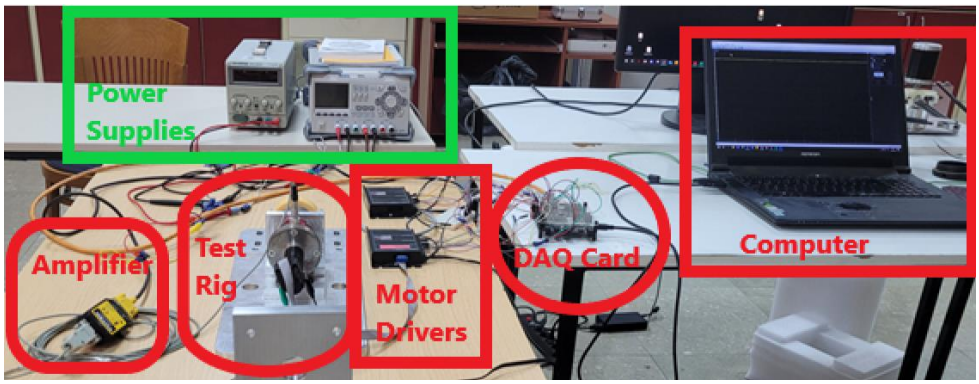

Figure 80: Test setup.

ESCON servo-controller module is used to control the current fed to the MR brake prototype and Maxon DC motor in the system. By using the analog inputs and outputs on these modules, the signals are controlled from the model created in MATLAB Simulink. Using these modules and the software simultaneously allows the current between 0 and 1 Ampere to be supplied and measured to the motor and brake system and monitor these values in real time. In addition, to provide speed control of the DC motor during experiments, rotational position information is obtained thanks to an encoder connected to the output shaft of the motor. Another important element for the experiments is the torque sensor. For this task, Futek's FSH03985 model reaction torque sensor is assigned and used. Since the analog output voltage obtained from the reaction torque sensor, which is placed between the DC motor and the brake system, is not sufficient to be read and processed on the control card, it is connected to the Futek CSG110 module. Thanks to the CSG110 module, the voltage values obtained from the torque sensor are increased to a level that can be read by the control card, and it maps the torque values between 0 and 1.1 N.m to values between 0-10 volts. Rigol DP832 (12 Volt) and GW Instek SPS-3610 DC power supply (15 Volt) were used, respectively, for the power supply of the mentioned 2 ESCON servo-controller modules and the CSG110 module. V-DAQ RT-4 data acquisition (DAQ) card was used to process the data coming from the sensors and to control the system via computer. The data sent to the computer by the DAQ card includes the data obtained from the encoder, torque sensor and current feedback sensors on the motor drivers. The data sent to the DAQ card by the computer includes the necessary control signals that are mapped to operating voltage values at the motor drivers in order to control the supplied current to the DC motor and the MR brake prototype. The signals sent to and received from the DAQ card are observed and processed by the Simulink Desktop Real-Time software used on the computer with using 2 kHz sampling rate.

5.2. Test Procedures and Results

During the tests carried out on the developed MR brake prototype, it was aimed to measure the off-state torque and the maximum torque capacity; to establish the relationship between current and torque; and to determine the system's bandwidth. The details of the performed tests are given in following sections.

5.2.1. Determination of the Off-state Torque

Off-state torque is the torque observed in the brake system required to start the rotation of the output shaft of the brake system from stationary status while current is not supplied through the coil and braking is not intended. Three different scenarios were used in the tests performed to determine the closed state torque of the MR brake.

In the first scenario, the neodymium magnets (used to seal the MR fluid filled in the MR brake prototype) and the spacers were removed from the system. After the related parts were removed from the MR brake prototype and MR fluid is not filled, the prototype was connected to the test setup and the tests were carried out. The aim of these tests is to observe the torque values caused by the friction between the bearing elements and the inertial properties of the system. Other torque values that will contribute the off-state torque such as the attraction force caused by the magnetic flux between the magnets and the MR fluid to be found between the magnets were excluded in this scenario.

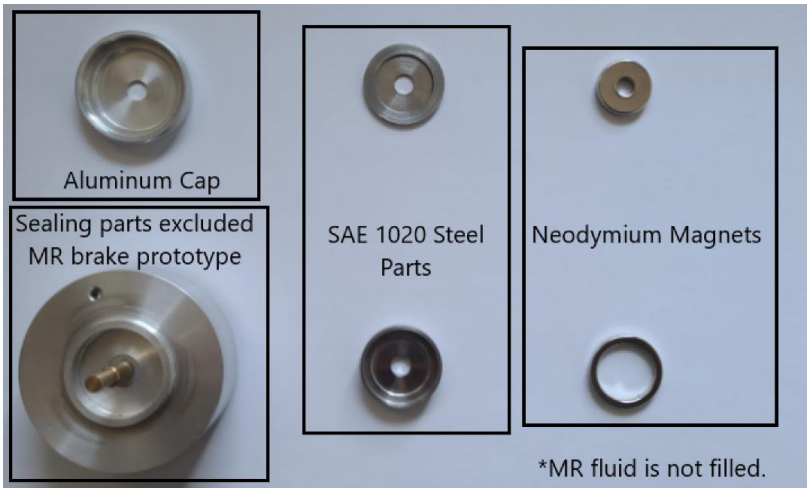

Figure 81: MR Brake prototype without MR fluid and parts related with sealing.

In the second scenario, magnets to seal the MR fluid are included in the MR brake prototype, but the MR fluid is not filled into the system again. In these tests, it was aimed to check whether the attraction force between the magnets has any effect on the off-state torque, together with the inertial properties of the system and the friction between the bearing elements.

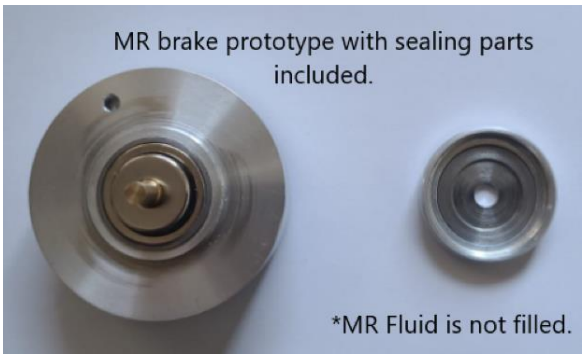

Figure 82: MR Brake prototype without MR fluid.

In the third scenario, tests were carried out by assembling all parts of the brake system and filling the MR fluid. In these tests, it was aimed to measure the off-state torque that the system will have in a real use case.

Figure 83: MR brake prototype.

In the first and second scenario tests, no current was fed to the MR brake prototype and the DC motor was driven at a constant 50 RPM speed. In the third scenario, while the DC motor is driven at the same speed, the part of the graph (between 0 and 0.5 seconds time interval, where no current is supplied to the MR brake prototype) is used which was plotted during the tests to reveal the current-torque relationship. The related graph is given in Figure 84.

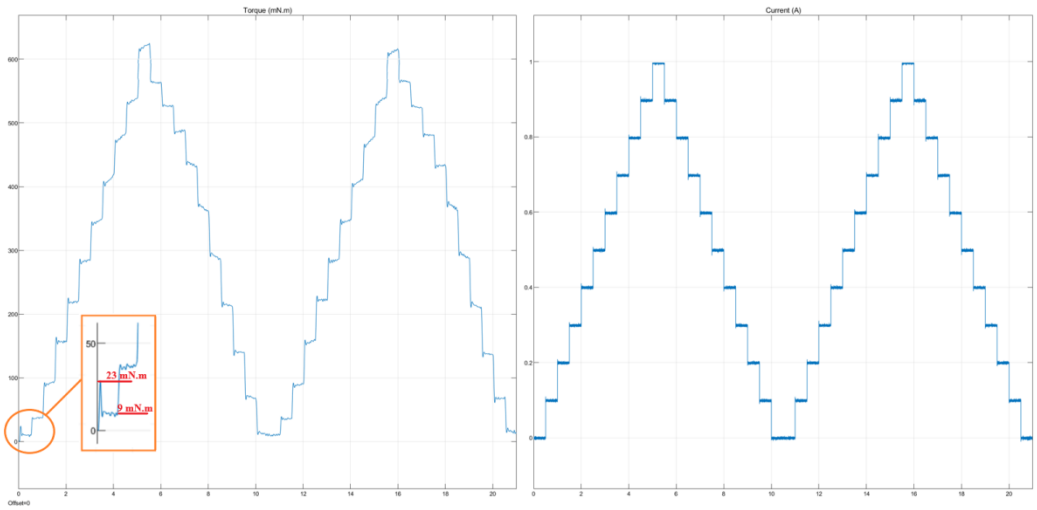

Figure 84: Graphic display of off-state torque value.

The data obtained from the torque sensor were analyzed over MATLAB Simulink Real-time. As a result of the tests, the off-state torque values corresponding to the relevant scenarios are given in Table 15.

Table 15: Experimentally obtained off-state torque results.

Scenarios (performed @50 RPM)	**Off-state torque values (mN.m)**
Scenario #1 (No magnets, no MR fluid)	~9
Scenario #2 (No MR fluid)	~20
Scenario #3	~23

When the results in Table 11 are examined, it is observed that the off-state torque nearly doubled between the first and second scenarios. The reason for this situation is that the neodymium magnets assembled to the system to provide sealing are placed in the system in such a way that the polarization directions are opposite to each other, and due to the attraction force formed between these magnets, the shaft is pushed in a certain direction, increasing the force on the Teflon bush used for bedding and causing more frictional force. This situation is illustrated in Figure 85.

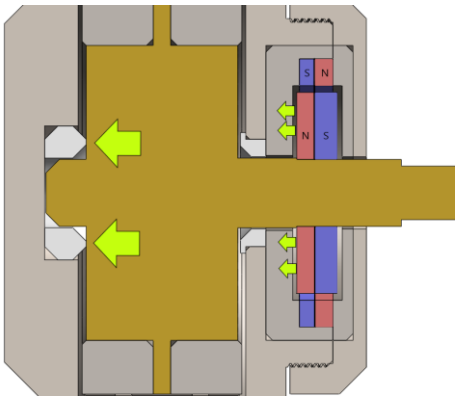

Figure 85: The effect of the force between the neodymium magnets on the Teflon bearing.

In the third scenario, it can be seen that there is a slight increase in off-state torque when compared with the second scenario. The reason for this increase after filling the MR fluid to the system is that, the MR fluid, which is located in the region with low magnetic flux density and far from the magnet centers of the sealing region, makes a constant braking in the radial direction due to the alignment of metal particles in the direction of the weak magnetic flux vectors. Since the magnetic flux affecting the MR fluid is weak and the region is close to the center of rotation, the contribution of this situation over off-state torque was expected to be low. This situation is illustrated in Figure 86.

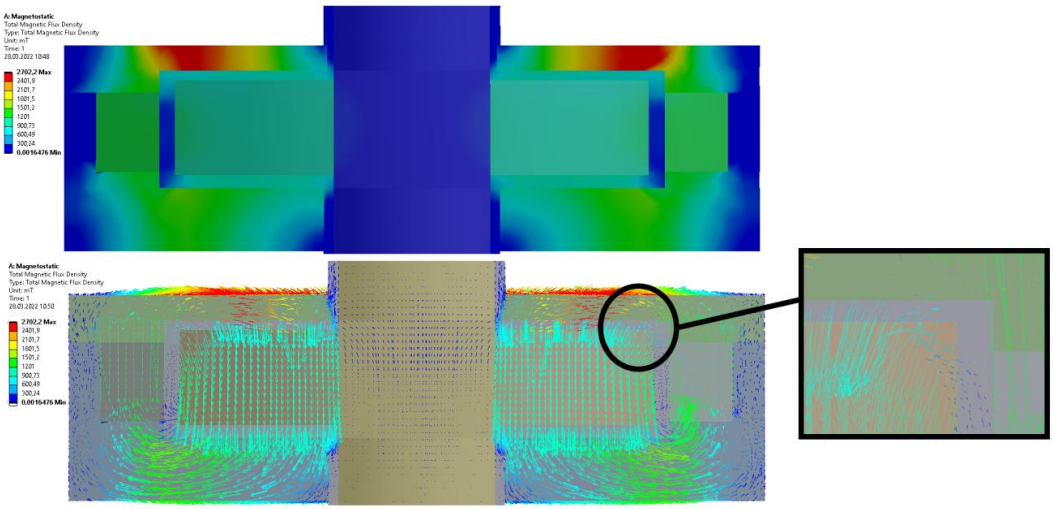

Figure 86: Region with low magnetic flux density and weak magnetic flux vectors on the sealing part.

The parameters affect the off-state torque after filling the MR fluid can be listed as:

- The amount of MR fluid that settles in the region with low magnetic flux density,
- The magnitudes of the radial components of the magnetic flux vectors,
- The distance from the center of the iron particles in the MR fluid aligned on the respective regions.

It is not possible to calculate these parameters theoretically using analytical/numerical methods, but only to be measured experimentally. Also, even experimentally obtained, these parameters cannot be measured separately but obtained in a dependent manner within each other. When the experimental results are examined, the effect of these dependent parameters on the off-state torque was calculated as ~3 mN.m and the total off-state torque value of the MR brake prototype was measured as approximately 23 mN.m.

5.2.2. System Characterization

MR fluid was added to the developed MR brake system at the last stage of the off-state torque determination experiments. In order to use the developed brake system in any system, certain tests must be carried out in order to reveal its electronic and mechanical specifications. Also, additional tests must be performed to characterize the behavior of the system to be controlled.

The first stage of the characterization tests covers the validation of the expected output torque of the system obtained through magnetic analysis. During these tests, the torque capacity and the dynamic range of the brake system is determined. The torque capacity of the system is the torque output that it will exhibit at the maximum current value it can operate. The maximum current value at which the system can operate is determined by the standards of the characteristics of the cables wound on the coil part. The characteristics of the coil wire used in the system and the measured coil parameters are given in Table 16.

The test procedure to measure the torque capacity is as follows: while the DC motor was driven at a constant speed of 50 RPM, current signals were sent to the brake system in

increasing and decreasing manner. For this varying current input, a stair function is used with a step size of 100 mA and a step time of 500 ms between increments within 0 and 1 A range. The current is supplied to the MR brake starting from 0 A and increases by 100 mA every 0.5 seconds. After it reaches to 1 A (which is maximum operable current for the system), it starts to decrease in the same manner. Supplied current signal is given in Figure 87.

Table 16: Characteristics of coil wire and MR brake coil.

Coil Wire Specifications	Coil Wire Type	AWG 26
	Wire diameter (mm)	0.405
	Resistance per unit length (mΩ/m)	133.9
	Ampacity at 60 °C (A)	1.3
MR Brake Coil Specifications	Number of turns	~210
	Measured resistance (Ω)	3.78
	Maximum allowable current (A)	1
	Measured power consumption (W)	~3.7 - 3.8

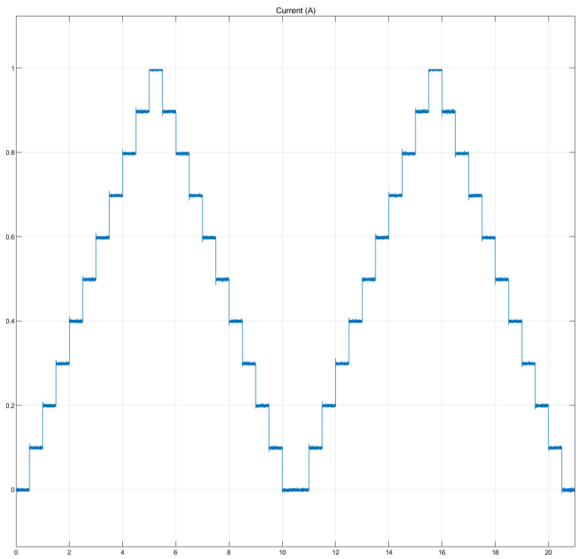

Figure 87: Stair function used for current supply to the MR brake prototype.

During this process, the torque sensor measures the torque generated between the DC motor connected to the sensor and MR brake. With the current supplied, the coil inside the brake magnetizes and magnetic flux starts to flow over the MR fluid causing the yield strength and the braking torque increase. The current supplied to the MR brake and the torque measured by torque sensor were recorded and also monitored in real-time. As a result, the graph in Figure 88 is obtained. Based on the measurements, it was seen that the developed MR brake produces 620.17 mN.m of braking torque when 1 A is supplied. When the results of the magnetic analysis and the measurements were compared, the difference between the calculated (587.25 mN.m, see Section 3.5.1) and measured torque output (620.17 mN.m) is calculated as 32.92 mN.m. When this difference is converted to percent value (5.61%), it can be concluded that the magnetic analysis' results and the mathematical models developed for the system are highly accurate.

After the validation of the torque capacity, in order to control the system with an open loop manner and determine the other system specifications, the next sequence of tests were performed. In these tests, the aim is to to reveal the relationship between the supplied current and the output torque and develop a control model.

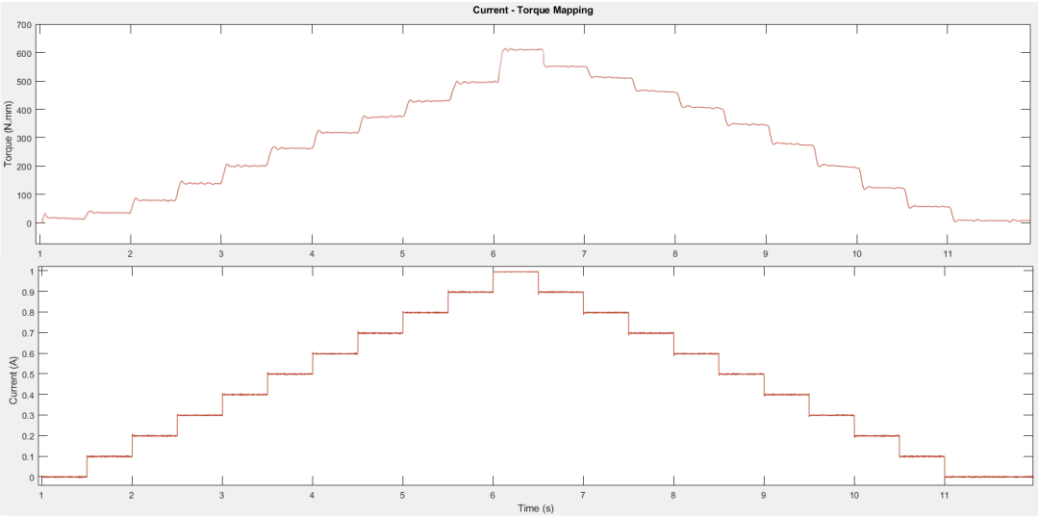

Figure 88: Torque-time (above) and current-time (below) graphs.

For this task, the same procedures were followed and the tests were carried out for different operating current intervals. To keep the control of the system simple, the torque values corresponding 0-0.8 A and 0-0.6 A are measured and used. By using these current

and torque data, hysteresis loops for different current intervals are derived and the effects of non-linear magnetization/demagnetization in the braking system on braking torque are investigated. Hysteresis curves for different operating current intervals are shown in Figure 89 and Figure 90.

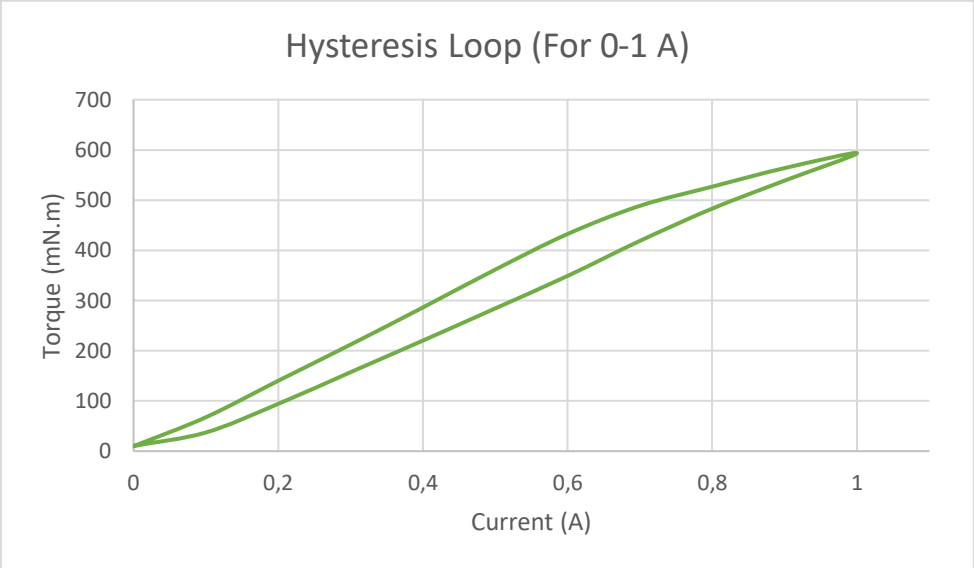

Figure 89: Hysteresis loop for 0-1 A operating current interval.

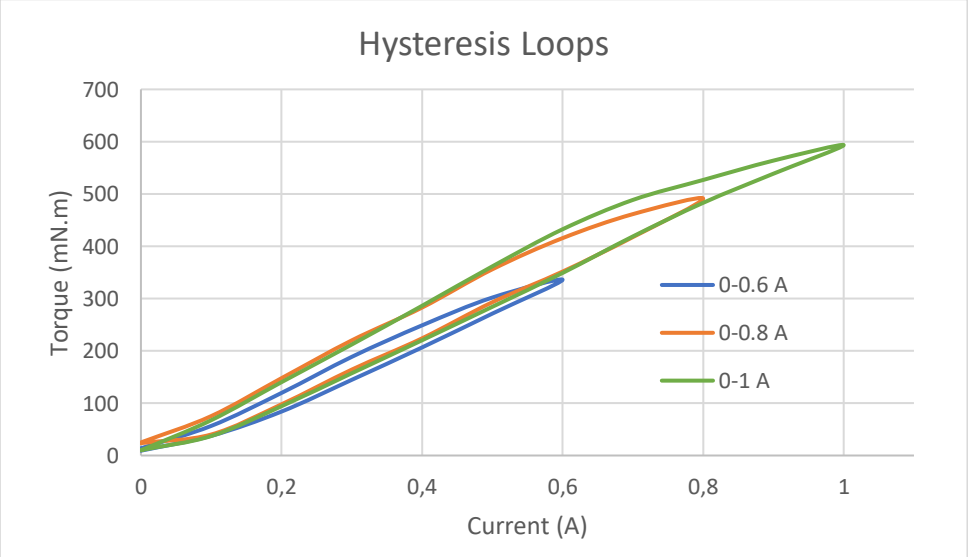

Figure 90: Hysteresis loops for different operating current intervals.

By using the data within the hysteresis loops, the relationship between the current and the torque is established. For each hysteresis loop, 4th-order polynomial equations are fitted for increasing and decreasing trends of the current. With the help of the derived equations, the inverse control of the system was established so that the system takes the desired torque values as inputs and computes the current to be supplied to achieve that input. The reason these equations are derived for different operating currents is related with the magnetically hysteric behavior of system. As can be seen in Figure 85, for a selected torque value, there exists two different current values that the selected torque could be obtained. However, it can also be seen that, for lower desired torques, hysteresis loop becomes narrower and the horizontal distance between current values decrease. Since the control of the system is aimed to be established in an open loop manner (no sensors are going to be used on the glove to measure and correct the torque), for applications requiring lower torques, equation sets for narrower hysteresis loops can be used; in this way, the system can provide more accurate results. The calculated constants for the 4th degree polynomial equations were tabulated and given in the Table 17.

After the torque-current relations are established, the response of the system against various signals were analyzed.

First test signal is selected as step input and applied on the MR brake to measure the rise time, settling time, overshoot, peak time and lastly the steady state error experimentally. The system response against a constant torque demand signal (which has 600 mN.m amplitude) is measured 10 times and averaged to estimate the parameters accurately. The resultant graph and measured parameters are given in Figure 91 and Table 18 respectively.

Table 17: Calculated polynomial constants for torque-current relation.

	Desired Torque Interval (mN.m)	**a**	**b**	**c**	**d**	**e**
If desired torque values are increasing	0-330	-88,62E-12	73,47E-09	-21,44E-06	41,59E-04	-3,44E-02
	330-480	-10,25E-12	10,35E-09	-35,97E-07	20,66E-04	2,23 E-02
	480 or higher	-56,81E-13	96,97E-10	-53,89E-07	26,74E-04	-12,80E-03
If desired torque values are decreasing	0-330	20,34E-13	16,26E-09	-82,60E-07	27,60E-04	-35,24E-03
	330-480	15E-12	-86,79E-10	64,81E-08	16,92E-04	-28,32E-03
	480 or higher	91,79E-13	-58,06E-10	44,14E-08	15,71E-04	-13,01E-03
$y = \boldsymbol{a}x^4 + \boldsymbol{b}x^3 + \boldsymbol{c}x^2 + \boldsymbol{d}x + \boldsymbol{e}$ (x: desired torque & y: brake input current)						

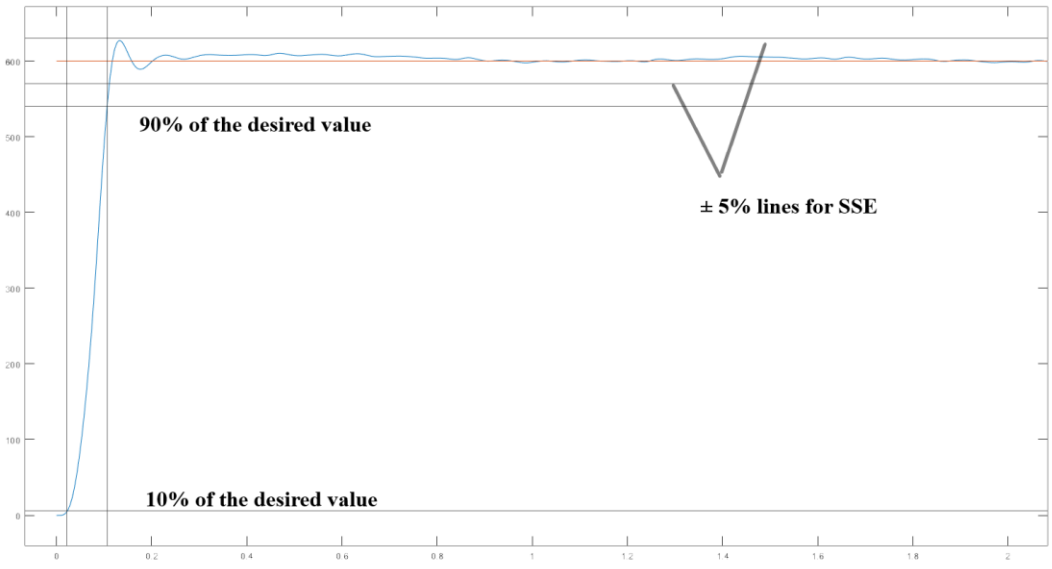

Figure 91: Response of the system to a step input torque demand signal.

Table 18: Measured system characteristics.

Torque demand (mN.m)	600
Rise time (ms)	50.2
Peak time (ms)	115.5
Overshoot (%)	2.37
Settling time (ms)	145.6
SSE	± 10 mN.m

The next series of tests were performed in order to determine the bandwidth of the system. To compute the bandwidth of the system, series of sine wave signals with increasing frequencies were applied and the responses were compared. As a first step, root mean square error between the sinusoidal input and output signals were compared to determine whether the current-torque relation is established accurately.

$$RMSE = \sqrt{\frac{\sum_{i=1}^{n}[T_{input}(i) - T_{response}(i)]^2}{n}} \quad (17)$$

By using Equation 17, root mean square error is obtained as 6.49% for signals compared at 1 rad/s frequency given in Figure 92 (with 2 kHz sampling rate and for 100 seconds).

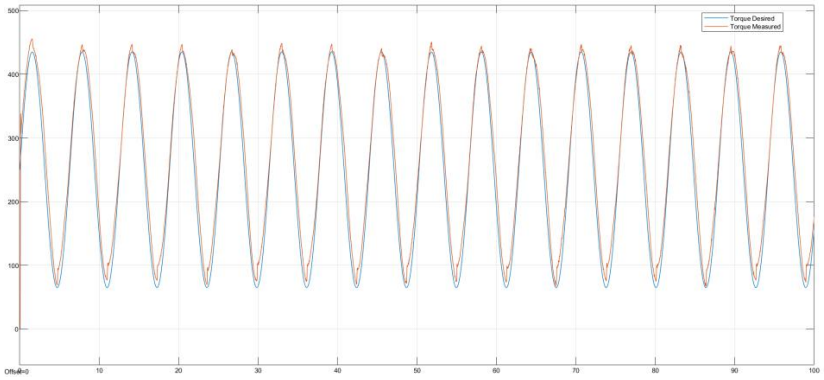

Figure 92: Torque demand and measured torque signals at 1 rad/s frequency.

During frequency tests, the magnitude ratio between the input and response signals were measured and expressed in terms of logarithm by using the Equation 18:

$$Logarithmic\ Gain = 20 \log_{10} \left| \frac{T_{response}}{T_{input}} \right| \quad (18)$$

The bandwidth of a system defined as the range of frequencies that the system can respond to the changes at the input signal within a specified range of degradation in performance. The threshold for the performance degradation is often defined as 70.7% of the magnitude ratio (or -3 dB in terms of logarithmic gain). The frequency tests were performed between 1 rad/s to 1000 rad/s frequency range and the resultant graphs were provided in Appendix G. Based on the experimental results, - 3 dB gain ratio is achieved at 65 rad/s which defines the bandwidth of the system. It is important to note that, even though the magnitude ratio between the signals around 65 rad/s frequency is more than -3 dB, there exist a phase between the signals which nearly equals to 160°; indicating that the response of the system is delayed. Experimentally obtained Bode plot of the developed MR brake system and the phenomena observed during experiments are illustrated in Figure 93 and Figure 94 respectively.

In order to find the possible reason for this delay in the system, all elements in the test setup were evaluated. No problems were detected during the observations made on the torque sensor, DC motor and flexible coupling. Therefore, other possible reasons such the main computer used in the DAQ system and complicated software algorithms were evaluated. The possible amounts of the delay might occur within the data acquisition systems and software algorithms are analyzed and given in the Table 19.

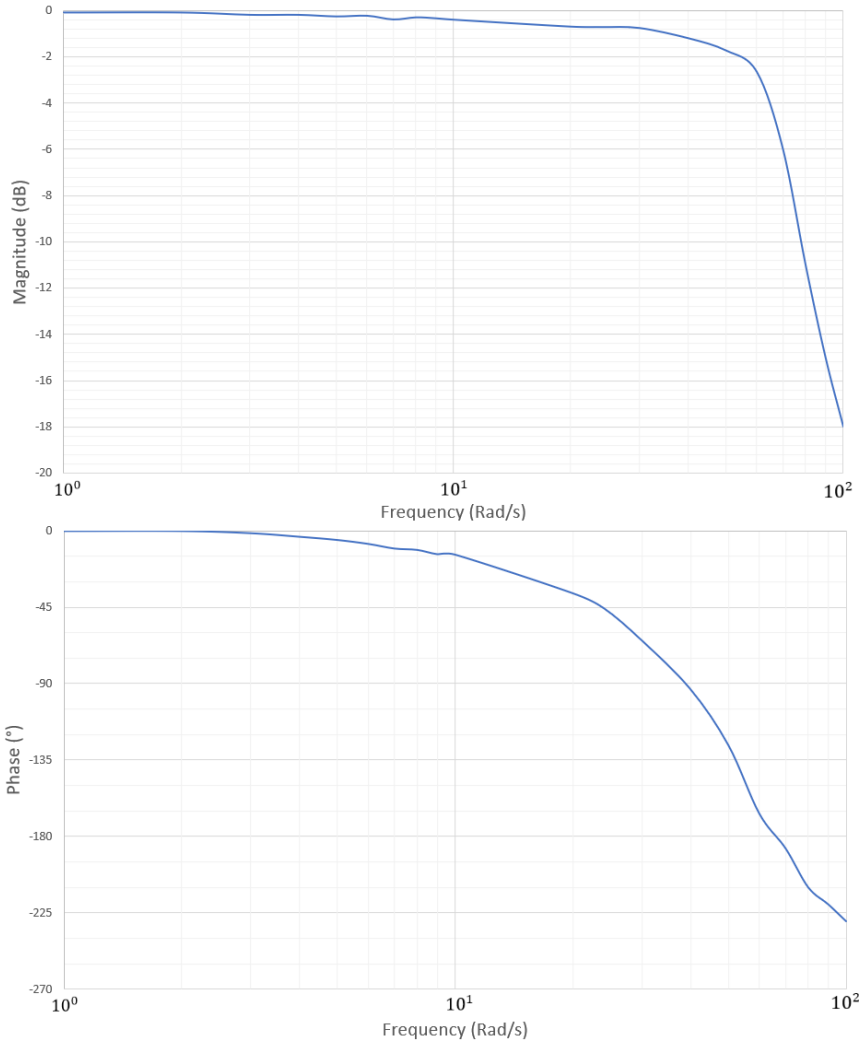

Figure 93: Experimentally obtained Bode-plot of the MR Brake.

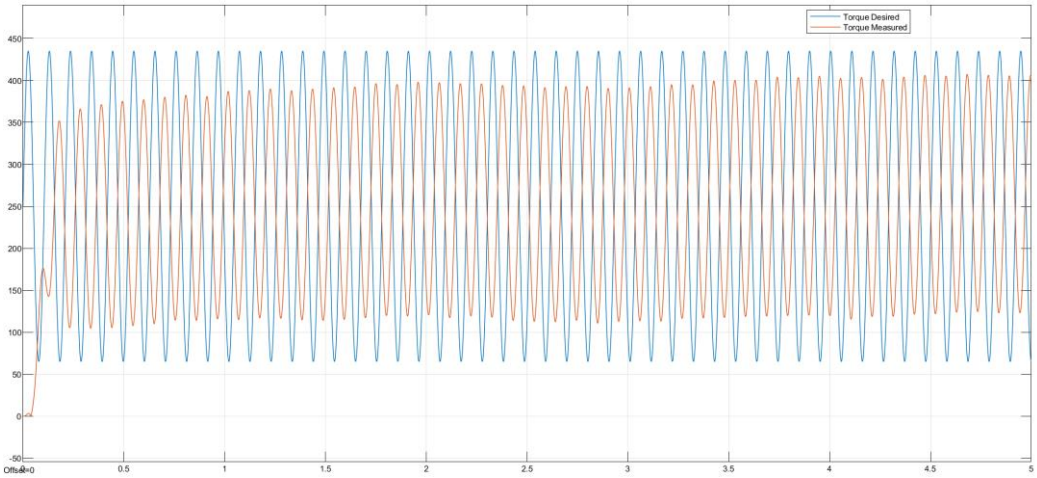

Figure 94: Comparison of torque demand and response signals at 65 rad/s.

Table 19: Delay comparison chart.

Reasons of Delay	Delay Amount
Signal Conditioning (ADC&DAC)	Nanoseconds to seconds.
Hardware Communication	Microseconds to tens of milliseconds.
Software/Memory Transfer	Microseconds to several seconds.
Logic/Algorithms	Microseconds to many seconds.

Since the delay depends on both the performance of the computer and the underlying software algorithms, only necessary algorithms were permitted to be run on a PC with higher performance; however, the no improvements were achieved in terms of the phase delay. After the investigations and repeated tests, it was concluded that the observed phase shift is a feature of the developed MR brake system. When this system is compared with another MR brake previously developed in the IzTech Robotics Laboratory that uses dynamic oil seals to keep the MR fluid inside the system, the only reason that may cause this problem is considered to be the permanent magnets used in the sealing parts system of the system. It is thought that the strong magnetic field created by the magnets in the sealing part polarizes the steel parts with high magnetic permeability in the interior section where the braking torque is obtained, and the external magnetic field created by the current fed to the system causes a disturbance in the total magnetic field resulting with the unexplainable phase shift observed at high frequencies. A new test setup, details of which are given in the future work section, makes it possible to identify and verify the source of this problem.

Experimentally obtained data is transferred to the MATLAB System Identification Toolbox and the following transfer function is obtained that fits 86.41% of the estimation data.

$$T.F. = \frac{1}{1.077\ 10^{-5}\ s^3 + 6.062\ 10^{-4}\ s^2 + 0.04688\ s + 0.9866}$$

The Bode plot in which the experimentally obtained data are compared with the estimated transfer function, can be seen in Figure 95.

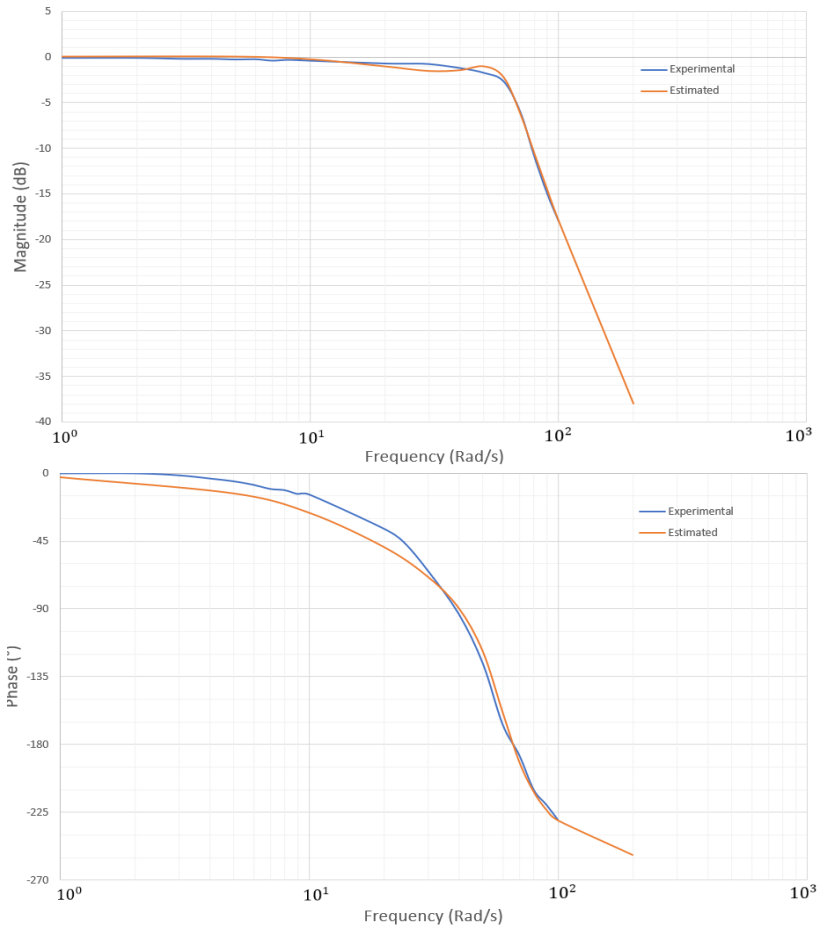

Figure 95: Comparison of the experimental and estimated data on the Bode plot.

The control of the developed brake systems on the glove will be carried out using open-loop control system, since the output forces/torques obtained from the brake system are not measured by any sensors placed on the fingertips. Therefore, it is seen that the only situation that may disturb the stability of the system during the use of the calculated transfer function in an open-loop manner will be the torque demand signals required at high frequencies. However, since the frequencies of the force signals required to be supplied to the fingertips to simulate daily activities are approximately 2 Hz (12.57 rad/s), and the frequencies required for power grip becomes even lower, the developed MR brake system is found to be suitable to be used in a haptic glove application.

5.3. Conclusion

In this chapter, the specifications of the developed MR brake are analyzed. In the first section of the chapter, information about the data acquisition and control systems used for the tests are given in detail. By using these mentioned systems, experimental studies were performed to validate the results obtained through analyses; and, to obtain detailed specifications of the MR brake system. The specifications of the developed system obtained though tests are given in Table 20.

Table 20: Specifications of the developed MR brake system.

MR Brake Features		
(1)	Mass (g)	206
(2)	Outer Shell Diameter (mm)	50.25
(3)	Total Length (mm)	38
(4)	Number of Turns in the Coil	200
(5)	Maximum operational current (A)	1
(6)	Braking Torque (mN.m)	620.17
(7)	Off-state Torque (mN.m)	23
(8)	Dynamic Torque Range (mN.m)	597.17
(9)	Torque/Mass Ratio (N.m/kg)	2.90
(10)	Bandwidth (rad/s)	65
(11)	Power Consumption (W)	4

As can be seen in the 1st, 2nd, 3rd and 6th items given in the Table 20, the manufactured prototype meets the design criteria mentioned in Chapter 4-Section 1.

As mentioned in Chapter 3 - Section 1, previously developed MR brakes and the ones used in the haptic glove applications suffers from high off-state torque due to the dynamic sealing elements used to seal the fluid inside the brake systems. Furthermore, in the works of Nam et al. (2008) and Winter & Bouzit (2007), the off-state torque in their developed MR brakes used in Smart Glove and MRAGES are 25% and 10% of the maximum torque output respectively. Thanks to the new sealing design (Chapter 4-Section 4), the friction between rotary parts and the dynamic sealing elements were eliminated. The off-state torque within the brake system was measured as 23 mN.m corresponding to 3.71% of the maximum torque output.

An important metric used to measure the performance of the MR brakes based on the architectures they possess, is the torque-to-mass (TMR) ratio. Based on the work of Qin et al. (2018), typical TMR values for drum, disk and multi-disc architectures were given as 1.369, 1.075 and 3.692 Nm/kg respectively. As presented in the Chapter 4, an improved drum type MR brake was designed in this work to achieve manufacturability in small volumes with better torque output features. Based on the test results, TMR of the developed MR brake is obtained as 2.90 N.m/kg, which is 280% more compared to a typical drum-type MR brake architecture.

5.4. Future Works

After obtaining the prototype specifications, possible improvements to be for the future versions of the MR brake system are revealed and listed as follows:

- Shaft attachments and the shaft diameter: If a manufacturer with better manufacturing capabilities were found, the shaft attachments can be hollowed and the shaft diameter can be reducing as shown in Figure 96. By this way, the rotating mass can be reduced from 70.85 grams to 35.94 grams (50.92%).

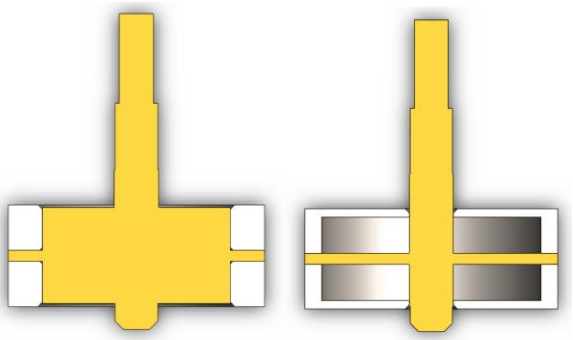

Figure 96: Actual design of the rotary parts (left) and the improved version (right).

- Radially polarized neodymium magnets: As stated in the “Sealing Design” section (3.4), in the current prototype, 2 axially polarized neodymium magnets were used. In order to direct the magnetic flux density vectors to achieve sealing, 2 additional

parts with high magnetic permeability are designed and manufactured. Based on the results given at the “Determination of the Off-State Torque” section, the off-state torque occurred in the MR brake nearly doubled after the assembly of the magnets. The reason for this situation is explained as, the attraction force formed between magnets cause the shaft to be pushed over the Teflon bush and increasing the frictional force.

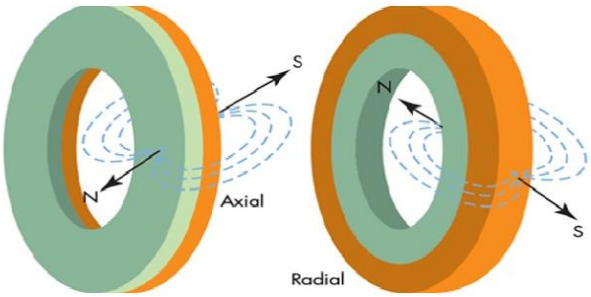

Figure 97: Axially (left) and radially (right) polarized magnets (Source: Moermond, n.d.).

By switching to radially polarized magnets as shown in Figure 97, the off-state torque will be reduced since the shaft is no longer pushed in the axial direction. Beside this, the additional steel parts will no longer be required and can be extracted. By this way, the total length of the system can be reduced further. It should be noted that radial magnets are significantly rare and have to be produced specifically based on the requirements such as polarization directions, hole diameters, outer diameters and thicknesses. Due to these reasons, these magnets will increase the cost significantly.

- Increasing the number of non-magnetic parts on the magnetic flux path: As stated in Chapter 3, when the magnetic flux density vectors are forced to pass over the MR fluid more with the help of the parts introduced to the magnetic flux path with low magnetic permeabilities, the torque output of the system will increase proportionally. In the current design, 3 non-magnetic parts were used on the magnetic flux path. This number is determined based on the advice of the manufacturer and their machining capabilities. If a manufacturer with better machining capabilities can be found, additional parts can be produced and assembled to increase the torque capacity of the system.

- Changing the MR fluid: In the prototyped MR brake, LORD Corp.'s MRF-140 CG is being used as the magnetorheological fluid. Since the viscosity and the variable shear strength of the fluid directly affects the off-state and braking torque respectively, a magnetic fluid with better features could be used if it is found.

- Vertical test rig: In the Bode plot obtained at the last stage of the system characterization tests, an unexplained phase delay was observed on the phase plot. It is thought that the most likely reason for the phase shift observed in the system is, the strong magnetic field obtained from the neodymium magnets used in the sealing part combines with the magnetic field created by the supplied current, affecting the inner parts of the system made of steel material and causing a complex magnetic effect on the system. By creating a new test rig as shown in Figure 98, it can be ensured that the MR brake in the system works in an upright position so that the magnets in the sealing part can be removed and the leakage of the MR fluid in the system is prevented.

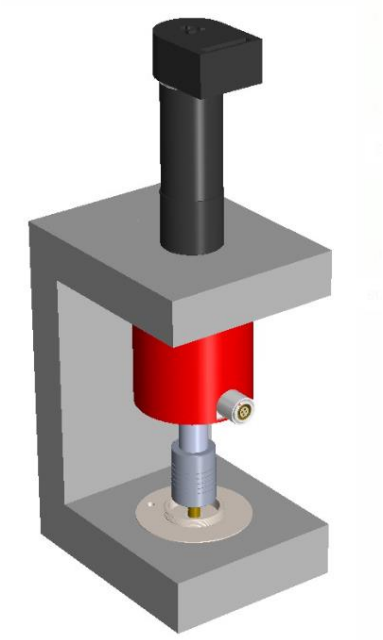

Figure 98: Vertical Test Rig.

By ensuring an environment where MR fluid will not spill while the MR brake can still operate, the effects of magnets extracted from the system can be examined. By comparing the obtained results with the current results, more detailed information about the effects of magnets in the sealing section can be obtained.

CHAPTER 6

CONCLUSION

In this thesis, the designs of the MR brake systems aimed to be used in the conceptually designed haptic glove for virtual reality applications are presented.

The work begun with reviewing the literature to find the haptic feedback gloves developed in the laboratory environment and commercially available ones. As a result of the literature review 26 different gloves were found, examined, and classified according to their properties. After the examinations, the problems occurred in most of the gloves are detected to be insufficient force feedback, heavy ground units and safety issues. It has been observed that the source of these problems is caused by the actuators used in these systems. At this point, magnetorheological fluid-based brake systems are found to be great candidates and chosen as the main actuation units to be used in the developing haptic glove in the scope of this thesis.

Magnetorheological fluid-based brake systems were analyzed in details and the design of the actuation system architecture of the glove is started. As a result of the researches carried out, different architectures used for MR brake systems were revealed and compared to determine which architecture can meet the conditions and criteria required for a haptic glove application most. Following the determination of the actuation systems to be used in the system as MR brakes, a conceptual design of an efficient force transmission system has been realized to transfer the force/torque to the user's fingertips obtained from these brake systems.

When the different architectures of MR brakes were examined by considering their conveniences to be used in haptic glove applications, it was found that the most appropriate architecture was the drum-type MR brakes due to their low weights, small sizes and the least number of parts required to be manufactured in narrow tolerances; however, their torque output is needed to be increased within an improved design. Following the determination of the architecture to be used, the common problems occur in MR brakes (both originated due to the architecture and independent of the architecture)

were evaluated and combined with the requirements to be used for a haptic glove application, the final design criteria were determined.

Following the determination of the design criteria, the mathematical models required to determine and estimate the output torque of the system were created and the design of the solid models was realized. To find the best design parameters and to estimate the approximate value of the output torque to be obtained from the design, magnetic analyzes were performed by using the developed solid models. In the proposed design, an improved drum-type MR brake is developed where:

- The low output torque problem occur in drum-type architectures is solved by implementing non-magnetic materials to the magnetic flux path, to force flux density vectors were to pass MR fluid additional times,
- High off-state torque and sticky wall problems observed in MR brakes (independent of architectures) have been solved by designing an efficient sealing mechanism and implementation of one-way bearings respectively.

After the desired results were obtained in the performed magnetic analyses, technical drawings of each solid model were prepared and the production of the parts was started. Manufactured parts were then assembled to perform validation tests and experiments. During production and assembly, an important note was taken to help future designers of the brake system. The production of parts should be provided by a single manufacturer so that each part should be machined in coordination with the related parts they are in contact with. If the parts are produced by different manufacturers and desired to be assembled, it is very likely to encounter problems related with tolerances during assembly.

Following the assembly of the brake system, a test rig was built and the brake system was connected to this setup to perform a series of experiments. The aim of the tests was to verify the results obtained in magnetic analyzes and to reveal the characteristics of the system. First series of the tests were performed to determine the off-state torque that the developed MR brake system has and validate the sealing of the MR fluid inside the brake system. It has been observed that the proposed sealing mechanism is both capable of keeping the MR fluid inside the system without any leakage and able reduce the high off-state torque observed in MR brakes. When the works of Nam et al. (2008) and Winter & Bouzit (2007) are examined, the off-state torque observed in their

MR brakes used in haptic glove applications are 25% (5.54 to 26 N) and 10% (1.9 to 6 N) of the maximum torque output respectively. The off-state torque observed in this design was measured as 23 mN.m corresponding to 3.71% of the maximum torque output.

The next series of tests were performed to determine the maximum torque output of the system, which is measured as 620.17 mN.m. As stated in the Chapter 5- Section 3, torque-to-mass ratio is an important metric to classify the performances between different architectures of MR brakes. Based on the experimental work, TMR of the developed MR brake is obtained as 3.01 Nm/kg, which is 280% more compared to a typical drum type MR brake architecture and about 81.52% of a multi-disc type MR brake. As specified in the design requirements, brake systems are required to produce and transmit a force of at least 7 N to the user's fingertips. This value represents the minimum force required for fingers to perform daily tasks. However, it could be increased to 100 N~400 N for power grip motion. It has been observed that only the actuators used in the Wolverine glove are able to generate forces for the power grip motion when compared to the actuators in the reviewed gloves. Actuators in the Wolverine can produce 100 N of force feedback but due to the self-locking mechanisms, variable stiffness cannot be modeled. At the current state, proposed MR brake system is able to deliver 106.92 N of force feedback to the fingertips of the user during a fully powered braking sequence. However, if the sticky wall problem can be solved by using external sensors and/or control algorithms, this value can be increased up to 310 N by winding the cables directly to the shaft instead of a pulley coupled with a one-way bearing.

After the determination of the dynamic torque range of the developed system is completed, the relationship between current and torque is established. While establishing the current-torque relationship, two set of functions were created for the increasing and decreasing trends of the current supplied to the system to reduce the effect of magnetic hysteresis for different intervals of operating currents. By using these functions, frequency tests were performed and the tracking error between the desired and measured torque signals were measured with a margin of error of 6.49%. During the frequency tests, sinusoidal torque demand signals started from 1 rad/s frequency to 1000 rad/s were sent and the response of the system was measured. As a result of these frequency tests, the bandwidth of the MR brake system is found as 65 rad/s. Experimentally obtained frequency data is then transferred to the MATLAB System Identification Toolbox to estimate a transfer function. It has been observed in the literature that most of the MR

brakes developed for different applications and using different architectures have a first-order transfer function. The transfer function of the developed MR braking system was obtained as third order and fit the experimental data with 84% accuracy. When the reason behind obtaining the third-order transfer function is investigated, it is seen that two axially polarized neodymium magnets used in the sealing part of the system affect the total magnetic field formed in the system and although no issues were observed on the magnitude plots that the system, the phase angle between the input and output signals has affected significantly. However, since the developed brake systems are aimed to be used in an open-loop manner within the glove system and the required frequencies for force feedback signals are around 2 Hz, these systems were found to be suitable to be in a haptic glove applications.

When the current and voltage characteristics of the developed system are examined, 1 A current and 4 V voltage are required to obtain the highest output torque. Since the brake system works with a low power consumption of 4 Watts, the risk of harming the user by an electrical shock in case of any malfunction is prevented. Additionally, since these brake systems are not capable of providing any motion thanks to their resistive nature, any physical harm such as sudden and powerful pull of the fingers in case of malfunction is completely prevented.

The developed brake system can transmit a force of 106.92 N to the fingertips. This value is 15 times more than 7N required to simulate the daily activities. The reason for this situation is to obtain a system suitable for simulating the force required for power grip motion. However, if the objective of the modeling of the power grip is completely abandoned and a system that can only provide 7 N force feedback is aimed, it is possible to obtain a system that is 52.4% smaller in volume (18.4 mm outer shell diameter and 13.56 total length). Thanks to this arrangement that can be made, a lighter and more compact system can be obtained with easier placement in the limited area on the hand.

REFERENCES

An, Jinung, and Dong Soo Kwon. 2004. “In Haptics, the Influence of the Controllable Physical Damping on Stability and Performance.” *2004 IEEE/RSJ International Conference on Intelligent Robots and Systems (IROS)* 2: 1204–9. https://doi.org/10.1109/IROS.2004.1389560.

“AvatarVR.” n.d. Accessed April 16, 2022. https://avatarvr.es/.

Avraam, More, Mihaita Horodinca, Iulian Romanescu, and André Preumont. 2010. “Computer Controlled Rotational MR-Brake for Wrist Rehabilitation Device.” *Journal of Intelligent Material Systems and Structures* 21 (15): 1543–57. https://doi.org/10.1177/1045389X10362274.

Blake, Jonathan, and Hakan B. Gurocak. 2009. “Haptic Glove with MR Brakes for Virtual Reality.” *IEEE/ASME Transactions on Mechatronics* 14 (5): 606–15. https://doi.org/10.1109/TMECH.2008.2010934.

Bouzit, M., and G. C. Burdea. 2006. U.S. Patent No. 7,138,976. 7,138,976, issued 2006.

Bouzit, Mourad, Grigore Burdea, George Popescu, and Rares Boian. 2002. “The Rutgers Master II - New Design Force-Feedback Glove.” *IEEE/ASME Transactions on Mechatronics* 7 (2): 256–63. https://doi.org/10.1109/TMECH.2002.1011262.

Bouzit, Mourad, George Popescu, Grigore Burdea, and Rares Boian. 2002. “The Rutgers Master II-ND Force Feedback Glove.” *Proceedings - 10th Symposium on Haptic Interfaces for Virtual Environment and Teleoperator Systems, HAPTICS 2002,* 145–52. https://doi.org/10.1109/HAPTIC.2002.998952.

Chen Chen, Fai, Silvia Appendino, Alessandro Battezzato, Alain Favetto, Mehdi Mousavi, and Francesco Pescarmona. 2013. “Constraint Study for a Hand Exoskeleton: Human Hand Kinematics and Dynamics.” *Journal of Robotics* 2013. https://doi.org/10.1155/2013/910961.

Choi, Inrak, Elliot W. Hawkes, David L. Christensen, Christopher J. Ploch, and Sean Follmer. 2016. “Wolverine: A Wearable Haptic Interface for Grasping in Virtual Reality.” *IEEE International Conference on Intelligent Robots and Systems* 2016-November (November): 986–93. https://doi.org/10.1109/IROS.2016.7759169.

"Contact CI." n.d. Accessed April 16, 2022. https://contact.ci/#maestro-product.

CyberGlove. 2007. "CyberGrasp Manual, Version 2.0." San Jose, CA.

"Cynteract." 2013. 2013. https://www.cynteract.com/.

DextaRoboticsInc. 2019. "DEXMO Development Kit 1 User Manual [V3.0]." https://oss-main.dextarobotics.com/specifications_en-us.pdf.

exiii. 2018. "Exiii - Wearable Haptic Technology for XR." 2018. https://exiii.jp/2018/10/02/exos_wrist_dk2_en/.

Gang, Han Gyeol, Seung-Bok Choi, and Jung Woo Sohn. 2016. "Design of Haptic Master Featuring Small-Sized MR Brakes." *Https://Doi.Org/10.1117/12.2219076* 9799 (April): 916–21. https://doi.org/10.1117/12.2219076.

Ghazaly, Mariam Md, Tawfik Ahmed Yahya, Aliza Che Amran, Zulkeflee Abdullah, Mohd Amran Md Ali, Ahmad Hilkam Jamaludin, and Nursabillilah Mohd Ali. 2016. "Force Characterization Of A Tubular Linear Electromagnetic Actuator Using Finite Element Analysis Method (FEM)." *Jurnal Teknologi* 78 (11): 217–25. https://doi.org/10.11113/JT.V78.9901.

Habib, Sahar Refaat, and Nashwa Nabil Kamal. 2010. "Stature Estimation from Hand and Phalanges Lengths of Egyptians." *Journal of Forensic and Legal Medicine* 17 (3): 156–60. https://doi.org/10.1016/J.JFLM.2009.12.004.

Haption. n.d. "Haption Hglove." Accessed April 16, 2022. https://www.haption.com/fr/products-fr/hglove-fr.html.

HaptX Inc. 2013. "Haptic Technology for VR and Robotics - Tactile, Force, and Motion | HaptX." 2013. https://haptx.com/technology/.

In, Hyunki, Brian Byunghyun Kang, Min Ki Sin, and Kyu Jin Cho. 2015. "Exo-Glove: A Wearable Robot for the Hand with a Soft Tendon Routing System." *IEEE Robotics and Automation Magazine* 22 (1): 97–105. https://doi.org/10.1109/MRA.2014.2362863.

Ito, A, W Bosworth, A T Visser, J Grimson, and W Yang. 1983. "Fermi Lab B VS. H CURVES FOR 1008 AND 1020 STEELS TM-1197 6023.000." *International Nuclear Information System (INEA)*, June. https://lss.fnal.gov/archive/test-tm/1000/fermilab-tm-1197.pdf.

Jasuja O.P., and Singh G. 2004. “Estimation of Stature from Hand and Phalange Length.” *Journal of Indian Academy of Forensic Medicine* 26 (3): 100–106. https://indianjournals.com/ijor.aspx?target=ijor:jiafm&volume=26&issue=3&article=003.

Jenkins, J.W. 1963. U.S. Patent No. 3,082,792. 3,082,792, issued 1963.

Jibin, Zou, and Lu Yongping. 1992. “Numerical Calculations for Ferrofluid Seals.” *IEEE Transactions on Magnetics* 28 (6): 3367–71. https://doi.org/10.1109/20.179812.

Johnston, G., W. C Kruckemeyer, and R. E. Longhouse. 1998. U.S. Patent No. 5,848,678. 5,848,678, issued 1998.

Kern, Thorsten A. 2009. “Engineering Haptic Devices: A Beginner’s Guide for Engineers.” *Engineering Haptic Devices: A Beginner’s Guide for Engineers*, 1–472. https://doi.org/10.1007/978-3-540-88248-0.

Kim, Jinho, and Junghwan Chang. 2007. “A New Electromagnetic Linear Actuator for Quick Latching.” *IEEE Transactions on Magnetics* 43 (4): 1849–52. https://doi.org/10.1109/TMAG.2006.892289.

KOMEDA, Takashi, Shinichi UCHINO, Yoshiyuki TAKAHASHI, Mario ELASYEH, Yukio KAWAKAMI, Hiroyuki KOYAMA, and Shin-ichiro YAMAMOTO. 2005. “Development of a Haptic Glove to Use a Master-Slave Rehabilitation Robot Hand System.” *Proceedings of the JFPS International Symposium on Fluid Power* 2005 (6): 745–48. https://doi.org/10.5739/ISFP.2005.745.

Koyama, Tatsuya, Ikuo Yamano, Kenjiro Takemura, and Takashi Maeno. 2002. “Multi-Fingered Exoskeleton Haptic Device Using Passive Force Feedback for Dexterous Teleoperation.” *IEEE International Conference on Intelligent Robots and Systems* 3: 2905–10. https://doi.org/10.1109/IRDS.2002.1041713.

Koyanagi, Ken ’, Yuki Fujii, and Junji Furusho. 2005. “Development of VR-STEF System with Force Display Glove System.” *Proceedings of the 2005 International Conference on Augmented Tele-Existence - ICAT ’05*. https://doi.org/10.1145/1152399.

Krishnan, R. 1987. “Selection Criteria for Servo Motor Drives.” *IEEE Transactions on Industry Applications* IA-23 (2): 270–75. https://doi.org/10.1109/TIA.1987.4504902.

Kunii, Yasuharu, Yoshiaki Nishino, Toshio Kitada, and Hideki Hashimoto. 1997. "Development of 20 DOF Glove Type Haptic Interface Device - Sensor Glove II." *IEEE/ASME International Conference on Advanced Intelligent Mechatronics, AIM*, 132. https://doi.org/10.1109/AIM.1997.653003.

Lee, Kyung Sun, and Myung Chul Jung. 2015. "Three-Dimensional Finger Joint Angles by Hand Posture and Object Properties." *Https://Doi.Org/10.1080/00140139.2015.1108458* 59 (7): 890–900. https://doi.org/10.1080/00140139.2015.1108458.

Lindberg, T. 1993. U.S. Patent No. 5,186,286. 5,186,286, issued 1993.

Liu, Tonggang, Yusheng Cheng, and Zhiyi Yang. 2005. "Design Optimization of Seal Structure for Sealing Liquid by Magnetic Fluids." *Journal of Magnetism and Magnetic Materials* 289 (March): 411–14. https://doi.org/10.1016/J.JMMM.2004.11.116.

LORD Corp. 2016. "Magneto-Rheological (MR) Fluid." 2016. http://www.lord.com/products-and-solutions/active-vibration-control/industrialsuspension- systems/magneto-rheological-(mr)-fluid.

Ma, Zhou, and Pinhas Ben-Tzvi. 2015a. "RML Glove-an Exoskeleton Glove Mechanism with Haptics Feedback." *IEEE/ASME Transactions on Mechatronics* 20 (2): 641–52. https://doi.org/10.1109/TMECH.2014.2305842.

———. 2015b. "Design and Optimization of a Five-Finger Haptic Glove Mechanism." *Journal of Mechanisms and Robotics* 7 (4). https://doi.org/10.1115/1.4029437/377682.

Moermond, Jack. n.d. "Magnetic Field Sensors – Are Magnets Different? - AUTOMATION INSIGHTS." https://automation-insights.blog/2010/04/26/magnetic-field-sensors-%E2%80%93-are-magnets-different/.

Najmaei, Nima, Peyman Yadmellat, Mehrdad R. Kermani, and Rajni v. Patel. 2014. "Application of Magneto-Rheological Fluid Based Clutches for Improved Performance in Haptic Interfaces." *Proceedings - IEEE International Conference on Robotics and Automation*, September, 832–37. https://doi.org/10.1109/ICRA.2014.6906951.

Nam, Y. J., M. K. Park, and R. Yamane. 2008. “Smart Glove: Hand Master Using Magnetorheological Fluid Actuators.” *Https://Doi.Org/10.1117/12.783776* 6794 (January): 681–86. https://doi.org/10.1117/12.783776.

Perret, J., and vander Poorten. 2018. “Touching Virtual Reality: A Review of Haptic Gloves .” In *16th International Conference on New Actuators* , 1–5. https://ieeexplore.ieee.org/abstract/document/8470813.

Plexus. 2021. “Plexus / High-Performance VR/AR Gloves.” 2021. http://plexus.im/.

Precision Microdrives. n.d. “Eccentric Rotating Mass Vibration Motors - ERMs - Precision Microdrives.” Accessed April 22, 2022a. https://www.precisionmicrodrives.com/eccentric-rotating-mass-vibration-motors-erms.

———. n.d. “Linear Resonant Actuators – LRAs - Precision Microdrives.” Accessed April 22, 2022b. https://www.precisionmicrodrives.com/linear-resonant-actuators-lras.

Qin, Huanhuan, Aiguo Song, Zhan Gao, Yuqing Liu, and Guohua Jiang. 2018. “A Multi-Finger Interface with MR Actuators for Haptic Applications.” *IEEE Transactions on Haptics* 11 (1): 5–14. https://doi.org/10.1109/TOH.2017.2709321.

Rankin, P. J., J. M. Ginder, and D. J. Klingenberg. 1998. “Electro- and Magneto-Rheology.” *Current Opinion in Colloid & Interface Science* 3 (4): 373–81. https://doi.org/10.1016/S1359-0294(98)80052-6.

Redmond, Brittany, Rachel Aina, Tejaswi Gorti, and Blake Hannaford. 2010. “Haptic Characteristics of Some Activities of Daily Living.” *2010 IEEE Haptics Symposium, HAPTICS 2010*, 71–76. https://doi.org/10.1109/HAPTIC.2010.5444674.

Rice, Martin S., Cathy Leonard, and Mike Carter. 1998. “Grip Strengths and Required Forces in Accessing Everyday Containers in a Normal Population.” *The American Journal of Occupational Therapy* 52 (8): 621–26. https://doi.org/10.5014/AJOT.52.8.621.

Richard, P., and Ph Coiffet. 1999. “Dextrous Haptic Interaction in Virtual Environments: Human Performance Evaluations.” *Robot and Human Communication - Proceedings of the IEEE International Workshop*, 315–20. https://doi.org/10.1109/ROMAN.1999.900359.

Rosenberg, L. B., and B. D. Adelstein. 1993. “Perceptual Decomposition of Virtual Haptic Surfaces.” *Proceedings of 1993 IEEE Research Properties in Virtual Reality Symposium, VRAIS 1993*, 46–53. https://doi.org/10.1109/VRAIS.1993.378264.

Schweber, Bill. 2021. “Haptics Components, Pt 1: LRA, ERM, and Piezo Actuators - Power Electronic Tips.” June 2, 2021. https://www.powerelectronictips.com/haptics-components-pt-1-lra-erm-and-piezo-actuators/.

SenseGlove. 2017. “SenseGlove for Research Applications.” 2017. https://www.senseglove.com/solutions/senseglove-for-research/.

“Senso.” 2015. 2015. https://senso.me/.

Shafer, Alex S., and Mehrdad R. Kermani. 2011. “Design and Validation of a Magneto-Rheological Clutch for Practical Control Applications in Human-Friendly Manipulation.” *Proceedings - IEEE International Conference on Robotics and Automation*, 4266–71. https://doi.org/10.1109/ICRA.2011.5980258.

Szczęch, Marcin. 2019. “Magnetic Fluid Seal Critical Pressure Calculation Based on Numerical Simulations:” *Https://Doi.Org/10.1177/0037549719885168* 96 (4): 403–13. https://doi.org/10.1177/0037549719885168.

Szczech, Marcin, and Wojciech Horak. 2017. “Numerical Simulation and Experimental Validation of the Critical Pressure Value in Ferromagnetic Fluid Seals.” *IEEE Transactions on Magnetics* 53 (7). https://doi.org/10.1109/TMAG.2017.2672922.

“VRtouch DK Data Sheet.” 2017. https://31a099b0-57f4-4cfb-a98f-fd78d508843b.filesusr.com/ugd/54e189_ed1c52ee29724c11b233004375424b59.pdf.

Wang, Lefan, Turgut Meydan, and Paul Ieuan Williams. 2017. “A Two-Axis Goniometric Sensor for Tracking Finger Motion.” *Sensors (Switzerland)* 17 (4). https://doi.org/10.3390/S17040770.

Winter, Scott H., and Mourad Bouzit. 2007. “Use of Magnetorheological Fluid in a Force Feedback Glove.” *IEEE Transactions on Neural Systems and Rehabilitation Engineering* 15 (1): 2–8. https://doi.org/10.1109/TNSRE.2007.891401.

Yun, Sung Sik, Brian Byunghyun Kang, and Kyu Jin Cho. 2017. “Exo-Glove PM: An Easily Customizable Modularized Pneumatic Assistive Glove.” *IEEE Robotics and Automation Letters* 2 (3): 1725–32. https://doi.org/10.1109/LRA.2017.2678545.

Zheng, Yukai, Dangxiao Wang, Ziqi Wang, Yu Zhang, Yuru Zhang, and Weiliang Xu. 2018. “Design of a Lightweight Force-Feedback Glove with a Large Workspace.” *Engineering* 4 (6): 869–80. https://doi.org/10.1016/J.ENG.2018.10.003.

Zinn, Michael, Bernard Roth, Oussama Khatib, and J. Kenneth Salisbury. 2016. “A New Actuation Approach for Human Friendly Robot Design:” *Http://Dx.Doi.Org/10.1177/0278364904042193* 23 (4–5): 379–98. https://doi.org/10.1177/0278364904042193.

APPENDIX A
FUTEK TFF400 REACTION TORQUE SENSOR
DATA SHEET

Figure A: FUTEK TFF400 Reaction Torque Sensor (Source: FUTEK,2017)

Table A: Product specifications of TFF400 reaction torque sensor.

SPECIFICATIONS	
PERFORMANCE	
Nonlinearity	±0.2% of RO
Hysteresis	±0.2% of RO
Nonrepeatability	±0.05% of RO
ELECTRICAL	
Rated Output (RO)	1 mV/V nom (5 in-oz) 2 mV/V nom (10 in-oz to 500 in-lb)
Excitation (VDC or VAC)	18 max
Bridge Resistance	350 Ohm nom (5 to 1000 in-oz) 700 Ohm nom (100 to 500 in-lb)
Connection	4 Pin LEMO® Receptacle (EGG.0B.304.CLL)
Wiring/Connector Code	CC4
MECHANICAL	
Weight (approximate)	9 oz [250 g]
Safe Overload	300% (5 to 1000 in-oz) of RO 150% (100 in-lb to 500 in-lb) of RO
Material	Aluminum
IP Rating	IP40
TEMPERATURE	
Operating Temperature	–60 to 200°F (–50 to 93°C)
Compensated Temperature	60 to 160°F (15 to 72°C)
Temperature Shift Zero	±0.002% of RO/°F (0.0036% of RO/°C)
Temperature Shift Span	±0.002% of Load/°F (0.0036% of Load/°C)
CALIBRATION	
Calibration Test Excitation	10 VDC
Calibration (standard)	5-pt CW
Calibration (available)	5-pt CW & CCW
Shunt Calibration Value	60.4 kOhm (10 to 1000 in-oz) 100 kOhm (5 in-oz, 100 to 500 in-lb)

APPENDIX B

FUTEK MODEL CSG 110 DATA SHEET

Figure B: FUTEK CSG 110 AMPLIFIER MODULE

Table B: FUTEK CSG 110 DATASHEET

ELECTRICAL SPECIFICATIONS				
PARAMETER	**MIN**	**TYPICAL**	**MAX**	**UNIT**
Power Supply[6]	14		26	VDC
Current Draw[7]		30		mA
Output Impedance (voltage)		< 1 Ohms		Ohms
Output Impedance (current)			700	Ohms
Sensor Impedance	100			Ohms
Bandwidth	1000		25000	Hz
Common Mode Rejection Ratio	120			dB
Noise		15		mV p-p
Output Span Range	–10		10	% of Rated Output
Output Zero Range	–10		10	% of Rated Output
Gain Drift with Temperature	–25	X	25	PPM of FSR per degree Celsius
Gain Non-Linearity (Better than)	–0.01	X	0.01	% of FSR
Zero Drift with Temperature	–25	X	25	PPM of FSR per degree Celsius

APPENDIX C

V-DAQ DATA ACQUISITION BOARD DATA SHEET

Figure C: V-DAQ control and data acquisition board.

Table C: V-DAQ Product Specifications

Quadrature Encoder Inputs

Number of Inputs	: 2
Sensor Supply	: 5V
Counter Size	: 32 bits
Max. Count Freq.	: 1 MHz

Digital Inputs

Number of Inputs	: 8
Voltage Level	: Selectable 3.3V / 5V
Leakage Current	: ± 2 µA

Analog Inputs

Number of Inputs	: 4 Single-Ended or 2 Differential
Input Range	: ±12V, ±6V, ±3V (Single-Ended) ±24V, ±12V, ±6V (Differential)
Resolution	: 16 bits
SNR + Distortion	: 91 dB (±24V Differential) 83 dB (±3V Single-Ended)
INL	: ±1 LSB (Typ)
Offset Error	: ±2 mV (Typ)
Gain Error	: ±1 %FSR (Max)

Integrated Motor Driver

Number of Drivers	: 2 Brushed DC or 1 Stepper
Voltage Range	: 6-48 V Wide Input Range
Max. Drive Current	: 2A (per driver)

PWM Outputs

Number of Outputs	: 4
Resolution	: 16 bits (depends on freq.)
Voltage Level	: Selectable 3.3V / 5V
Max. Freq.	: 65 KHz

Digital Outputs

Number of Outputs	: 8
Voltage Level	: Selectable 3.3V / 5V
Max. Drive Current	: 4 mA (per channel)

Analog Outputs

Number of Outputs	: 4
Output Range	: 0-5V, 0-10V, 0-10.8V ±5V, ±10V, ±10.8V
Resolution	: 16 bits
INL	: ±16 LSB (Max)
Offset Error	: ±6 mV (Max)
Gain Error	: ±0.08 %FSR (Max)
DC Output Impedance	: 0.5 Ω
Capacitive Load Stability	: 4000 pF
Max. Load	: 2 kΩ
Short-Circuit Current	: 20 mA
Slew Rate	: 3.5 V/µs
Output Noise	: 80 µV RMS (@100 kHz)

Relay Output (Solid State)

Number of Outputs	: 2
Blocking Voltage	: 60 V (Max.)
Max. Load Current	: 700 mA
Isolation	: 1500 Vrms Input/Output

APPENDIX D

MAXON DRIVES

D.1. Planetary Gearhead GP 26 A Ø26 mm, 0.75–4.5 Nm

Figure D.1: MAXON Planetary Gearhead.

Table D.1: MAXON Planetary Gearhead Specifications

General information	
Gearhead type	GP
Outer diameter	26 mm
Version	Standard version
Gearhead Data	
Reduction	181 : 1
Absolute reduction	87723/484
Max. motor shaft diameter	3 mm
Number of stages	3
Max. continuous torque	4.5 Nm
Max. intermittent torque	6.2 Nm
Direction of rotation, drive to output	=
Max. efficiency	70 %
Average backlash no load	0.8 °
Mass inertia	0.31 gcm²
Gearhead length (L1)	39.5 mm
Max. transmittable power (continuous)	20 W
Max. transmittable power (intermittent)	30 W
Technical Data	
Radial play	max. 0.1 mm, 5 mm from flange
Axial play	0 - 0.4 mm
Max. radial load	140 N, 12 mm from flange
Max. force for press fits	120 N
Max. continuous input speed	8000 rpm
Max. intermittent input speed	12000 rpm
Recommended temperature range	-30...+100 °C
Number of autoclave cycles	0
Product	
Weight	93 g

D.2. RE 25 Ø25 mm, Graphite Brushes, 20 Watt

Figure D.2: MAXON DC Motor.

Table D.2: MAXON DC Motor Specifications

Values at nominal voltage	
Nominal voltage	12 V
No load speed	9620 rpm
No load current	68.1 mA
Nominal speed	8310 rpm
Nominal torque (max. continuous torque)	27.5 mNm
Nominal current (max. continuous current)	2.45 A
Stall torque	268 mNm
Stall current	23.2 A
Max. efficiency	84 %
Characteristics	
Terminal resistance	0.517 Ω
Terminal inductance	0.057 mH
Torque constant	11.5 mNm/A
Speed constant	828 rpm/V
Speed / torque gradient	37.1 rpm/mNm
Mechanical time constant	5.62 ms
Rotor inertia	14.5 gcm²
Thermal data	
Thermal resistance housing-ambient	14.4 K/W
Thermal resistance winding-housing	5.08 K/W
Thermal time constant winding	29.3 s
Thermal time constant motor	543 s
Ambient temperature	-30...+100 °C
Max. winding temperature	+155 °C
Mechanical data	
Bearing type	ball bearings
Max. speed	14000 rpm
Axial play	0.05 - 0.15 mm
Radial play	0.025 mm
Max. axial load (dynamic)	20 N
Max. force for press fits (static)	60 N
(static, shaft supported)	1000 N
Max. radial load	35 N, 5 mm from flange
Other specifications	
Number of pole pairs	1
Number of commutator segments	11
Number of autoclave cycles	0
Product	
Weight	110 g

D.3. Encoder HEDL 5540

Figure D.3: MAXON Motor Encoder.

Table D.3: MAXON Motor Encoder Specifications

General information	
Counts per turn	500
Number of channels	3
Line Driver	DS26LS31
Max. mechanical speed	12000 rpm
Shaft diameter	3 mm
Technical Data	
Supply voltage Vcc	5.0V ± 10.0%
Driver used logic	EIA RS 422
Max. angular acceleration	250000 rad / s²
Output current per channel	-20...20 mA
Signal rise time	180 ns
Measurement condition for signal rise time	CL=25pF, RL=2.7kOhm,
Signal fall time	40 ns
Measurement condition for signal fall time	CL=25pF, RL=2.7kOhm,
Phase shift	90 °e
Phase shift, inaccuracy	45 °e
Index synchronized to AB	Yes
Max. moment of inertia of code wheel	0.6 gcm²
Operating temperature	-40...+100 °C
Orientation of encoder output to motor flange	-1 °

D.4. Escon 50/5 Servo Controller

Figure D.4: MAXON 50/5 Servo Controller. (Source: MAXON,2018)

Table D.4: MAXON 50/5 Servo Controller Specifications

ESCON 50/5 (409510)			
Electrical Rating	Nominal operating voltage $+V_{CC}$	10…50 VDC	
	Absolute operating voltage $+V_{CC\,min}$ / $+V_{CC\,max}$	8 VDC / 56 VDC	
	Output voltage (max.)	0.98 x $+V_{CC}$	
	Output current I_{cont} / I_{max} (<20 s)	5 A / 15 A	
	Pulse Width Modulation frequency	53.6 kHz	
	Sampling rate PI current controller	53.6 kHz	
	Sampling rate PI speed controller	5.36 kHz	
	Max. efficiency	95%	
	Max. speed DC motor	limited by max. permissible speed (motor) and max. output voltage (controller)	
	Max. speed EC motor	150'000 rpm (1 pole pair)	
	Built-in motor choke	3 x 30 µH; 5 A	
Inputs & Outputs	Analog Input 1 Analog Input 2	resolution 12-bit; −10…+10 V; differential	
	Analog Output 1 Analog Output 2	resolution 12-bit; −4…+4 V; referenced to GND	
	Digital Input 1 Digital Input 2	+2.4…+36 VDC (R_i = 38.5 kΩ)	
	Digital Input/Output 3 Digital Input/Output 4	+2.4…+36 VDC (R_i = 38.5 kΩ) / max. 36 VDC (I_L <500 mA)	
	Hall sensor signals	H1, H2, H3	
	Encoder signals	A, A\, B, B\, (max. 1 MHz)	
Voltage Outputs	Auxiliary output voltage	+5 VDC (I_L ≤10 mA)	
	Hall sensor supply voltage	+5 VDC (I_L ≤30 mA)	
	Encoder supply voltage	+5 VDC (I_L ≤70 mA)	
Potentiometers	Potentiometer P1 (on board) Potentiometer P2 (on board)	240°; linear	
Motor Connections	DC motor	+ Motor, − Motor	
	EC motor	Motor winding 1, Motor winding 2, Motor winding 3	
Interface	USB 2.0 / USB 3.0	full speed	
Status Indicators	Operation	green LED	
	Error	red LED	
Physical	Weight	approx. 204 g	
	Dimensions (L x W x H)	115 x 75.5 x 24 mm	
	Mounting holes	for M4 screws	
Environmental Conditions	Temperature	Operation	−30…+45 °C
		Extended range *1)	+45…+85 °C Derating ➔Figure 2-1
		Storage	−40…+85 °C
	Altitude *2)	Operation	0…10'000 m MSL
	Humidity	5…90% (condensation not permitted)	

APPENDIX E

GW INSTEK SPS-3610 DC POWER SUPPLY DATA SHEET

Figure E: SPS-3610 DC Power Supply (Source: Farnell, 2018)

Table E: DC Power Supply Specifications

SPECIFICATIONS					
OUTPUT					
	SPS-1230	**SPS-1820**	**SPS-2415**	**SPS-3610**	**SPS-606**
Voltage **Current**	0 ~ 12V 0 ~ 30A	0 ~ 18V 0 ~ 20A	0 ~ 24V 0 ~ 15A	0 ~ 36V 0 ~ 10A	0 ~ 60V 0 ~ 6A
CONSTANT VOLTAGE OPERATION					
Regulation	Line regulation ≤5mV Load regulation ≤5mV				
Ripple & Noise	≤5mVrms, 100mVp-p 20Hz ~ 20MHz				
Recovery Time	≤500μS (50% Load change, Minimum load 0.5A)				
Temp. Coefficient	≤ 100ppm / °C				
Output Range	0 to rating voltage continuously adjustable				
CONSTANT CURRENT OPERATION					
Regulation	Line regulation ≤3mA Load regulation ≤3mA				
Ripple Current	≤3mArms (SPS-606) ≤5mArms (SPS-3610) ≤10mArms (SPS-2415) ≤10mArms (SPS-1820) ≤30mArms (SPS-1230)				
Output Range	0 to rating current continuously adjustable (HI/LO range switchable)				
METER					
Type **Accuracy**	3 1/2 digit, 0.39" LED display ± (0.5% of rdg + 2digits)				
INSULATION					
Chassis and Terminal **Chassis and AC Cord**	20MΩ or above (DC 500V) 30MΩ or above (DC 500V)				
POWER SOURCE					
AC 115V/ 230V ±15 %, 50/60Hz					
DIMENSIONS & WEIGHT					
128(W) x 151(H) x 295(D) mm, Approx. 3.2kg					

APPENDIX F

RESULTS OF THE FREQUENCY RESPONSE TESTS

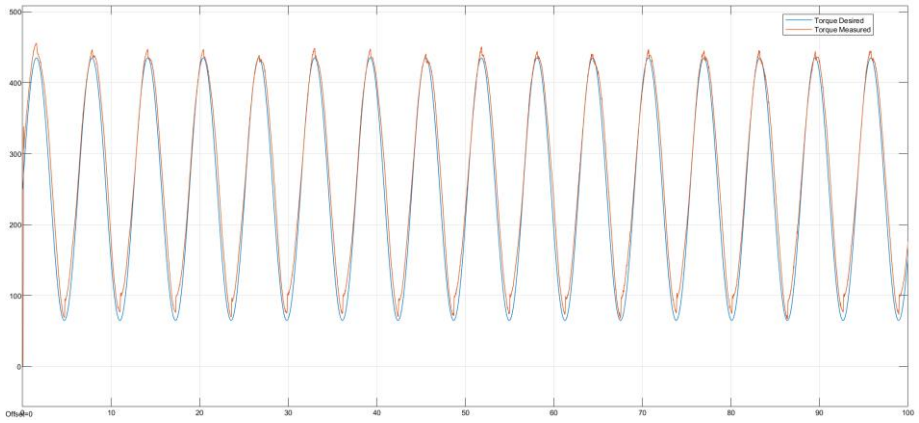

Figure F.1: Torque demand and response signals at 1 rad/s frequency.

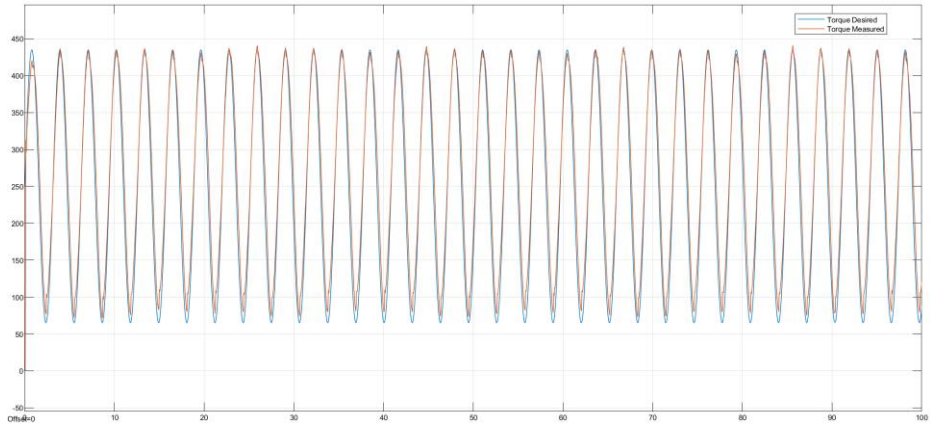

Figure F.2: Torque demand and response signals at 2 rad/s frequency.

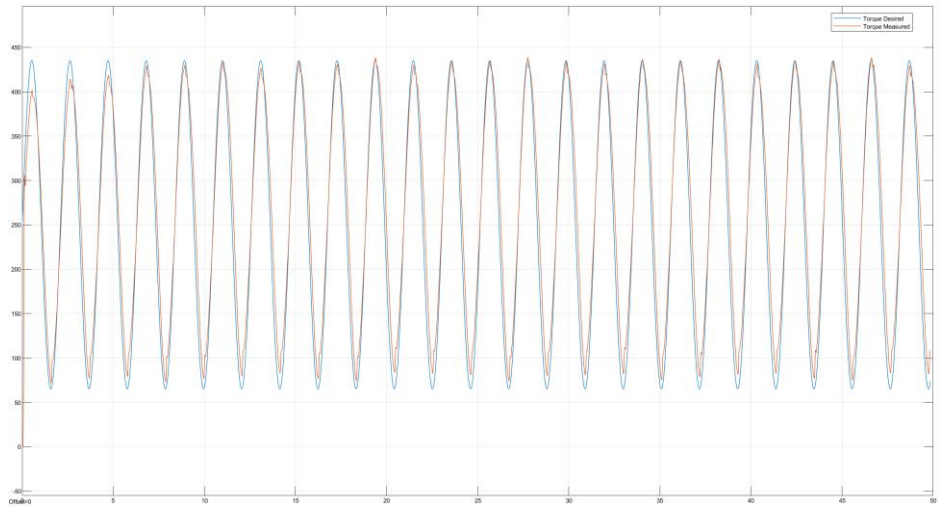

Figure F.3: Torque demand and response signals at 3 rad/s frequency.

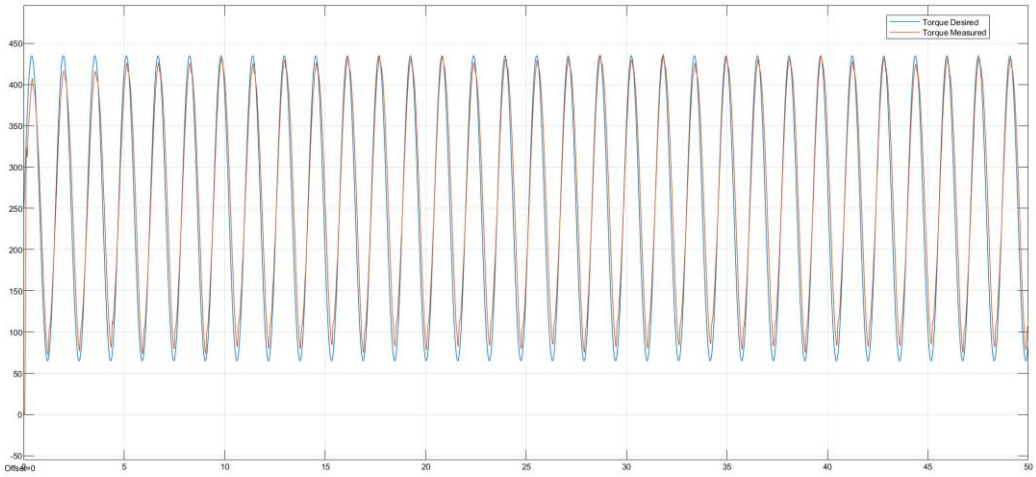

Figure F.4: Torque demand and response signals at 4 rad/s frequency.

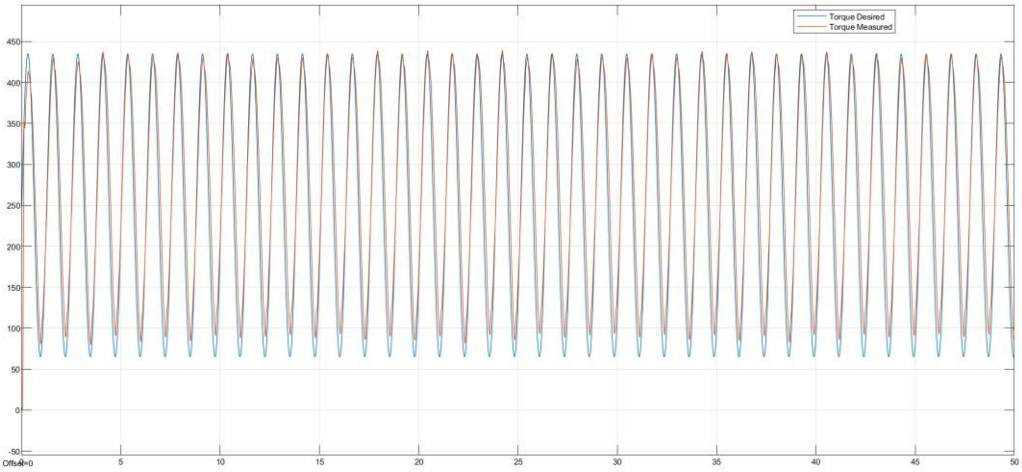

Figure F.5: Torque demand and response signals at 5 rad/s frequency.

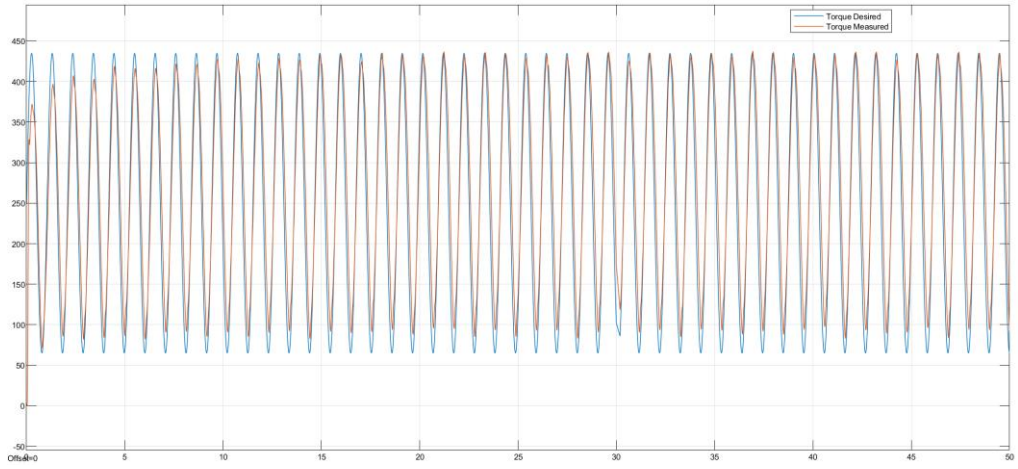

Figure F.6: Torque demand and response signals at 6 rad/s frequency.

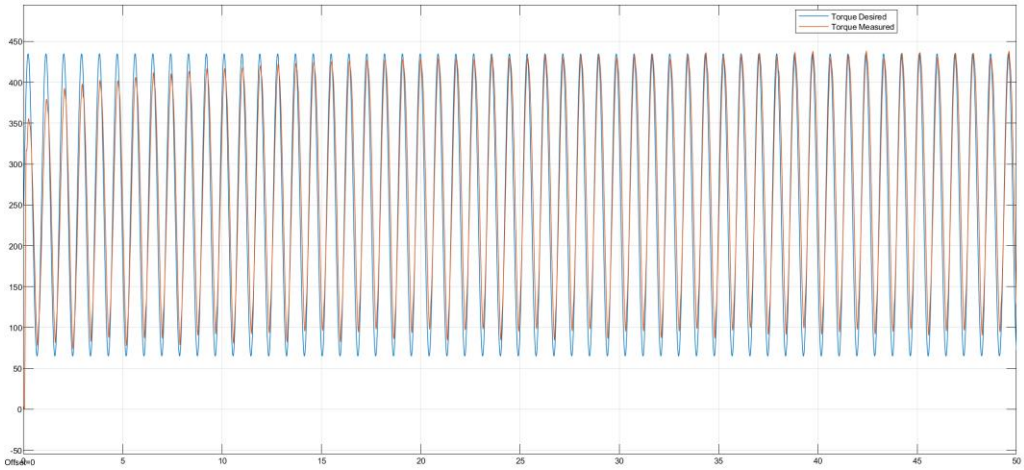

Figure F.7: Torque demand and response signals at 7 rad/s frequency.

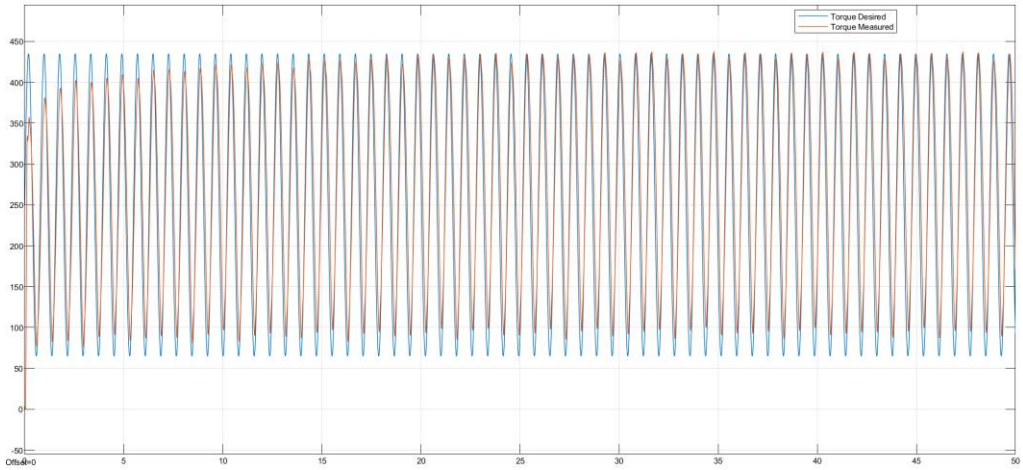

Figure F.8: Torque demand and response signals at 8 rad/s frequency.

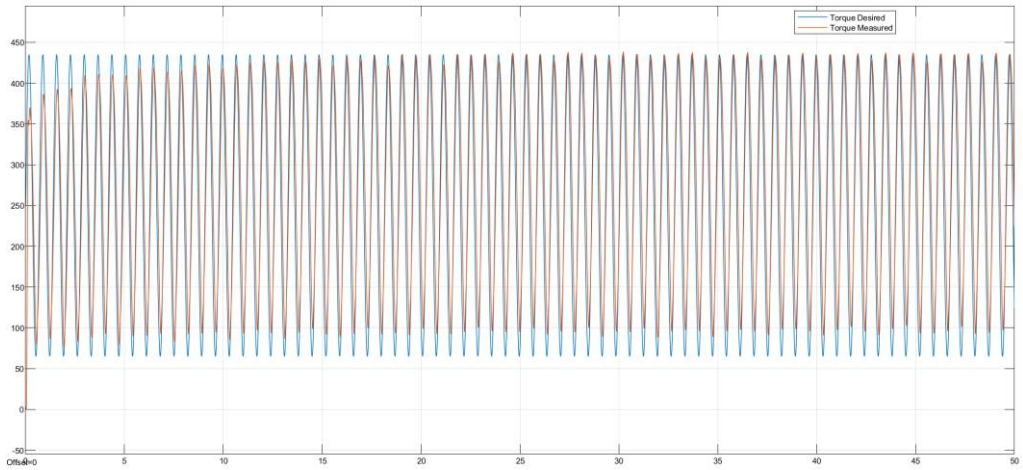

Figure F.9: Torque demand and response signals at 9 rad/s frequency.

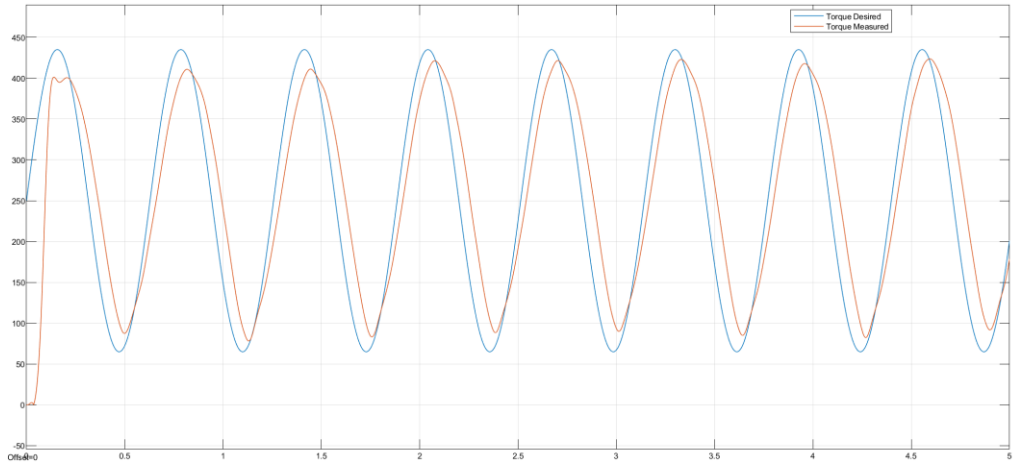

Figure F.10: Torque demand and response signals at 10 rad/s frequency.

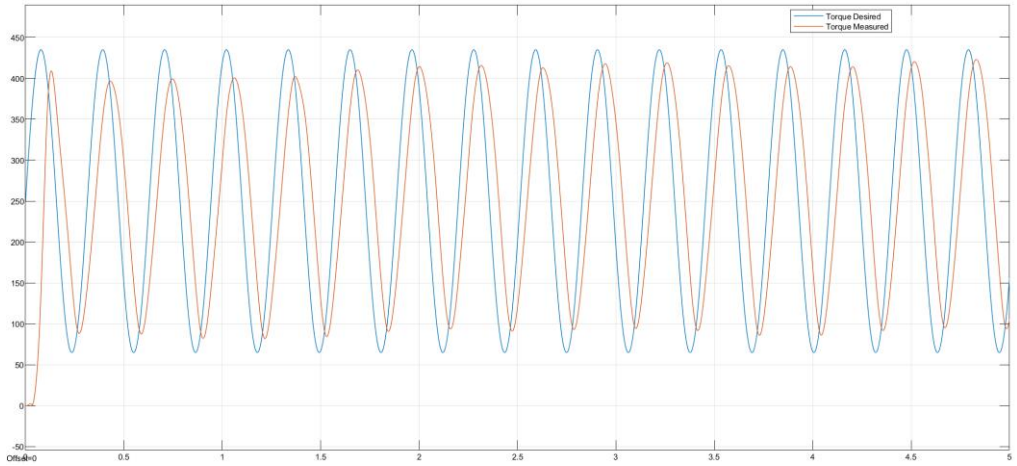

Figure F.11: Torque demand and response signals at 20 rad/s frequency.

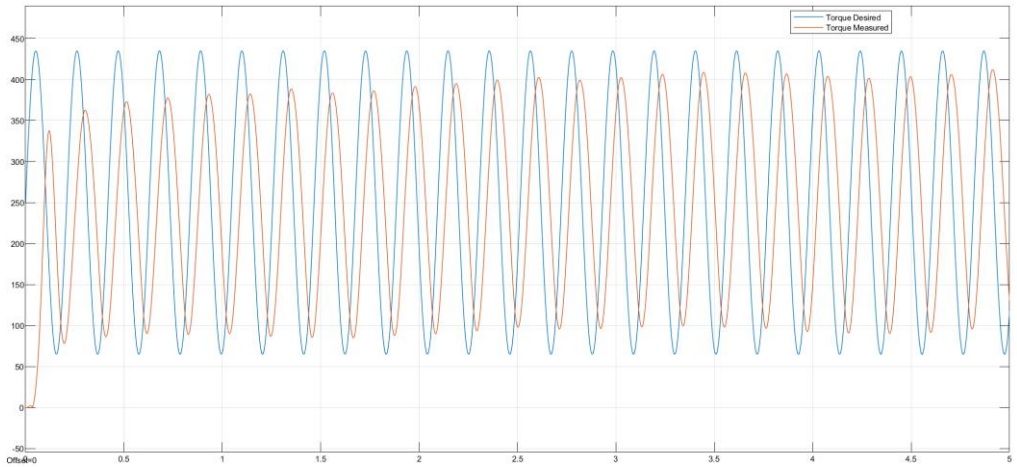

Figure F.12: Torque demand and response signals at 30 rad/s frequency.

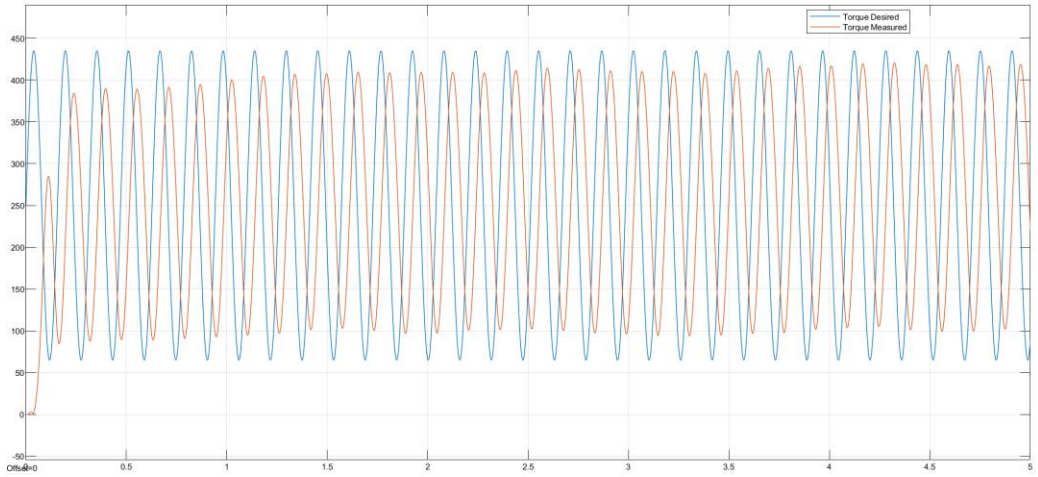

Figure F.13: Torque demand and response signals at 40 rad/s frequency.

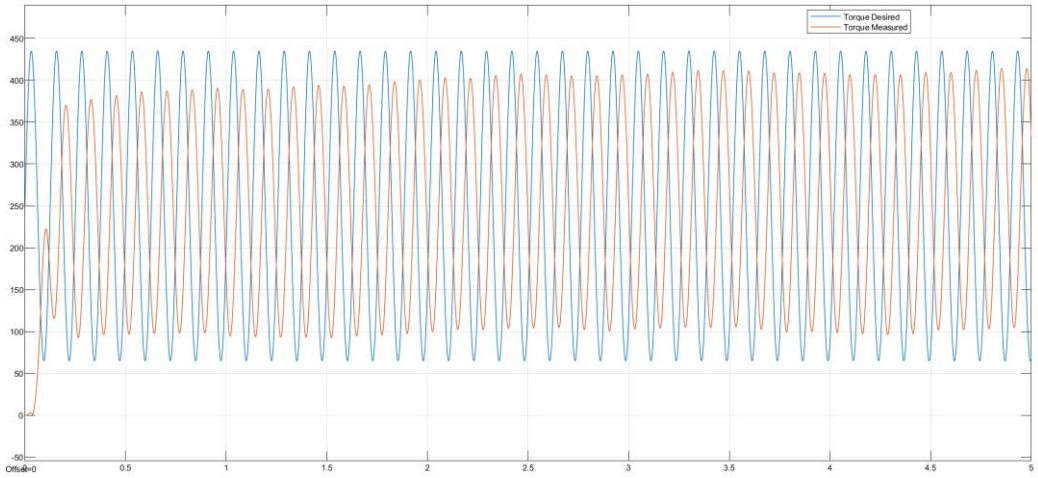

Figure F.14: Torque demand and response signals at 50 rad/s frequency.

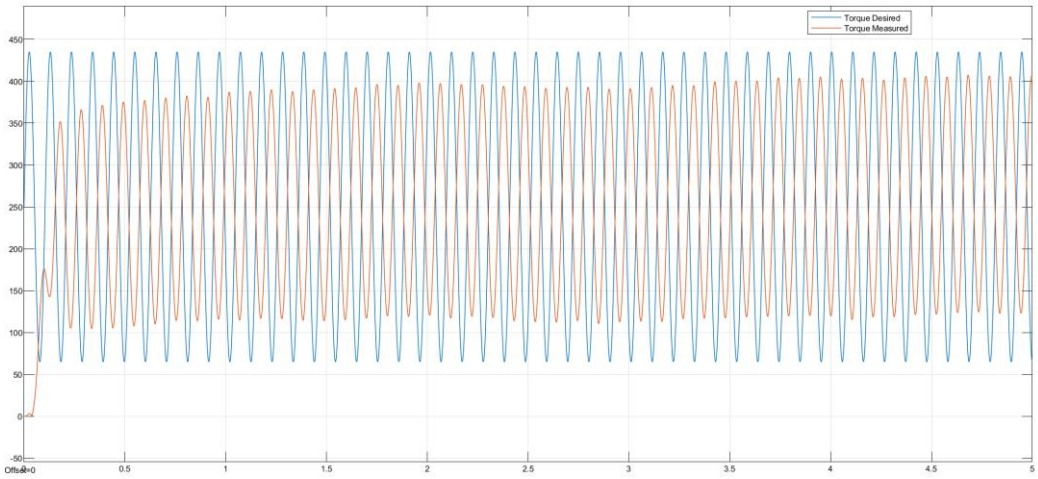

Figure F.15: Torque demand and response signals at 60 rad/s frequency.

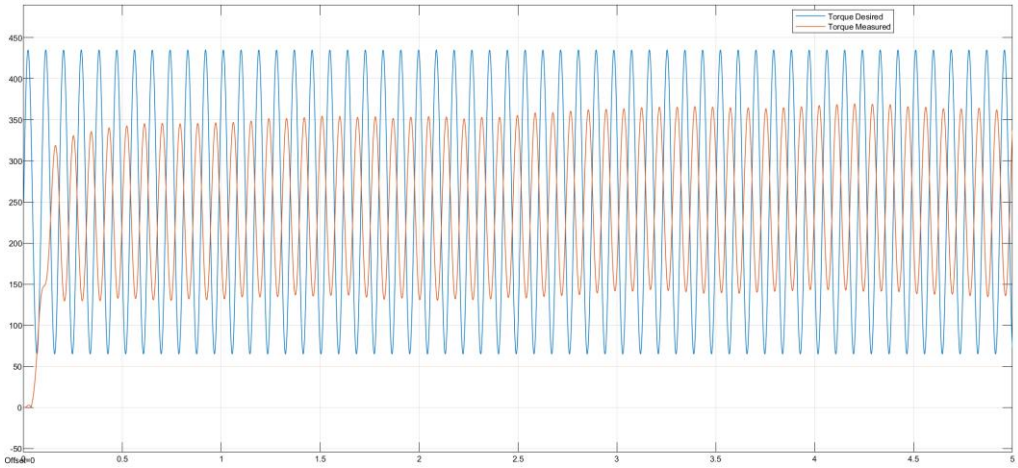

Figure F.16: Torque demand and response signals at 70 rad/s frequency.

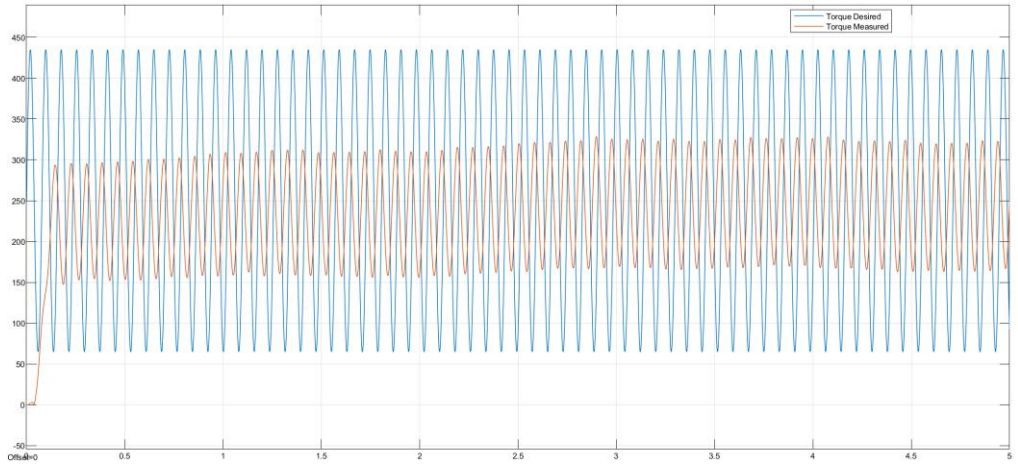

Figure F.17: Torque demand and response signals at 80 rad/s frequency.

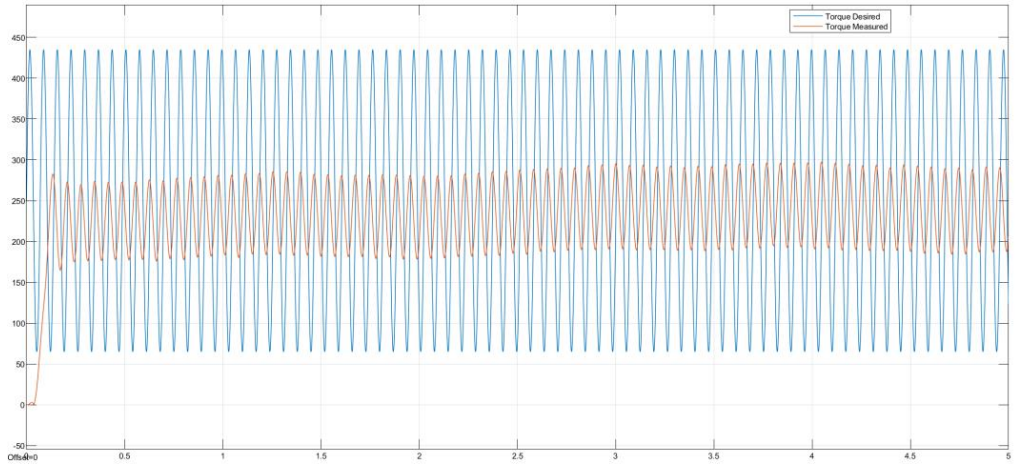

Figure F.18: Torque demand and response signals at 90 rad/s frequency.

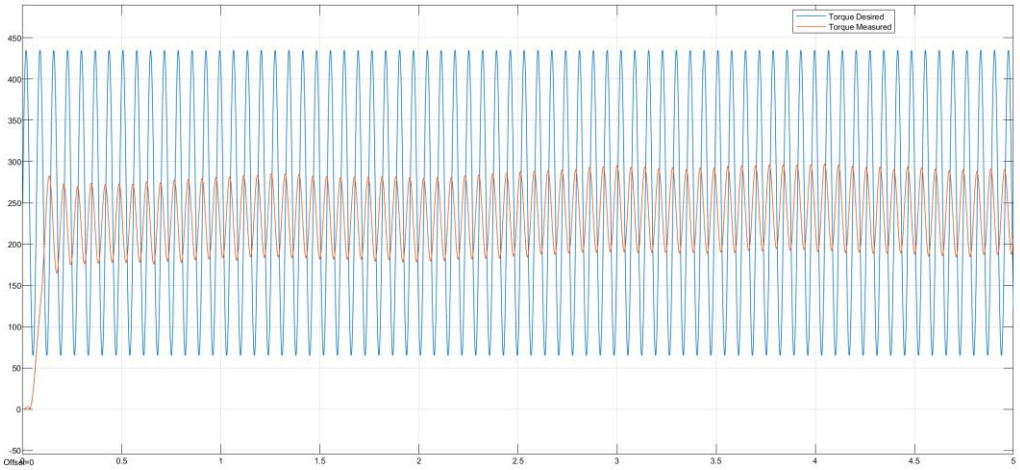

Figure F.19: Torque demand and response signals at 100 rad/s frequency.

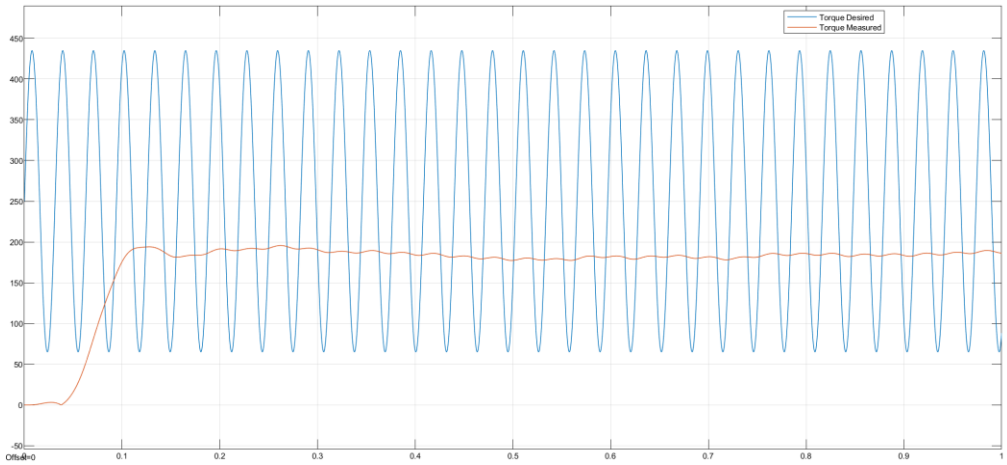

Figure F.20: Torque demand and response signals at 200 rad/s frequency.

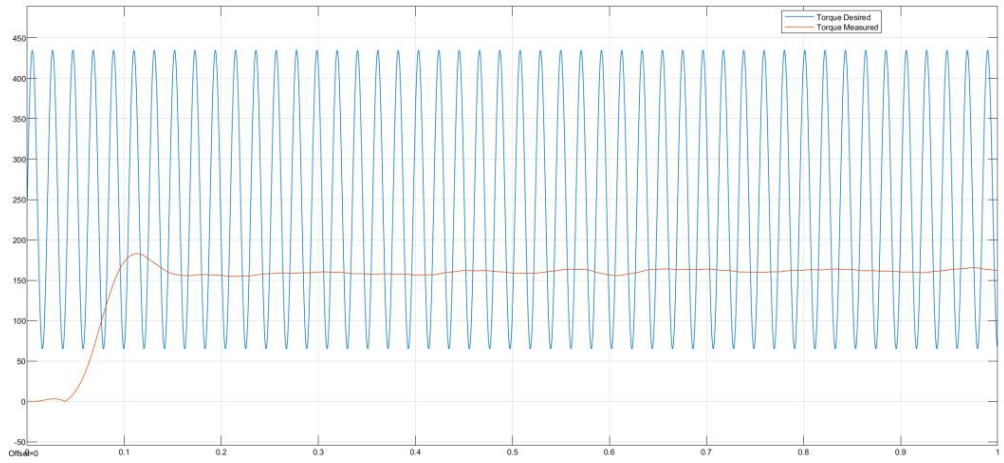

Figure F.21: Torque demand and response signals at 300 rad/s frequency.

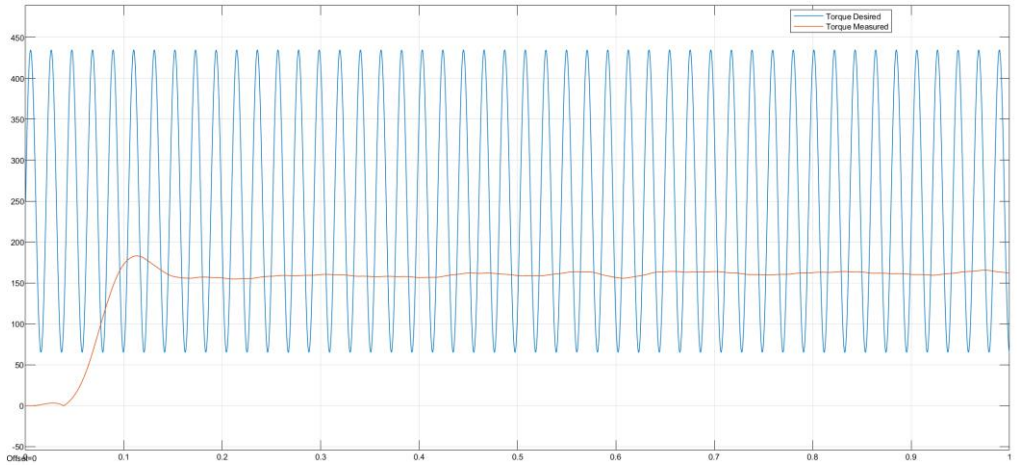

Figure F.22: Torque demand and response signals at 400 rad/s frequency.

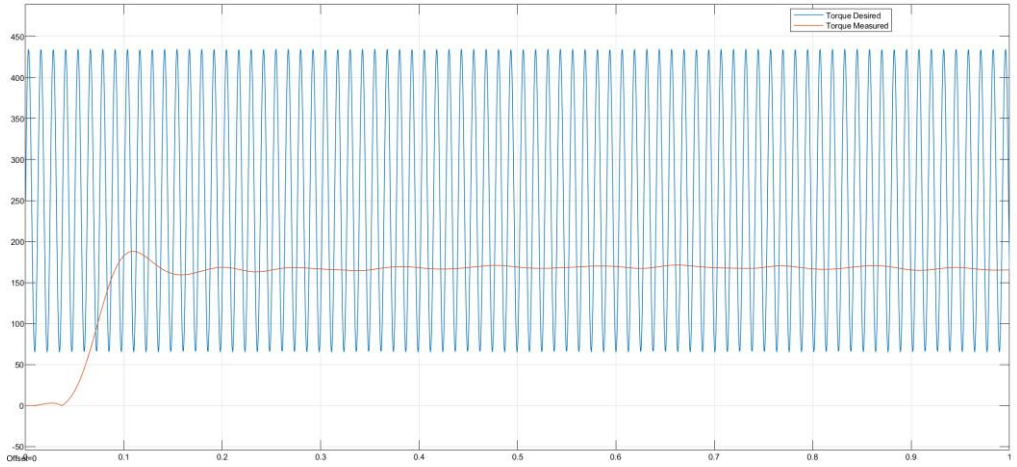

Figure F.23: Torque demand and response signals at 500 rad/s frequency.

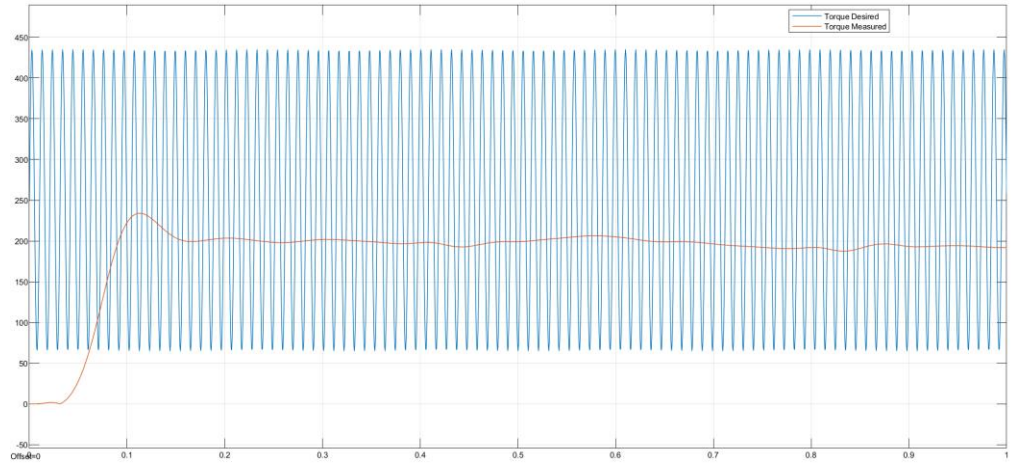

Figure F.24: Torque demand and response signals at 600 rad/s frequency.

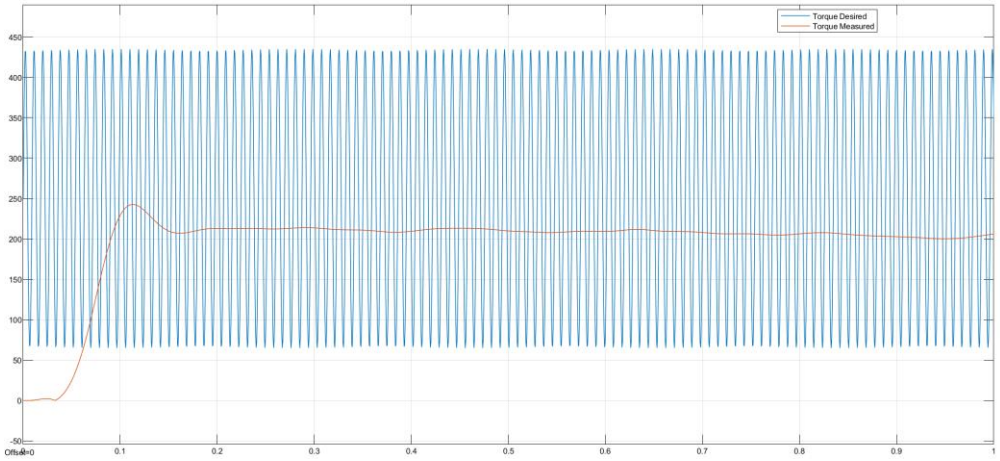

Figure F.25: Torque demand and response signals at 700 rad/s frequency.

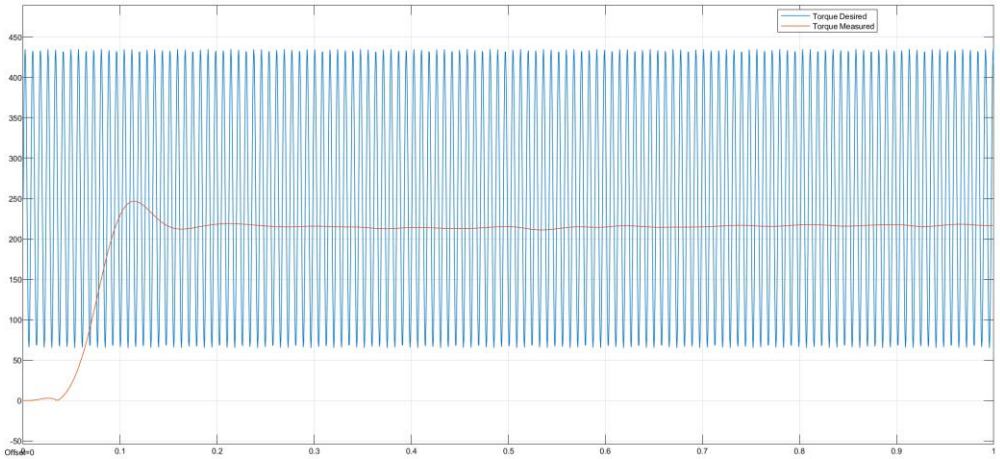

Figure F.26: Torque demand and response signals at 800 rad/s frequency.

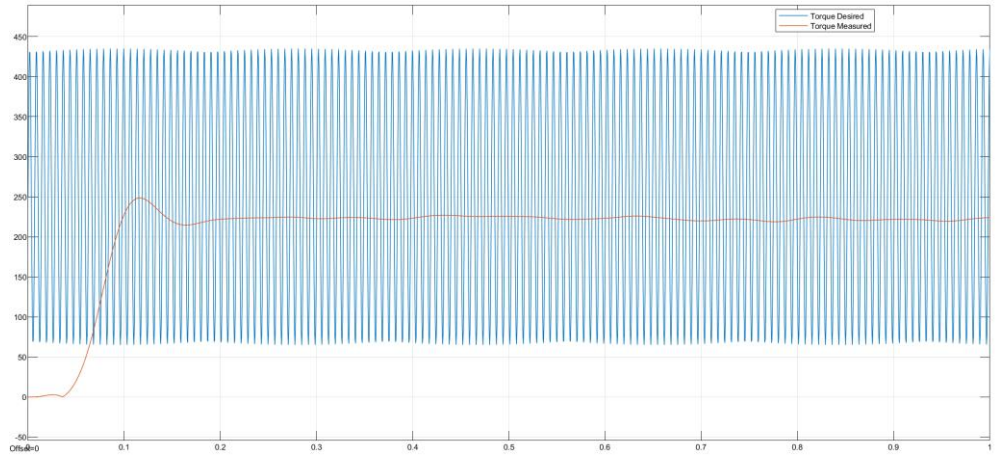

Figure F.27: Torque demand and response signals at 900 rad/s frequency.

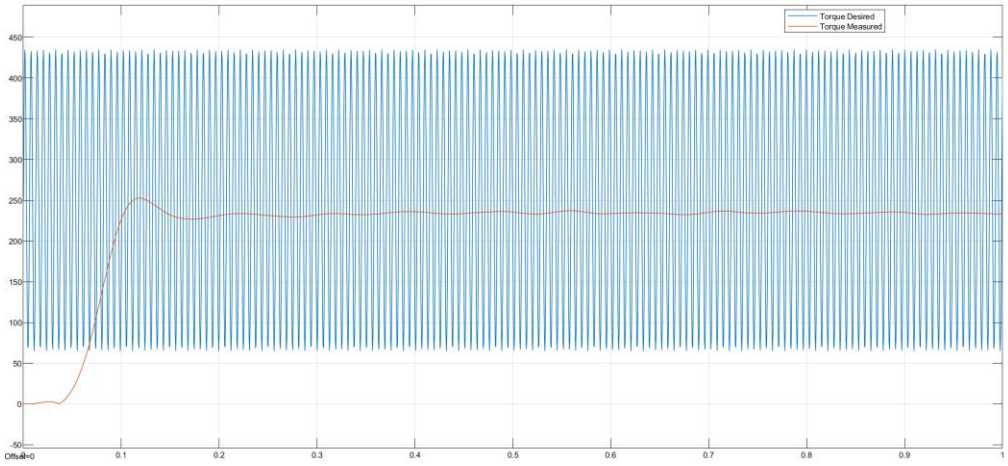

Figure F.28: Torque demand and response signals at 1000 rad/s frequency.